# Extreme heat and its impacts in a changing climate

Ethan D. Coffel

Submitted in partial fulfillment of the

requirements for the degree of

Doctor of Philosophy

in the Graduate School of Arts and Sciences

Columbia University

2018

Abstract

Extreme heat and its impacts in a changing climate

Ethan D. Coffel

Climate change has already increased the frequency, intensity, and duration of heat waves around the world. In the coming decades, this trend will continue and likely accelerate, exposing much of the world's population to historically unprecedented conditions. In some regions, extreme temperatures (as indexed by the annual maximum temperature) are projected to increase at a faster rate than mean daily maximum temperatures. This dissertation shows that under a high emissions scenario, by 2060 – 2080 models project that the most extreme temperatures could warm by 1 – 2°C more than the warm season average in some regions. This amplified warming of the most extreme temperatures is most pronounced in the eastern U.S., Europe, eastern China, and parts of the Amazon rainforest, and may have substantial implications for heat risk in these regions. This dissertation explores the physical mechanisms driving the projected amplified warming of extremes in climate models and assesses the associated uncertainty. It shows that the amplification is linked to reductions in cloud cover, increased net surface shortwave radiation, and general surface drying as represented by declines in the evaporative fraction.

In addition to rising temperatures, atmospheric humidity has been observed to increase in recent decades and models project this trend to continue. As a result, joint heat-humidity metrics indicating heat stress are likely to rapidly increase in the future. This dissertation explores how extreme wet bulb temperatures may change throughout the century and assesses the risk of exceeding a fundamental human heat tolerance limit that has been proposed in prior research. It then combines climate data with spatially explicit population projections to estimate the future population exposure to unprecedented wet bulb temperatures. Several regions stand out as being

at particular risk: India, the coastal Middle East, and parts of West Africa are likely to experience extremely high wet bulb temperatures in the future, and rapidly growing populations in these regions will result in large increases in exposure to dangerous heat stress. In some areas, it is possible that wet bulb temperatures could occasionally exceed the proposed human tolerance limit by 2080 under a high emissions scenario, but limiting emissions to a moderate trajectory eliminates this risk. Nevertheless, even with emissions reductions, large portions of the world's population are projected to experience unprecedented heat and humidity in the future.

The projected changes in extreme temperatures will have a variety of impacts on infrastructure and other human systems. This dissertation explores how more frequent and severe hot conditions will impact aircraft takeoff performance by reducing air density and limiting the payload capacity of commercial aircraft. It uses performance models constructed for a variety of aircraft types and projected temperatures to assess the payload reductions that may be required in the future. These payload limits, along with sea level rise, changes in storm patterns, increased atmospheric turbulence, and other effects of climate change, stand to have significant economic and operational impacts on the aviation industry.

Finally, this dissertation discusses evidence-based adaptation strategies to reduce the impacts of extreme heat in urban areas. It reviews a body of literature showing that effective strategies exist to both lower urban temperatures on a large scale and drastically reduce heat-related mortality during heat waves. Many adaptation techniques are not costly, but have yet to be widely implemented. Given the rapid increases in climate impacts that are projected in the coming decades, it will be essential to rigorously assess the cost-effectiveness of adaptation techniques and implement the most efficient strategies in both high- and low-income areas.

**Table of Contents**

**List of Figures**

**Acknowledgements**

I have many people to thank for their help, support, and friendship throughout graduate school. First and foremost Radley Horton, for being a fantastic advisor, pointing me towards interesting and impactful research topics but also giving me the time and freedom to explore my interests. I don't think I could have had a better graduate school experience. My committee members Arlene Fiore and Richard Seager, who always provided research advice and support. And Justin Mankin, who put in the time to give constructive and detailed feedback that helped push me to make my work better, both in its overall conception and in the details.

Finally my parents, who encouraged me to pursue science in the first place and supported me through the last 22 years of school.

**For Cynthia Miller, Scott Coffel, and the late Smoky Miranda**

# Introduction

Climate change is rapidly disrupting both the natural environment and human systems and will continue to do so throughout the 21st century. Many types of extreme weather events including heat waves, droughts, and floods are becoming both more intense and more frequent, resulting in unprecedented human impacts across the world. Through early 2018, the globe has warmed by approximately 1°C, with some regions – notably the Arctic – warming significantly more. There is currently little sign of the drastic emissions reductions that would be required to restrict warming to under 2°C as agreed to in the Paris Climate Accord in December, 2015. Weather disasters cost the United States over $300 billion in 2017[1], and weather-related damages are likely to continue rising due to development in vulnerable areas and increasingly frequent extreme events. Accordingly, it is essential that we understand the impacts that climate change will have on human and natural systems and consider adaptation strategies that can reduce our climate vulnerability.

A key threat from climate change is increasingly frequent and severe heat waves, and this dissertation will explore both the physical causes and potential impacts of increased heat and humidity. It will begin with an investigation of the amplified warming of the most extreme temperatures as compared to the mean, as well as the mechanisms driving the projected spatial variation in warming rates (Chapter 1). With that physical basis, it will then discuss rapid projected increases in population exposure to dangerous heat stress (Chapter 2), and present a case study that merges climate projections with system-specific data – here from aviation – to quantify the impact of climate change on aircraft takeoff performance (Chapter 3). It will conclude with an overview of potential adaptation strategies that have been shown to reduce heat

risk in urban areas (Chapter 4). Before considering these research questions, this dissertation discusses changing patterns of extreme weather and some of the methods used in climate impacts work.

**Extreme events**

In many regions, climate change will likely be first manifest by increasingly frequent and severe extreme weather events. There is robust evidence that many forms of extreme weather will increase in intensity and frequency as the planet warms[2], and attribution studies already show clear and strong links between anthropogenic warming and recent heat waves[3], heavy precipitation events[4], and droughts[5]. This section will review recent trends and future projections in a variety of forms of extreme weather.

Recent extreme events have been linked to climate change both statistically and through physical mechanisms. Statistical attribution has advanced greatly in recent years, facilitated by increased computing power and more efficient computational methods of comparing the historical likelihood of an event to its likelihood today. Such methods generally use model simulations of a pre-industrial climate to examine the statistics of an extreme event absent anthropogenic greenhouse forcing, and then compare these statistics to those found using a model with present-day forcing[5]. This method allows for an assessment of whether statistically significant changes in event frequency or intensity have occurred.

While the ability to statistically attribute individual events to climate change is recent, our understanding of the physical mechanisms driving changes in climate extremes is long-standing and robust. Such mechanisms can be classified as primarily thermodynamic – changes in the radiation budget, surface moisture, atmospheric humidity, and turbulent fluxes – or dynamic changes in the large-scale atmospheric circulation. Thus far, evidence suggests that

thermodynamic factors are the primary drivers of changes in extreme event frequency and intensity, although circulation changes may become increasingly important drivers as the climate continues to warm[6–8].

Heat waves are intensifying due to rising background temperatures driven by increased net surface radiation resulting from greenhouse gas forcing, which allows for larger sensible heat fluxes during atmospheric circulation regimes that produce clear skies and heightened local radiative input. Under such conditions, the surface dries through evapotranspiration and incoming energy is partitioned preferentially towards sensible heat flux, further raising temperatures in a positive feedback[9]. In addition, large-scale drying (as evidenced by declining precipitation minus evapotranspiration)[10] and reductions in the cloud cover fraction[11] are occurring in parts of the world – especially in southern and central Europe – which are both further increasing radiative input at the surface and decreasing latent heat fluxes, allowing for enhanced warming. There is some evidence for changes in Northern Hemisphere atmospheric circulation such that regimes conducive to heat waves are becoming more likely[6], but so far this dynamic process is likely secondary to thermodynamic changes in modifying the statistics of extreme heat events.

Cold extremes have become much less frequent across the world due to overall warming, and this trend is likely to continue[12]. However, it has been argued that wintertime changes in the northern hemisphere atmospheric circulation are favoring anomalous cold air excursions from the Arctic into the mid-latitudes[13]; these air masses are still warming, however, decreasing the overall occurrence of abnormally cold extremes. Regions which are projected to have declining winter snow cover are also projected to experience more rapid warming of wintertime

temperatures than the globe as a whole[14], likely due to the snow-albedo feedback enhancing warming as snow cover becomes less extensive[15] and surface albedo declines.

Warmer air holds more moisture according to the Clausius-Clapeyron relation, and observed increases in specific humidity have been attributed to warming[16]. Due to this higher background humidity, dynamical processes that result in precipitation – moisture convergence and convection – can generally produce larger precipitation totals[17,18]. Hurricane Harvey in 2017 is an example; while there is little evidence that the storm's path or intensity were affected by warming, its rainfall was likely substantially higher than it would have been in the pre-industrial climate[4]. While there are large uncertainties surrounding projected changes in seasonal and annual mean precipitation in some regions, there is generally agreement that precipitation variability[19] is likely to rise in many parts of the world, leading to some regions having a larger fraction of annual precipitation fall during extremes[20] which can lead to large increases in the frequency and intensity of wet seasons (as shown in Figure 0.1 in the Nile river basin).

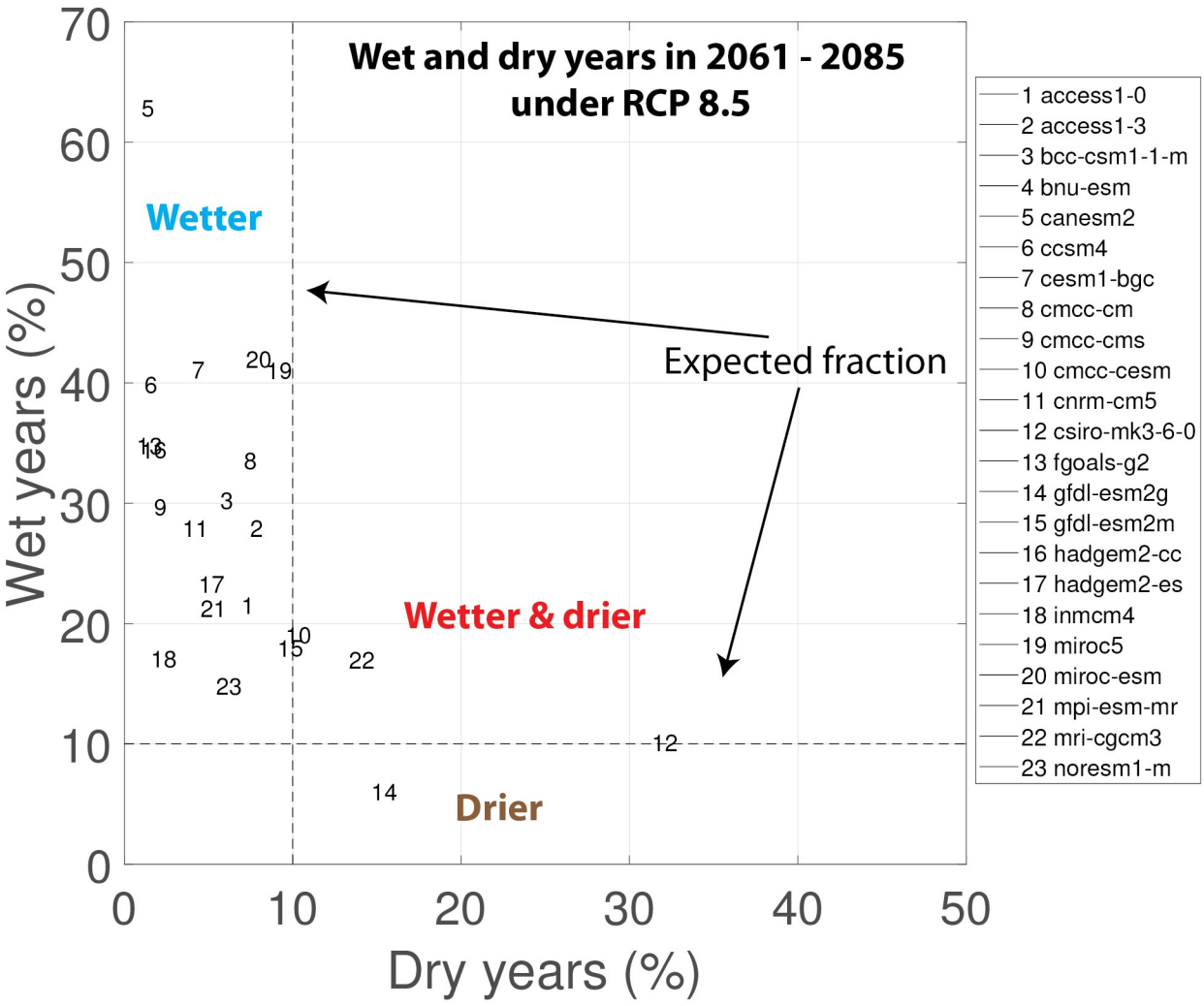


**Figure 0.1:** Projected fraction of future (2061 – 2085) years that are wet (> 90$^{th}$ percentile historical precipitation) or dry (< 10$^{th}$ percentile historical precipitation) in the Nile Basin under RCP 8.5 as compared to 1981 – 2005. Most CMIP5 models project an increase in the frequency of wet years and a decline in dry years, but due to temperature increases these models also project an increase in the frequency of concurrently hot and dry years. From Coffel, Keith, Lesk, Bower, Lee, Horton, (2018), in preparation.

Droughts are likely to increase in frequency and intensity in some regions[10]. Rising temperatures alone (that is absent changes in cloud cover, humidity and wind) increase potential evapotranspiration and can deplete soil moisture; this can lead to drought even without exceptional precipitation deficits[21,22]. Higher temperatures also result in more evaporative losses from reservoirs and rivers, and the projected widespread decline in snow cover will sharply limit

the ability of snow pack to store water[23]. Some parts of the world are likely to be at increased risk of long-term drought due to both local land-atmosphere coupling and large-scale circulation changes[24,25].

There is strong theoretical evidence that the strongest tropical cyclones may become more intense – even as the total number of tropical cyclones remains relatively steady – as air and sea surface temperatures rise[26]. Less evidence exists for possible changes in the frequency or intensity of mid-latitude storms[27,28], but such storms (and tropical cyclones as well) will likely produce more precipitation due to increased atmospheric moisture content, and all coastal storms will carry increased risks of flooding due to sea level rise[29]. There is robust evidence for changes in the mid-latitude storm track[28,30–32] which may impact regional precipitation patterns.

Taken together, climate change is either directly or indirectly intensifying most forms of extreme weather, except for cold. While there are still many outstanding research questions concerning how and why extremes will change in the future, there is very high confidence that the impacts of heat waves, floods, and droughts will increase in the coming decades. As the climate will continue to change in the coming decades regardless of emissions reductions, it is essential that we consider how to assess the relationships and the uncertainties between projected physical changes and potential disruption to ecosystems and human society.

**Climate impacts**

Research attention has increasingly turned to the effects of climate change on both human and natural systems, due to both an increased appreciation of the severity and breadth of the likely impacts and an improved ability to study region-specific changes. Climate impacts result both from direct physical damage caused by extreme events as well as from disruption due to

changes in mean temperatures or the seasonality and magnitude of precipitation. In addition, downstream effects of changing weather patterns and extremes on human societies may include increased conflict[33] and migration[34,35], the accelerated spread of vector-borne illness[36], and reduced economic performance[37], among many others. Investigating such impacts requires multi-disciplinary research merging climate science, economics, and other fields, and is only beginning to be explored.

Sea level rise is among the largest threats that climate change poses to society. Substantial uncertainties remain in the projected rate of sea level rise due to difficulty observing and modeling ice dynamics and melt processes in Antarctica and Greenland. However, sea levels have risen by nearly 1/3 meter in some parts of the world[38], and the trend in 21st century sea level rise projections has been upward in recent years as research has increasingly focused on instabilities that may lead to rapid ice loss from the world's largest ice sheets. The IPCC AR5 report suggests a worst case scenario of approximately 1 meter of sea level rise by 2100[39]; recent studies have suggested that higher amounts are possible[40,41], although models still struggle to reproduce known ice-sheet processes, leading to high uncertainty in the timing and magnitude of sea level projections[42,43]. In the near future sea level rise is likely to be experienced as a rapidly increasing coastal flood risk; even modest coastal storms may produce severe flooding in many regions due to the higher baseline water levels[29]. By the second half of the 21st century, coastal retreat may be necessary in some areas[44].

Human heat exposure is likely to be a severe and widespread threat from warming. Heat waves have killed tens of thousands of people in recent years, damaged crops[45], disrupted infrastructure[46], and reduced economic performance[37,47]. While crops and infrastructure are primarily affected by temperature, human health impacts depend on both temperature and

humidity. Research has proposed that when the wet bulb temperature exceeds the human skin temperature, about 35°C, the body will be unable to shed heat without artificial cooling, representing a theoretical limit to human tolerance to heat[48]. This threshold is almost never reached in the current climate, but Chapter 2 of this dissertation will show – and other research has confirmed[49,50] – that wet bulb temperatures approaching or exceeding 35°C are possible by the end of the 21st century. Health impacts from widespread exposure to such extreme heat stress are largely unknown, but recent heat waves with far lower wet bulb temperatures have caused substantial mortality, suggesting that heat-related illness and death could dramatically increase in the future[51]. Such heat is especially likely to occur in densely populated, rapidly growing, and currently low-income parts of northern India and West Africa, compounding the risk. However, as Chapter 4 will discuss, evidence-based adaptation strategies exist that can reduce the impacts of heat, especially in cities, which are particularly susceptible to heat waves due to the urban heat island effect. Aggressive adaptation efforts applied across the world have the potential to significantly reduce heat-related mortality, but thus far such measures have mostly been taken in a small number of mostly high-income regions.

Increasingly frequent climate extremes – especially heat and drought – coupled with changing seasonal climate patterns may have serious implications for agricultural production and global food supply stability. A substantial portion of historical crop yield variability has been attributed to climate[52], and high temperatures and moisture shortages are known to severely reduce the yields of major crops[53,54]. Rain-fed crops are particularly at risk; high temperatures increase evaporative demand, leading to moisture shortages which then allow leaf temperatures to rise. The existence of large-scale climate teleconnections introduces systemic risk into the food system – climate-induced crop failure in one region can increase food prices around the

world. Recent research has shown that ENSO teleconnections can result in unfavorable weather conditions affecting multiple agricultural breadbaskets during the same year[55]. Climate change is also likely to exacerbate multiple breadbasket risk, increasing the frequency of simultaneous hot and dry seasons around the world due to warming alone, regardless of changes in precipitation. Estimates of maize yield declines by mid-century range from 20 – 40% after accounting for potential changes in the spatial distribution of cropping[56], and declines are larger if cropping areas are assumed constant. Other major crops may experience similarly severe yield declines in the future. The effects of $CO_2$ fertilization on crops – whereby higher atmospheric $CO_2$ concentrations improve plant growth – present a significant source of uncertainty in estimating future agricultural productivity. Assessing the effects of fertilization requires process-based crop models; such models vary widely in sophistication but generally demonstrate that for some crops, fertilization may reduce the harmful effects of modest levels of warming, but cannot compensate for the larger temperature increases possible by the second half of the 21$^{st}$ century[57]. As a result, it is possible that some regions in the mid-latitudes may experience improved crop performance in the coming decades, but then have yields begin to decline as the harmful effects of warming exceeds the benefits of increased $CO_2$ concentrations.

Recent research has also shown that migration, conflict, and nation-level economic performance respond to fluctuations in temperature. Asylum applications rise during warm years[35], potentially due to the effects of heat, drought, and agricultural failure on local food and water security[34]. Conflict at a variety of scales, from inter-personal to war, is more likely at higher temperatures[58], and recent humanitarian crises – notably the war in Syria[33] – occurred in the context of severe drought and environmental stress. Labor productivity declines as temperatures rise, even for indoor workers[59]; in some locations, especially in the tropics, outdoor

work may be sharply curtailed during the hottest parts of the year due to heat stress[60] and its related health consequences[61] in the future. These societal impacts, coupled with the damaging effects of warming and extreme weather on infrastructure, public health, and ecosystems[62], are likely to combine to reduce future global economic output by a significantly larger sum than would be required to reduce greenhouse gas emissions and mitigate the effects of climate change[63]. It is also possible that climate change may prove difficult to reverse even with potential future reductions in greenhouse gas concentrations[64].

**Downscaling, bias correction, and uncertainty**

Using global coupled earth system models to assess regional climate impacts often requires techniques to relate relatively course model output to localized regions. Many climate models are run at resolutions of 1 – 2° latitude/longitude, limiting their ability to directly resolve small scale but essential climate processes including convection, cloud formation, and turbulent fluxes, in addition to orographic and coastal effects. Impacts research often employs a variety of downscaling methods to increase model resolution; such techniques are classified as statistical or dynamical[65]. Statistical downscaling uses observed relationships between large-scale climate variables such as geopotential height, humidity, or temperature to adjust the output of global climate models to better match historical observations at a specific location[66]. These methods can substantially reduce model bias, especially in mountainous or coastal regions. However, they must be used carefully, as they have no physical constraints and can therefore produce climate outcomes which are not spatially or temporally consistent[67]. Dynamical downscaling, by contrast, uses a high-resolution regional climate model (RCM) run over a limited geographical area to produce finer climate outputs than possible with a global model. RCMs are usually forced

at their boundaries by the output from a global model, allowing global scale dynamics to occur and influence the regional climate, thereby producing both high resolution and physically constrained results, but at the cost of computational intensity. RCMs have been shown to improve climate projection quality as compared with global models in some situations, but can also introduce unrealistic physical behavior due to the nesting of two different model grid resolutions[68].

In addition to downscaling, climate impact studies often employ a form of bias correction. Climate models generally contain biases in simulated temperature, precipitation, and other variables when compared with historical observations. Model bias arises for a variety of reasons, primarily the need to parameterize un-resolved climate processes. Biases are highly variable in space and time, affecting both the simulated mean climate and the climate variability. In addition, bias can vary in different parts of a variable's distribution – temperature bias, for instance, is often greatest at the highest and lowest values (Figure 0.2).

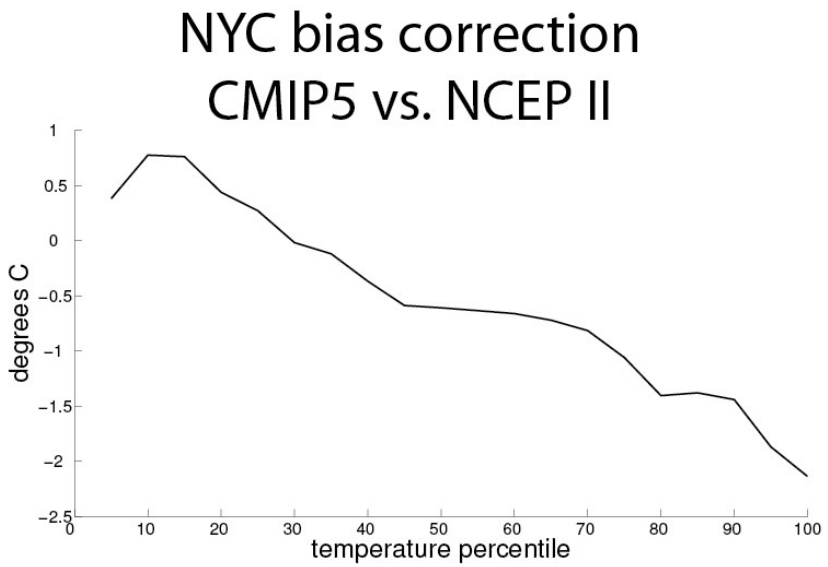


**Figure 0.2:** Multi-model mean bias in New York City daily maximum temperature across 27 CMIP5 models as compared to NCEP II Reanalysis in 1985 – 2005. Bias varies significantly across the temperature distribution, with the most extreme temperatures (> 90$^{th}$ percentile or <

10th percentile) having the largest biases. Similar biases are found using station data. From Coffel, Horton, 2015[69].

Bias correction techniques are often used alongside downscaling methods to create localized projections of absolute temperature or precipitation. These techniques range from simple adjustment of the distribution mean (the delta method) to more sophisticated methods that attempt to reshape the modeled variable distribution such that it matches observations[70]. As with statistical downscaling, such techniques can produce non-physical results and so must be used with care.

**Uncertainty analysis**

Due to the substantial and in some cases irreducible uncertainties inherent in climate projections, careful treatment of inter-model, inter-emissions scenario, and internal variability is essential to ensure that a robust range of plausible climate outcomes is presented. Much impacts research focuses on multi-model or ensemble mean results, without assessing the variability across models and ensemble members. Such a focus on the mean can mask drastic uncertainty in the magnitude and even direction of projected changes in climate variables.

It is sometimes useful to isolate the component of uncertainty which is intrinsic to the climate system and thus irreducible – as opposed to variation resulting from differences in model construction and parameterization schemes, which may decline as models continue to improve, or differences in emissions scenarios which depend on human choices. This irreducible uncertainty results primarily from internal variability, or chaotic behavior within the climate system, and can in some cases represents 10 – 50% of total uncertainty (Figure 0.3). Internal variability can be explored using multiple ensemble members of the same model – such as are

available through the NCAR Large Ensemble Community Project (LENS)[71] – allowing climate variation resulting solely from perturbed initial conditions to be assessed.

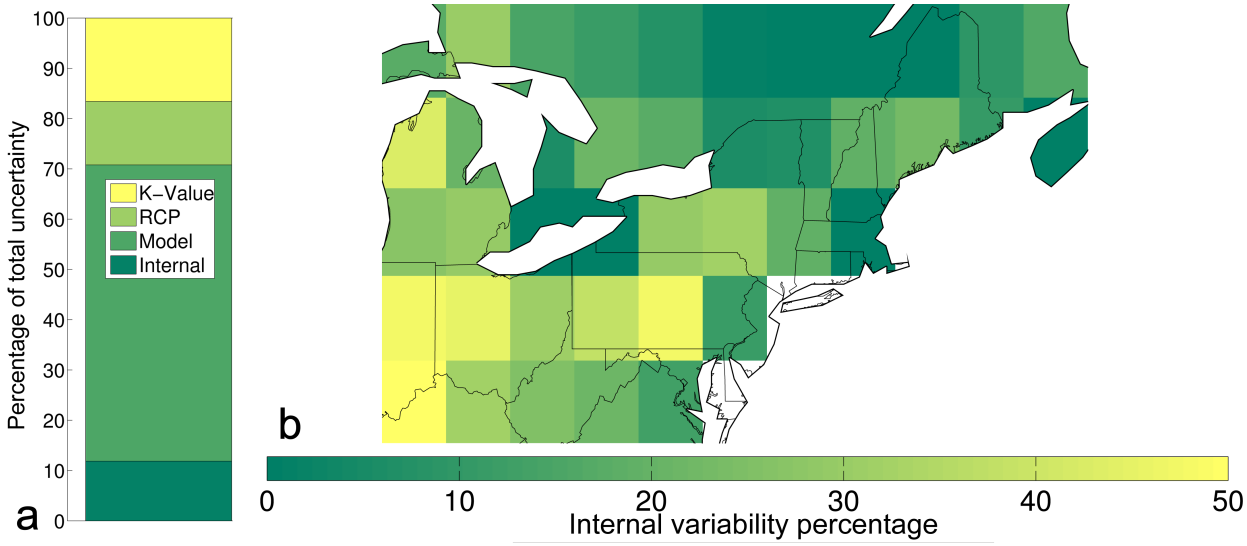


**Figure 0.3:** Fraction of total uncertainty resulting from internal variability in projections of the year after which air temperatures below -10°C will never again occur. Internal variability makes up approximately 10% of total variability region-wide, but up to 50% in some model grid cells. Generally, inter-model variability is the largest contributor to uncertainty. The K-Value is an estimated parameter related to the heat transfer rate through tree bark; variation in the parameter accounts for about 15% of total uncertainty, as shown in the bar plot. The other colors on the bar plot show variation due to emissions scenario (RCP), model variability (Model), and internal variability (Internal). From Lesk, Coffel, et al, 2017[62].

Climate impacts research is increasingly considering uncertainty and in particular the worst-case outcomes that may result from any combination of emissions, climate sensitivity, or impacted system sensitivity being higher than expected. Presentation of the full range of possible climate outcomes is essential to facilitate realistic adaptation planning[62], and understanding the sources of uncertainty helps assess the degree to which it may be reduced through technical and scientific advances.

**Dissertation overview**

This dissertation will focus primarily on how the causes and impacts of extreme heat may change in the future. Chapter 1 will describe the mechanisms that are leading to amplified warming of the most extreme temperatures as compared to the warm season average, investigate the physical processes driving this accelerated warming of extremes, and demonstrate its impacts on heat wave risk. Chapter 2 will investigate the joint risk of heat and humidity – referred to in this dissertation as heat stress – in the context of projected population growth, and assess the risk of some regions experiencing heat stress conditions beyond human tolerance. Chapter 3 will consider a specific impact of rising temperatures: the decline in aircraft takeoff performance due to lower air density in hot conditions, and the associated implications for airline operations. Finally, Chapter 4 will review adaptation strategies to reduce the impacts of extreme heat in urban areas, and a concluding section will focus on promising future research directions to improve our understanding of the impacts of climate change.

# Chapter 1 The amplified warming of extreme temperatures[14,72]

**Coffel, E. D.**, Mankin, J. S., Winter, J. M., & Horton, R. M. The amplified warming of extreme temperatures. *In preparation.*

Horton, R. M., **Coffel, E. D.**, Winter, J. M., & Bader, D. A. (2015). Projected changes in extreme temperature events based on the NARCCAP model suite. *Geophysical Research Letters*, *42*(18), 7722–7731. https://doi.org/10.1002/2015GL064914

## Introduction

The rate of climate change varies regionally and seasonally. The continents are warming faster than the oceans, due to the high heat capacity of water. Arctic amplification is warming the northern polar region at approximately twice the rate of the planet as a whole[73], due in part to the ice-albedo and snow-albedo feedbacks, stable stratification, increases in water vapor and clouds, and regional atmospheric circulation changes. Some regions, like the U.S. Southeast, have seen slowed warming in the past several decades due to aerosol emissions[74], dynamical processes, and natural variability[75]. Many parts of the world are projected to experience faster warming during the warm season than during other parts of the year, likely due to surface drying and land-atmosphere feedbacks[76]. In addition, in some areas the hottest days are projected to warm more than the warm season average. Other regions may experience enhanced warming of the coldest wintertime temperatures[77], due in part to the snow-albedo feedback associated with reduced snow cover.

Seasonal variations in warming rates are critical to potential future climate impacts. Projected rapid rises in wintertime minimum temperatures pose risks to ecosystems by, for example, potentially allowing pests to survive and spread[62,78,79], while amplified summertime warming raises the risk of extreme heat and associated impacts, including human mortality[51,80]

and other health concerns[61], agricultural losses to both livestock and crops[53,81], increased energy consumption and infrastructure damage[82,83], and reduced economic performance[37,59].

Prior research has suggested that the hottest temperatures will rise faster than daily-mean temperatures in some parts of the world in both global[77,84,85] and regional (Figure 1.1) climate models, even after accounting for potentially faster warming of the warm season as compared with the annual mean. In this chapter, this phenomena is quantified as the difference between projected warming of the annual maximum temperature (TXx) and the warm season mean daily maximum temperature (Tx) and is referred to as TXx amplification. Previous research has noted the asymmetric nature of changes to the temperature distribution in some areas, and increased temperature variability has been proposed to explain it[84,86,87], but so far this increased variability has not been observed[88]. This chapter will show that most of the warming amplification is linked to seasonal and sub-seasonal variation in warming rates that gives rise to changes in the shape of the temperature distribution in many locations, especially in the mid-latitudes.

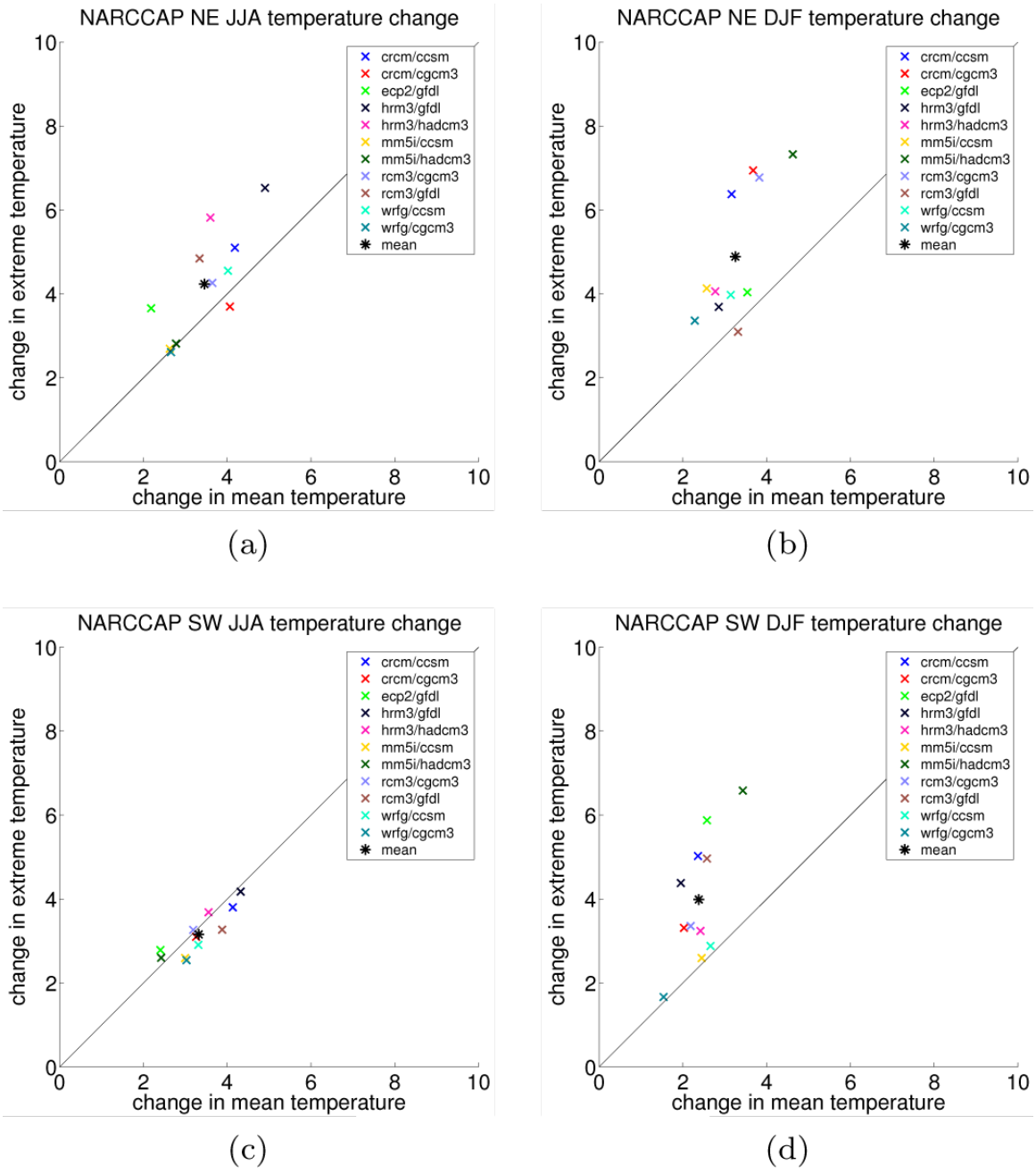


**Figure 1.1:** Projected change in mean daily maximum temperature (Tx) vs. change in annual maximum temperature (TXx) across the NARCCAP[89] regional climate models in the U.S. Northeast (a-b) and Southwest (c-d) in summer (JJA) and winter (DJF). In the Northeast, most models show extremes increasing more than the mean in both seasons, while in the Southwest this is true only in winter. From Horton, Coffel, et. al., 2015[14].

This chapter will first discuss the spatial distribution of the projected TXx amplification, and then identify the physical mechanisms that help to explain it in central Europe, the eastern United States, eastern China, and the Amazon rainforest. Prior work[14] using regional models has shown that TXx amplification in the U.S. does not occur alongside more intense synoptic conditions favorable to heat waves, as represented by positive 500 hPa geopotential height anomalies (Figure 1.2); anomalies during future heat waves are projected to have little change, even though future heat wave temperatures are projected to rise more than mean temperatures.

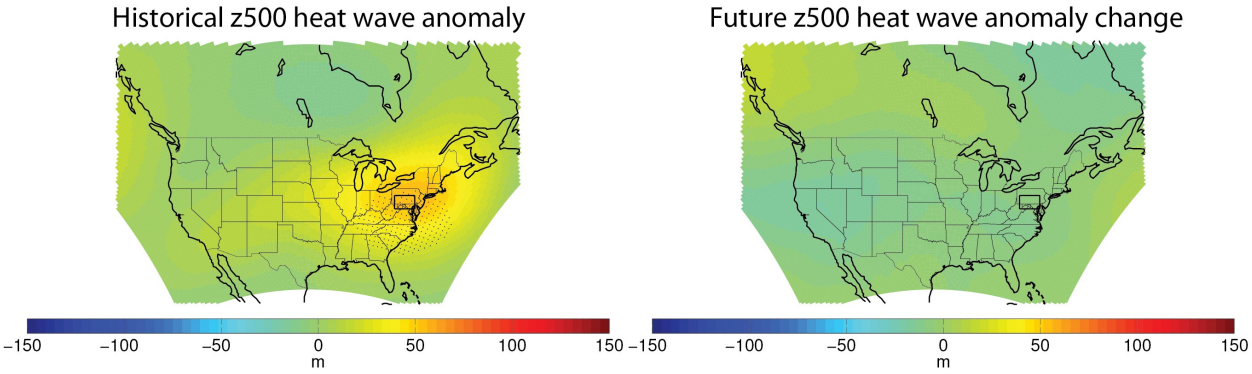


**Figure 1.2:** (left) 500 hPa geopotential height anomaly composited over each single hottest day per year in the Northeast U.S. (region shown in black box) between 1981 – 1998. (right) Change in the 500 hPa anomaly composited over the hottest days per year in the same region in 2051 – 2068 vs 1981 – 1998. Results using the NARCCAP[89] model suite. From Horton, Coffel, et. al., 2015[14].

This chapter will instead show that reductions in cloud cover coupled with surface drying result in increased net surface shortwave radiation and a preferential partitioning of increased energy input (due to greenhouse forcing) into sensible, as opposed to latent, heat flux in these regions. These changes increase the likelihood and the strength of a positive feedback between the land and the atmosphere in which temperature rise leads to increased evaporation, drying the surface and raising temperatures further[9]. As a result of this process, the warm season is projected to warm more than other parts of the year, and the highest daily temperatures are

projected to warm more than the warm season. This chapter will also demonstrate that this enhanced warm season warming substantially increases the recurrence frequency of historically extreme temperatures in some regions beyond what would be expected due to global mean warming alone. Finally, it will emphasize the importance of understanding the physical mechanisms driving projected temperature changes, as the strong dependence of warming on cloud and land-atmosphere interaction processes suggests substantial uncertainty in the magnitude of temperature projections and resulting heat risk.

**Data and methods**

This chapter uses 25 coupled climate models from the Coupled Model Intercomparison Project Phase 5 (CMIP5)[90] suite to project daily maximum temperatures (using the *tasmax* variable), along with monthly mean total column soil moisture (variable: *mrso*), sensible and latent heat fluxes (variables: *hfss*, *hfls*), surface radiation (variables: *rsds*, *rsus*, *rlds*, *rlus*), and cloud fraction (variable: *clt*) (Table 1). All models are forced with Representative Concentration Pathway 8.5 (RCP 8.5), a high-emissions scenario[91]. The chapter presents the forced response as the "projected change," which is defined as the difference between the future (2061 – 2079) and historical (1985 – 2004) period climatologies. These data are compared with the NCEP II[92] and ERA-Interim reanalysis products, also covering 1985 - 2004. All data are placed on a common 2° x 2° grid using linear interpolation to facilitate spatial comparison. Analyses are focused on the four regions that are most robustly projected to experience TXx amplification: the eastern United States, central Europe, the Amazon rainforest, and eastern China (Figure 1.3).


**Figure 1.3:** Selected regions.

The projected change (future minus historical) due to anthropogenic forcing is calculated for each variable, model, and grid cell. TXx amplification is calculated as the difference between the change in the annual maximum temperature and the mean daily maximum temperature during the local warm season. The Bowen ratio is calculated as $\frac{SH}{LH}$, and the evaporative fraction is calculated as $\frac{LH}{(LH+S\ )}$, where $SH$ and $LH$ are the sensible heat flux and latent heat flux, respectively. Bowen ratios greater than 100 are discarded (large values can be caused either by anomalous model heat fluxes or by the ratio growing large due to a small value of the denominator, latent heat flux). All projected changes are spatially averaged over each of the four selected regions. Multi-model robustness is assessed by showing the median change at each grid cell across all 25 models, and models are considered to be in agreement when more than 75% project the same direction of change.

Linear correlations between seasonally-averaged temperature and Bowen ratio are calculated for each model (and reanalysis) and each grid cell over the 1985 to 2004 historical

period. Regional mean correlations are then calculated by averaging over all grid cells in the region bounds.

Linear fits between variables are computed over all values within 2 standard deviations of the variable's mean; values outside of this range are considered outliers. Adjusted $R^2$ values are displayed to indicate fit robustness.

Monthly mean total column soil moisture change is calculated for each model separately by computing the change for each land grid cell in a region and averaging over the region's grid cells. The multi-model median change is then computed across all models. Snow mass change is computed similarly, but only grid cells with historical non-zero mean DJF snow cover in the ERA-Interim Land dataset are used to eliminate small snow totals which erroneously appear over large areas in certain models.

**Results and discussion**

Enhanced warming of extreme temperatures has two primary causes: the warm season warming more than the rest of the year, and the annual maximum temperature warming more than mean daily maximum temperatures during the warm season. Figure 1.4b demonstrates these two drivers of asymmetric temperature change in central Europe. Tx in the warm season (JJA) is projected to increase by 1 – 2°C more than the other seasons of the year, and TXx is projected to rise approximately 0.5 – 1°C more than warm season Tx. In all regions, warm season Tx is projected to rise by 2 – 8°C, making the amplification a substantial addition to the projected seasonal warming.

In most regions of the world, warming of the warm season Tx is projected to account for nearly all TXx change as shown in Figure 1.4a. In the eastern U.S., central Europe, eastern

China, and parts of the Amazon rainforest, however, models project that TXx will increase more than warm season Tx; in these four regions, warm season Tx change accounts for only 75 – 85% of total TXx change.

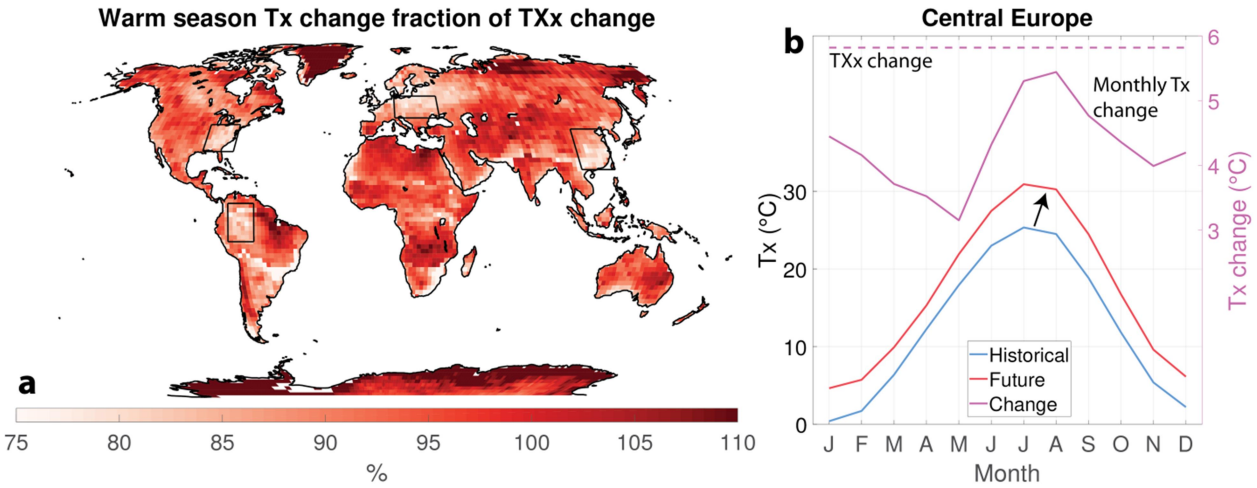


**Figure 1.4:** (a) Multi-model median fraction of annual maximum temperature (TXx) warming accounted for by warm season mean daily maximum temperature (Tx) change in 2060 – 2079 vs. 1985 – 2004 under RCP 8.5 across 25 CMIP5 models. (b) Demonstration of the effects of seasonal warming variability on the future temperature distribution in central Europe. The warm season warms more than the rest of the year, and TXx warms even more than the warm season, leading to amplified warming of the highest temperatures. From Coffel, Mankin, Winter, Horton, (2018), in preparation.

Moisture availability plays an important role in controlling temperatures during the warm season in these regions. Figure 1.5 shows the correlation between Bowen ratio and seasonal mean daily maximum temperature across the year in the CMIP5 models and NCEP II and ERA-Interim reanalysis products. Correlations are stronger during the warm season than during other parts of the year, especially in the eastern U.S. and central Europe. These higher correlations are due to generally higher warm season Bowen ratios than in other seasons, indicating a relatively more moisture-limited near-surface environment and thus more temperature response to changes in moisture availability.

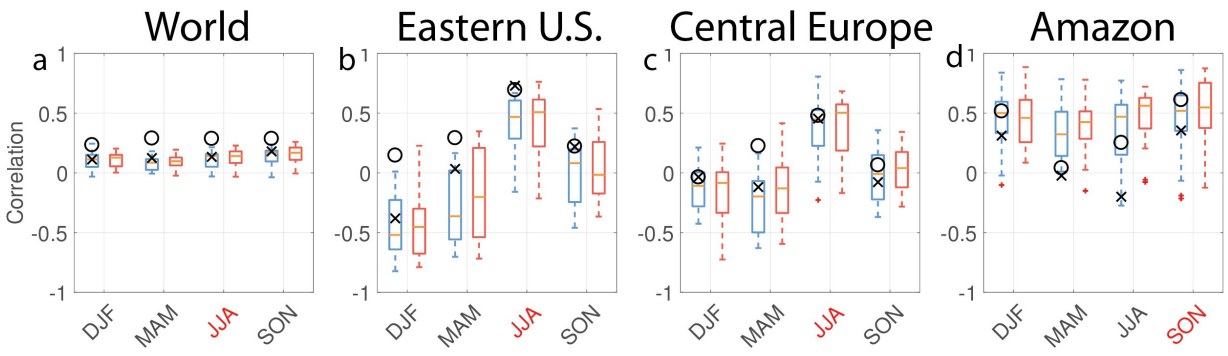


**Figure 1.5:** Historical (1985 – 2004; blue) and future (2060 – 2079; red) correlation between warm season Tx and Bowen ratio across 25 CMIP5 models. ERA-Interim (shown with an X) and NCEP II (shown with a circle) reanalysis products are plotted alongside the historical model distribution. In the eastern U.S., central Europe, and the Amazon, correlations during the warm season are higher than during other parts of the year, indicating a more moisture limited environment. Red lettering on the x-axis indicates the local warm season. From Coffel, Mankin, Winter, Horton, (2018), in preparation.

In addition to the stronger correlation between Bowen ratio and temperature during the warm season, these regions also have stronger land-atmosphere coupling as indicated by the correlation between soil moisture and Bowen ratio (Figure 1.6). This stronger coupling indicates that dry conditions will have more of an effect on the partitioning of energy into sensible and latent heat flux during the warm season than during the rest of the year; coupled with the higher correlation between Bowen ratio and temperature during the warm season (shown in Figure 1.5), warm season temperatures are seen to be generally more sensitive to changes in surface moisture content than during the rest of the year and thus will be influenced more by the warm season drying that is projected in the future.

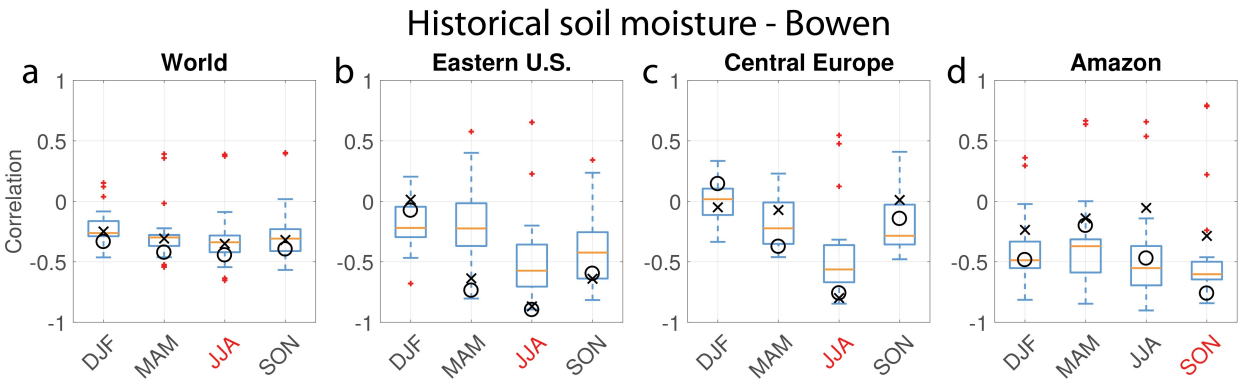


**Figure 1.6:** Historical (1985 – 2004) correlation between total column soil moisture and Bowen ratio in CMIP5 models (boxplots) and the NCEP II (open circle) and ERA-Interim (X) reanalysis products. Local warm seasons represented by red lettering on the x-axis. Red crosses indicate outlier models. From Coffel, Mankin, Winter, Horton, (2018), in preparation.

TXx amplification occurs in the context of this heightened warm season sensitivity of temperature to surface moisture. Figure 1.7a shows TXx amplification across the globe; the four selected regions are among the few large areas that are projected to have TXx warm more than the warm season. The null hypothesis, that TXx amplification is caused by random noise, is unlikely due to the statistical significance of the TXx amplification signal and the cross-model agreement on the spatial distribution and coherency of amplification; non-hatched areas in Figure 1.7a indicate that at least 75% of models agree on the direction of amplification and that the amplification is statistically significant ($P < 0.05$). The regions that see positive TXx amplification are the same that have low fractions of TXx warming explained by Tx warming in Figure 1.4a. The multi-model median amplification is approximately 1°C in all regions. Figure 1.7b-e show how TXx change varies with warm season Tx change across models in the four regions. TXx change tracks closely with warm season Tx warming ($R^2 > 0.8$ in all regions), but all regions also have a positive slope, indicating that projected TXx rises at a faster rate than warm season Tx across models; in Europe, for instance, a model that projects 1°C more Tx warming would project 1.25°C more TXx change. In all regions, almost all models fall above the

1-to-1 line, confirming that there is robust cross-model agreement on the existence and magnitude of TXx amplification. Only Greenland, Antarctica, and small parts of Siberia are projected to have significant negative TXx amplification – meaning that TXx increases less than the warm season on average.

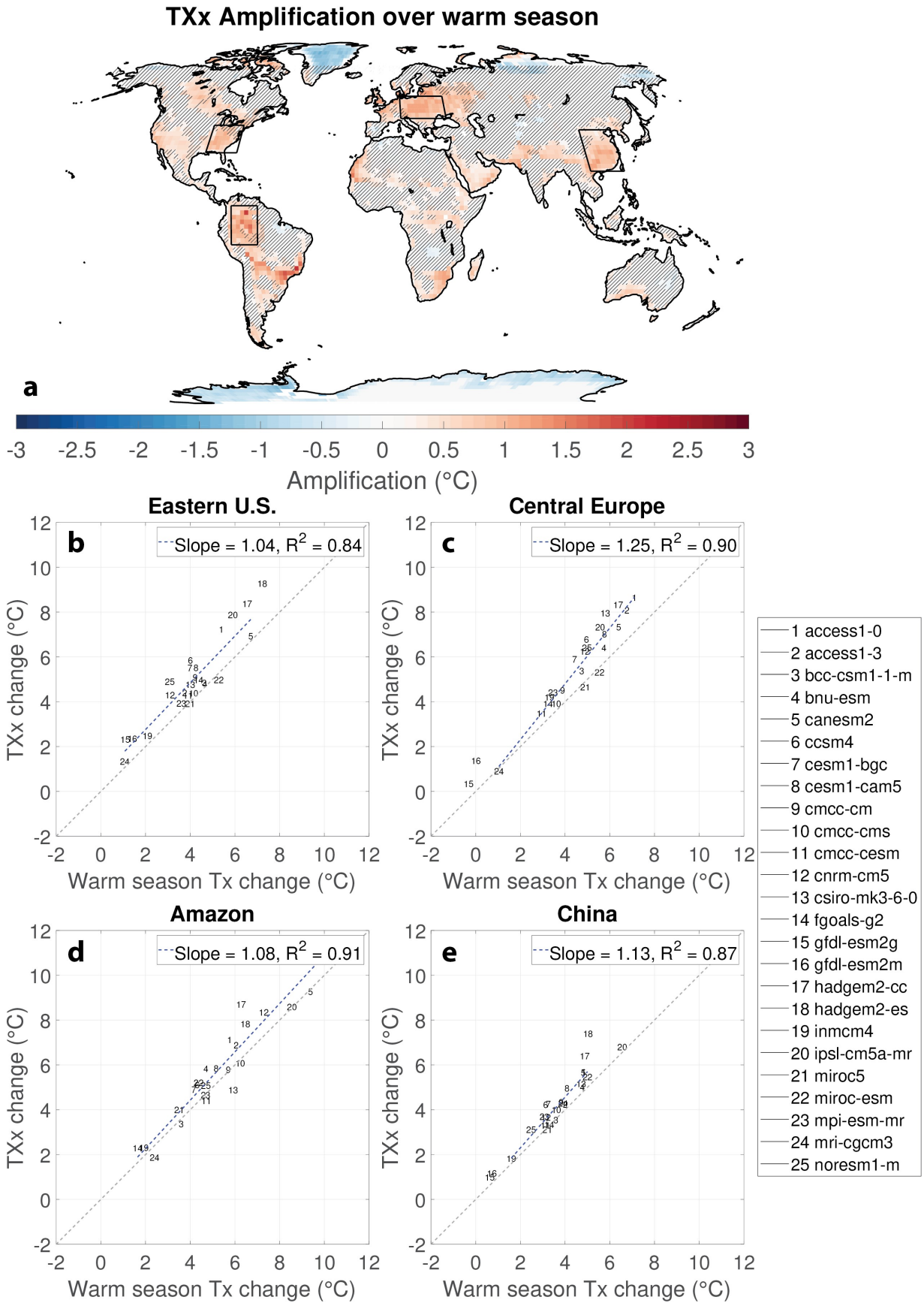
TXx Amplification over warm season
a
-3 -2.5 -2 -1.5 -1 -0.5 0 0.5 1 1.5 2 2.5 3
Amplification (°C)
Eastern U.S.
b
Slope = 1.04, R2 = 0.84
Central Europe
c
Slope = 1.25, R2 = 0.90
Amazon
d
Slope = 1.08, R2 = 0.91
China
e
Slope = 1.13, R2 = 0.87
TXx change (°C)
Warm season Tx change (°C)
1 access1-0
2 access1-3
3 bcc-csm1-1-m
4 bnu-esm
5 canesm2
6 ccsm4
7 cesm1-bgc
8 cesm1-cam5
9 cmcc-cm
10 cmcc-cms
11 cmcc-cesm
12 cnrm-cm5
13 csiro-mk3-6-0
14 fgoals-g2
15 gfdl-esm2g
16 gfdl-esm2m
17 hadgem2-cc
18 hadgem2-es
19 inmcm4
20 ipsl-cm5a-mr
21 miroc5
22 miroc-esm
23 mpi-esm-mr
24 mri-cgcm3
25 noresm1-m

**Figure 1.7:** (a): Multi-model median difference between projected TXx warming and warm season Tx warming in 2061 – 2085 vs 1981 – 2005 under RCP 8.5 across 25 CMIP5 models. Hatching indicates that the difference is not significantly different from zero (K-S test, 95%) or that less than 75% of models agree on the direction of amplification. (b-e): Projected warm season Tx change vs. TXx change in four selected regions. Models generally project TXx to warm more than warm season Tx. From Coffel, Mankin, Winter, Horton, (2018), in preparation.

Figure 1.8 shows the projected warm season change in four large-scale variables related to both warm season warming and TXx amplification: cloud fraction (a), sensible heat flux (b), net surface shortwave radiation (c), and evaporative fraction (d). These variables are correlated with each other; reduced cloud fraction increases net surface shortwave radiation, and a lower evaporative fraction signals that net surface radiative energy is preferentially partitioned into sensible heat flux as opposed to latent. In the four selected regions, models robustly project general drying; Europe has the most pronounced signal, with a 5 – 10% reduction in cloud cover, substantial increases in net surface shortwave radiation, an evaporative fraction decline of approximately 0.1, and increases in sensible heat flux of 10 – 20 $W/m^2$. China and the eastern U.S. are projected to have reduced cloud cover and more net surface shortwave radiation, but little change in evaporative fraction and smaller increases in sensible heat flux of less than 5 $W/m^2$. The Amazon has a sharp east-west gradient in projected change; drying increases closer to the Atlantic coast, but the entire region is projected to have reduced cloud cover and increased net surface shortwave radiation. The general drying trends projected in the four selected regions, coupled with the heightened sensitivity of temperature to surface moisture content during the warm season, contribute to the faster Tx warming that models project during the warm season as compared to the rest of the year. However, the warm season drying does not spatially correspond to projected TXx amplification.

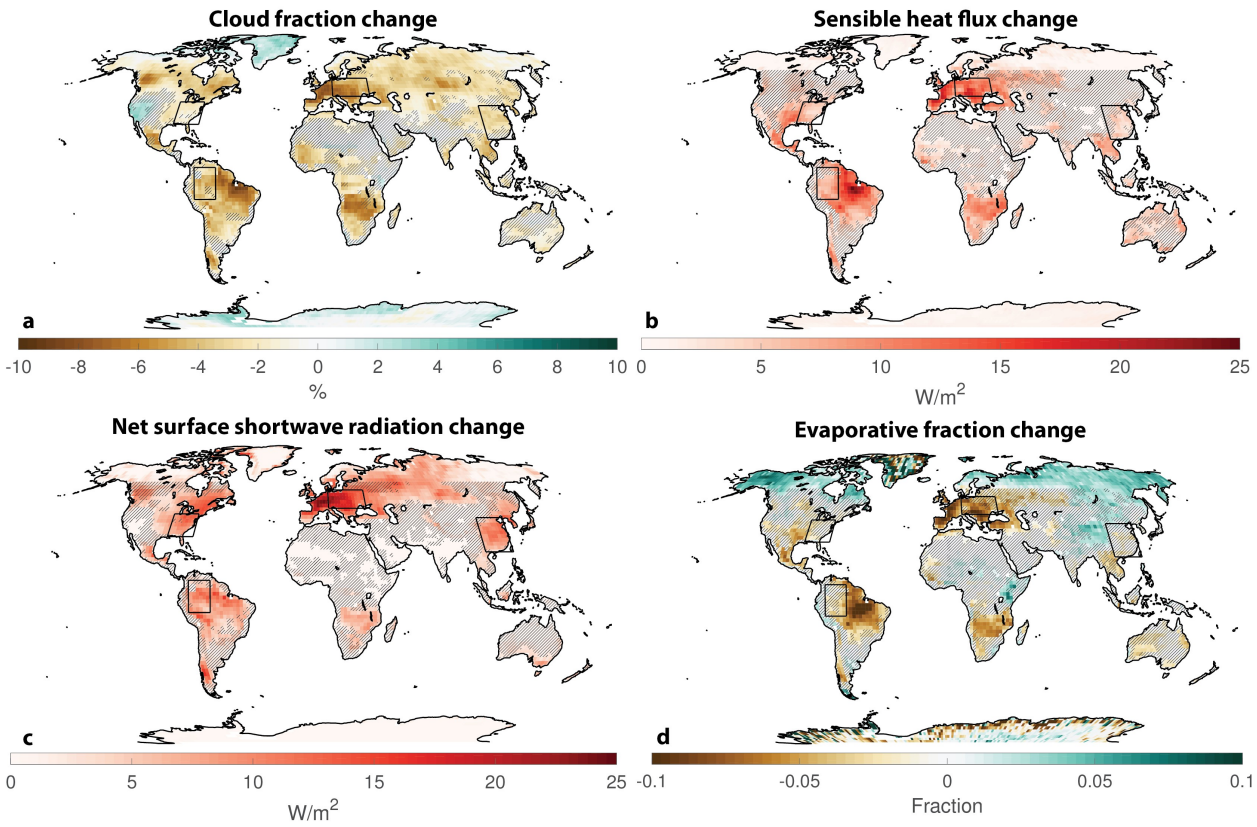


**Figure 1.8:** Multi-model median projected changes for the local warm season. Hatching shows regions with less than 75% model agreement on the direction of change. (a) Cloud fraction; (b) Sensible heat flux; (c) Net surface shortwave radiation; (d) Evaporative fraction. From Coffel, Mankin, Winter, Horton, (2018), in preparation.

At the daily scale, however, the amplification of evaporative fraction (defined as the change in evaporative fraction on the TXx day as compared to the change in the warm season mean) shows strong spatial correspondence with TXx amplification across the CMIP5 model ensemble. This spatial correspondence is examined by linearly regressing TXx amplification against evaporative fraction amplification over model grid cells. Regressions are performed for each model independently for the entire globe and for subsets of the globe in different climate zones. Climate zones are based on the mean warm season evaporative fraction and defined as follows: arid (mean warm season evaporative fraction of 0 – 0.1), semi-arid (0.1 – 0.33), temperate (0.33 – 0.75), and tropical (0.75 – 1). Figure 1.9 shows the regression slopes for each

of 22 models. Nearly all models show significant negative slopes over the full globe and for each climate zone, indicating that as evaporative fraction amplification becomes more negative (relative drying of the TXx day as compared to the warm season) in a grid cell, TXx amplification in that grid cell becomes more positive. However, the multi-model mean and median slopes differ between climate zones, with stronger relationships in arid and semi-arid regions than in temperature and tropical areas. These differences are due to the fact that at lower starting evaporative fractions, a decline represents a larger relative change, which allows for a larger increase in sensible heat flux and thus temperature. The dashed gray line in Figure 1.9 shows a cubic fit through the multi-model median slopes, demonstrating the non-linear relationship between evaporative fraction and temperature.

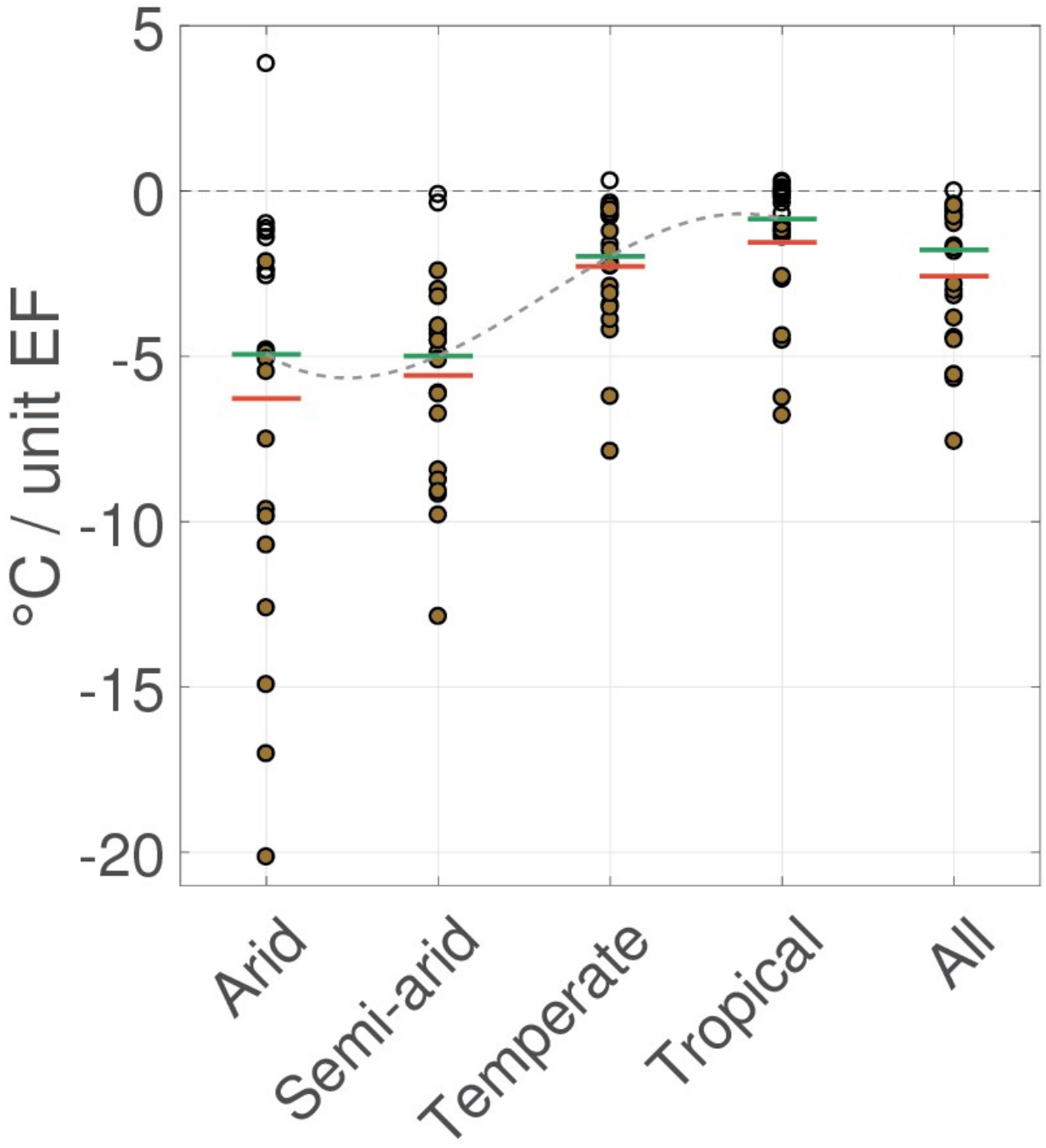


**Figure 1.9:** Linear regression slopes across grid cell evaporative fraction amplification and TXx amplification for each model over the full globe and each climate zone. Brown fill indicates a statistically significant ($P < 0.05$) regression coefficient. Green lines show the multi-model median, and red lines show the multi-model mean. The grey dashed line shows a cubic fit through the multi-model median slopes. From Coffel, Mankin, Winter, Horton, (2018), in preparation.

Evaporative fraction amplification also accounts for the magnitude of TXx amplification across the suite of CMIP5 models. Figure 1.10 shows the relationship between regionally averaged evaporative fraction amplification and regionally averaged TXx amplification across 22 models. All four selected regions show significant linear relationships ($P < 0.05$), with correlations ranging from -0.5 to -0.75. These results demonstrate that relative drying on the day of TXx controls both the occurrence and magnitude of TXx amplification within models and also modulates the magnitude of TXx amplification across the suite of models.

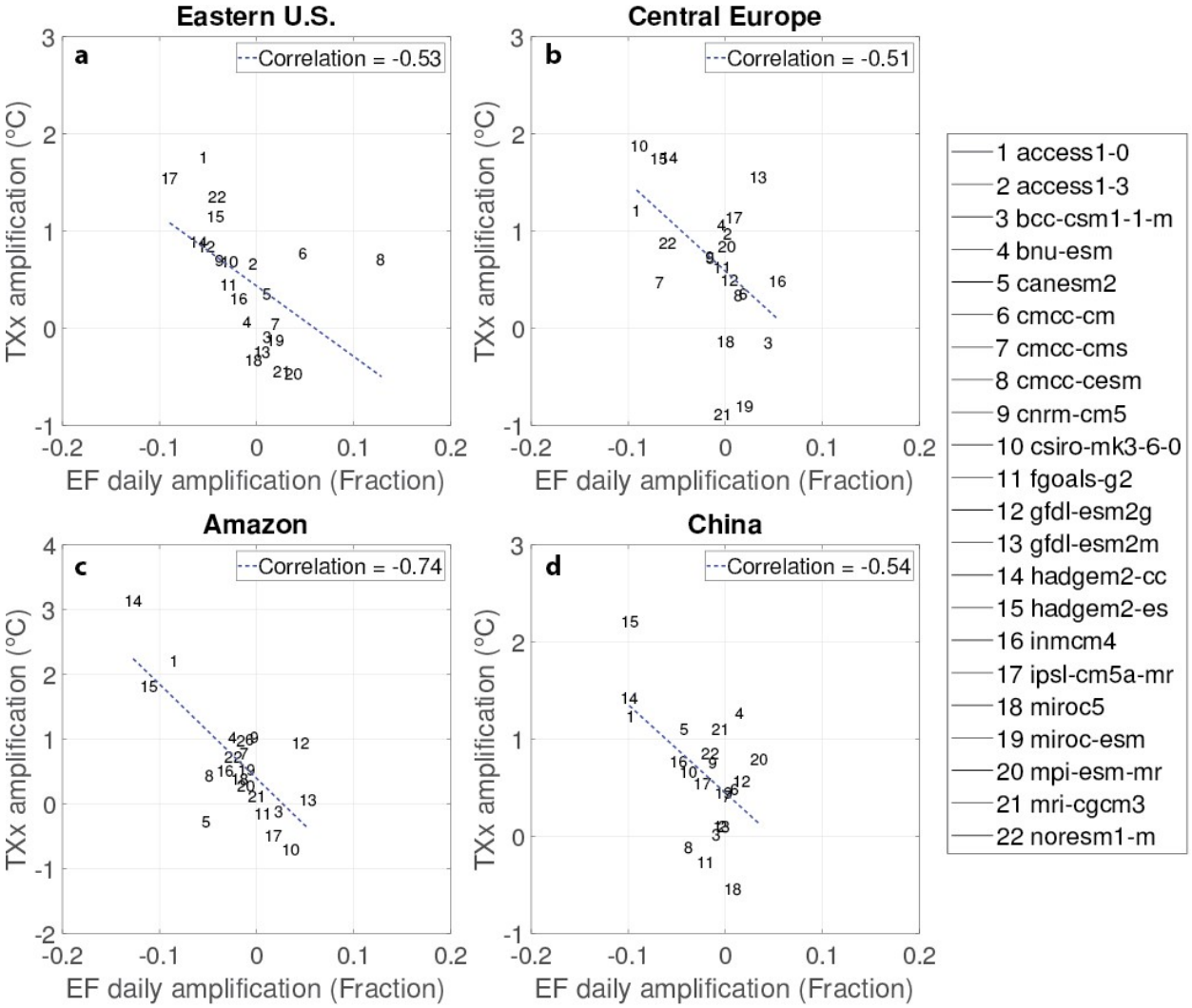

**Figure 1.10:** Relationships between regionally averaged evaporative fraction amplification and regionally averaged TXx amplification across CMIP5 models. Dashed blue lines indicate a significant linear relationship ($P < 0.05$) across models, and linear correlations are shown for each region. EF amplification substantially controls the magnitude of TXx amplification across models for all regions. From Coffel, Mankin, Winter, Horton, (2018), in preparation.

While evaporative fraction decline is associated with TXx amplification, this drying is not associated with a decline in wet bulb temperature. Figure 1.11 shows the multi-model median projected change in wet bulb temperature on the day of TXx. There is robust model agreement that the wet bulb temperature will see spatially consistent increases of 2 – 3°C across the globe. These increases occur even in regions that are drying and projected to have TXx amplification, indicating that the decline in evaporative fraction does not reduce surface specific humidity enough to offset the rise in temperature and prevent the wet bulb temperature from climbing.

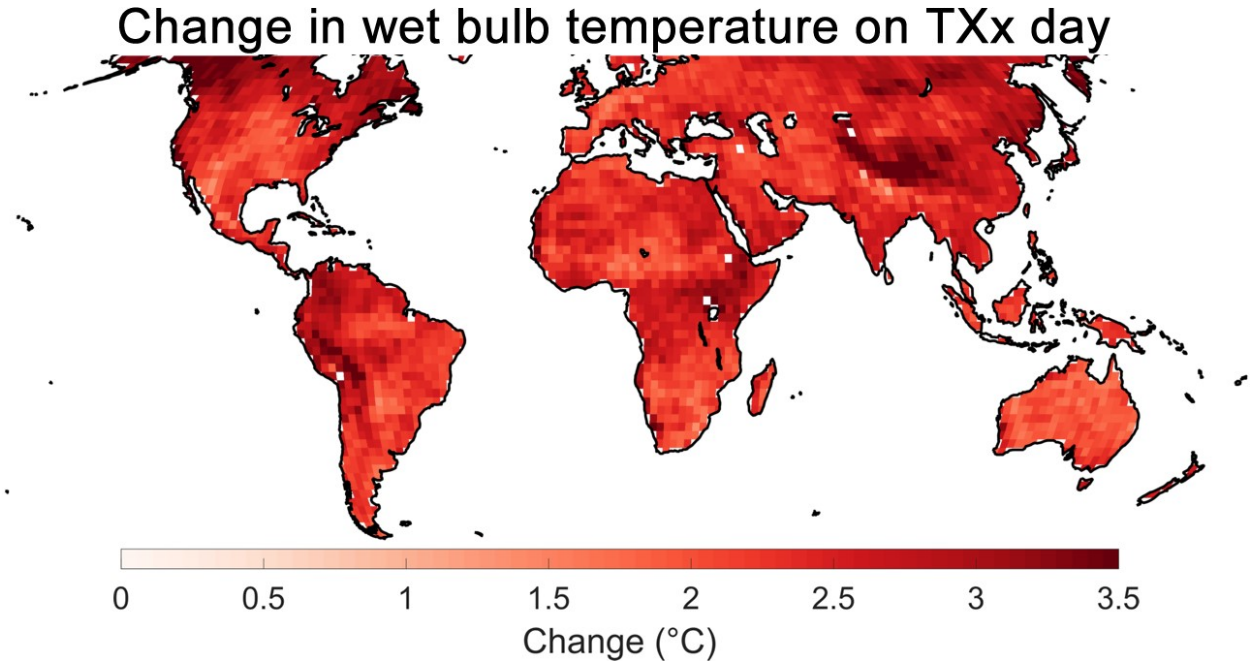


**Figure 1.11:** Projected change in the wet bulb temperature on the TXx day in 2061 – 2085 vs. 1981 – 2005 under RCP 8.5. Despite spatial variation in the magnitude of TXx change, wet bulb temperature change is spatially consistent, showing the modulating effect of humidity.

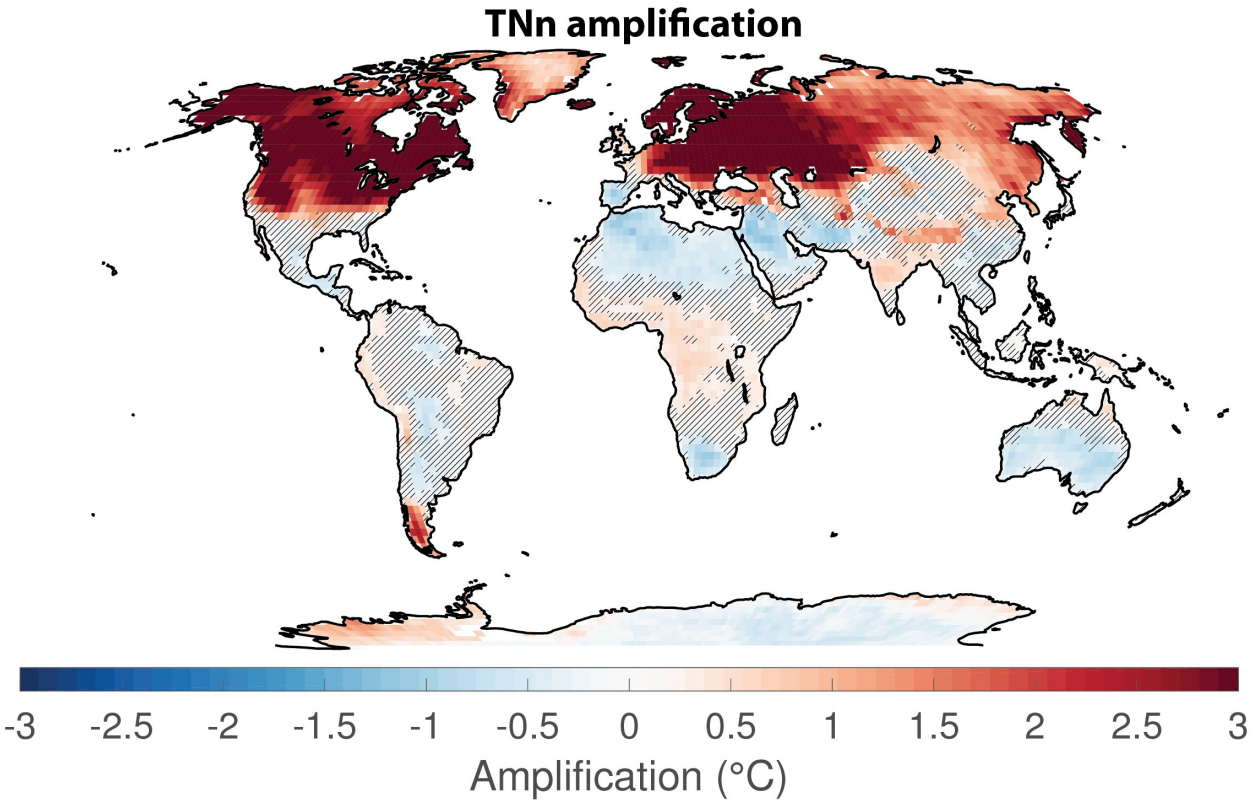


**Figure 1.12:** Multi-model median projected difference between annual minimum temperature (TNn) change and mean daily minimum temperature (Tn) change in 2060 – 2079 vs 1985 – 2004 across 25 CMIP5 models under RCP 8.5. Hatching indicates that less than 75% of models agree on the sign of amplification.

Amplification is also projected for extreme low temperatures. Figure 1.12 shows the multi-model median projected difference between warming of the annual minimum temperature (TNn) and the annual mean daily minimum temperature (Tn). In much of the Northern Hemisphere, TNn is projected to warm by at least 3°C more than Tn. There are strong linkages between wintertime (Dec – Feb, DJF) snow mass declines and TNn amplification. Figure 1.13a shows multi-model median projected DJF snow mass declines of 50% or more across much of the mid-latitudes. Snow mass is historically spatially correlated with DJF Tn anomalies in all regions with regular DJF snow cover; Figure 1.13b shows linear fits between normalized (for

each grid cell) historical DJF snow mass anomalies and historical normalized DJF Tn anomalies in the NCEP II and ERA-Interim reanalysis products and across 25 CMIP5 models. Most models have comparable temperature responses to snow as compared with reanalysis, with more snow mass corresponding to negative temperature anomalies. Three models, however, stand out as having a positive slope: FGOALS-G2, Hadgem2-CC, and Hadgem2-ES. Projected TNn amplification is also spatially associated with snow mass decline; Figure 1.13c shows that grid cells with high levels of TNn amplification also have large declines in snow mass across models. Reductions in surface albedo associated with snow melt likely contribute to this TNn amplification.

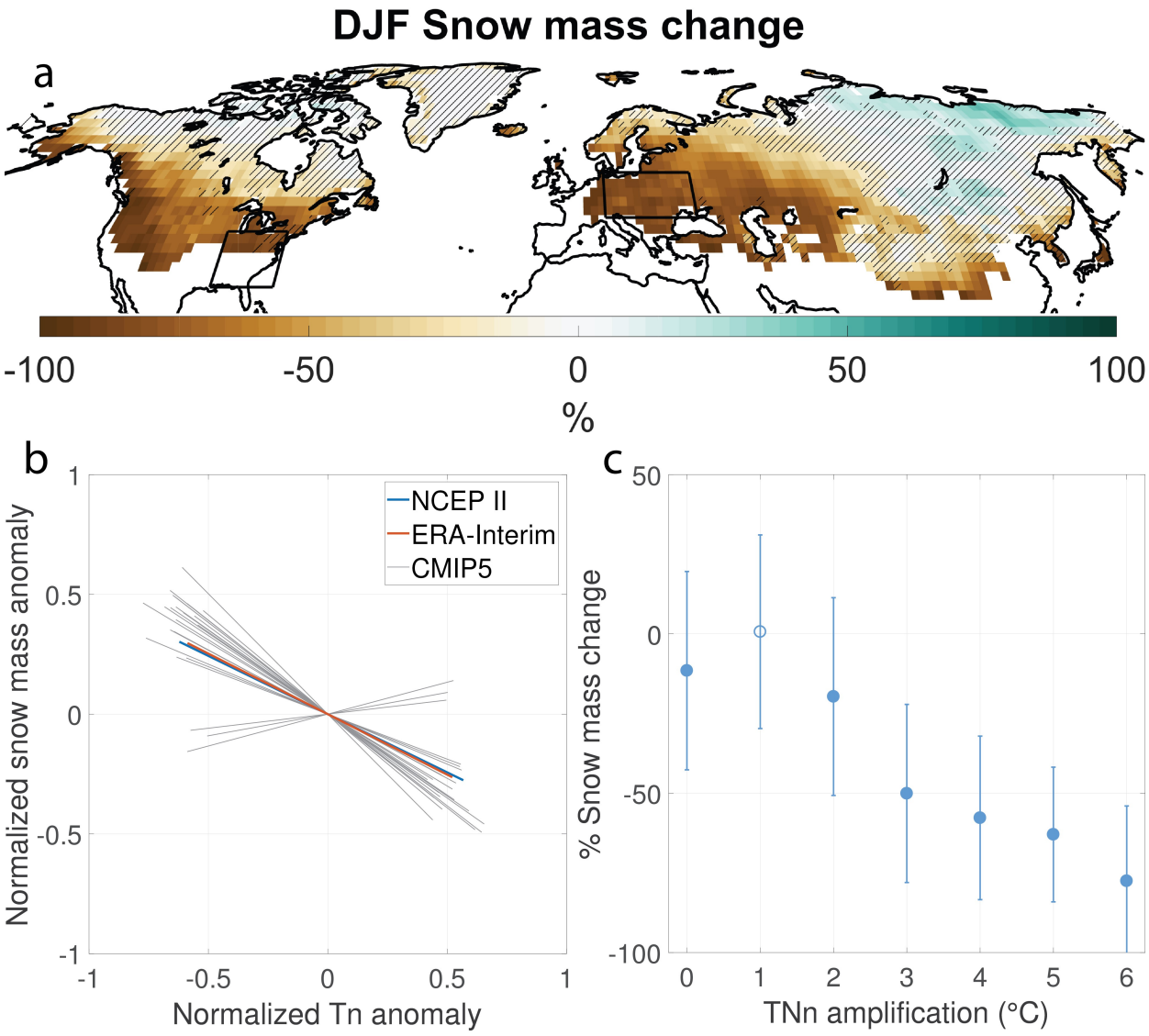


**Figure 1.13:** (a): Multi-model median projected DJF snow mass change in 2060 – 2079 as compared to 1985 – 2004. Hatched regions show less than 75% model agreement on the direction of change. (b): Relationships between normalized monthly-mean snow mass anomaly and normalized monthly-mean Tn anomaly in DJF between 1985 – 2004, averaged across all Northern Hemisphere grid cells. Gray lines show 23 CMIP5 models, and blue and orange lines show the NCEP II and ERA-Interim reanalyses. (c): Multi-model median projected snow mass change for grid cells with different levels of TNn amplification. Error bars show the standard deviation across all grid cells with the same level of TNn amplification. Filled markers indicate that at least 75% of grid cells with a given level of TNn amplification have the same direction of snow mass change.

Prior studies have shown that seasonal warming can explain most of the projected change in heat wave statistics[76]. We find that in most locations that is the case, but in four key regions – the eastern U.S., central Europe, the Amazon rainforest, and eastern China – the most extreme temperatures increase significantly more than the warm season overall. Previous research has proposed increased daily temperature variability as a driver of the projected asymmetric warming of extremes[86,93], but no significant changes in temperature variability have been observed so far[88]. This chapter, however, shows that most extreme temperature warming can be attributed to seasonal mean temperature changes, but in some regions, the most extreme temperatures are increasing substantially more than the season on average. This increased warming of extremes is due to land-atmosphere interactions that create a positive feedback between surface drying and temperature rise during the warm season as a whole and particularly in the short-term heat waves during which the annual maximum temperature occurs.

The increased warming of the warm season (as compared to the rest of the year) has a substantial effect on the occurrence frequency of historically extreme temperatures. In central Europe, the amplified summertime warming is projected to result in 10 days per month above the historical, seasonal 95$^{th}$ percentile Tx, and 4 days in spring, (March – May; Figure 1.14) by 2060 – 2079. Historically, 1 – 2 days per month would be expected to exceed the 95$^{th}$ percentile. In the eastern U.S., this figure is 17 days per month in the summer, and 8 days in the spring. In the Amazon, where temperature variability is lower, the warm season (September – November) is projected to experience 27 days per month above the historical, seasonal 95$^{th}$ percentile Tx, and 22 days in December – February, when slower warming is expected. The projected TXx amplification will occur on top of this heightened warm season warming, further increasing temperatures during heat waves by 1 – 2°C.

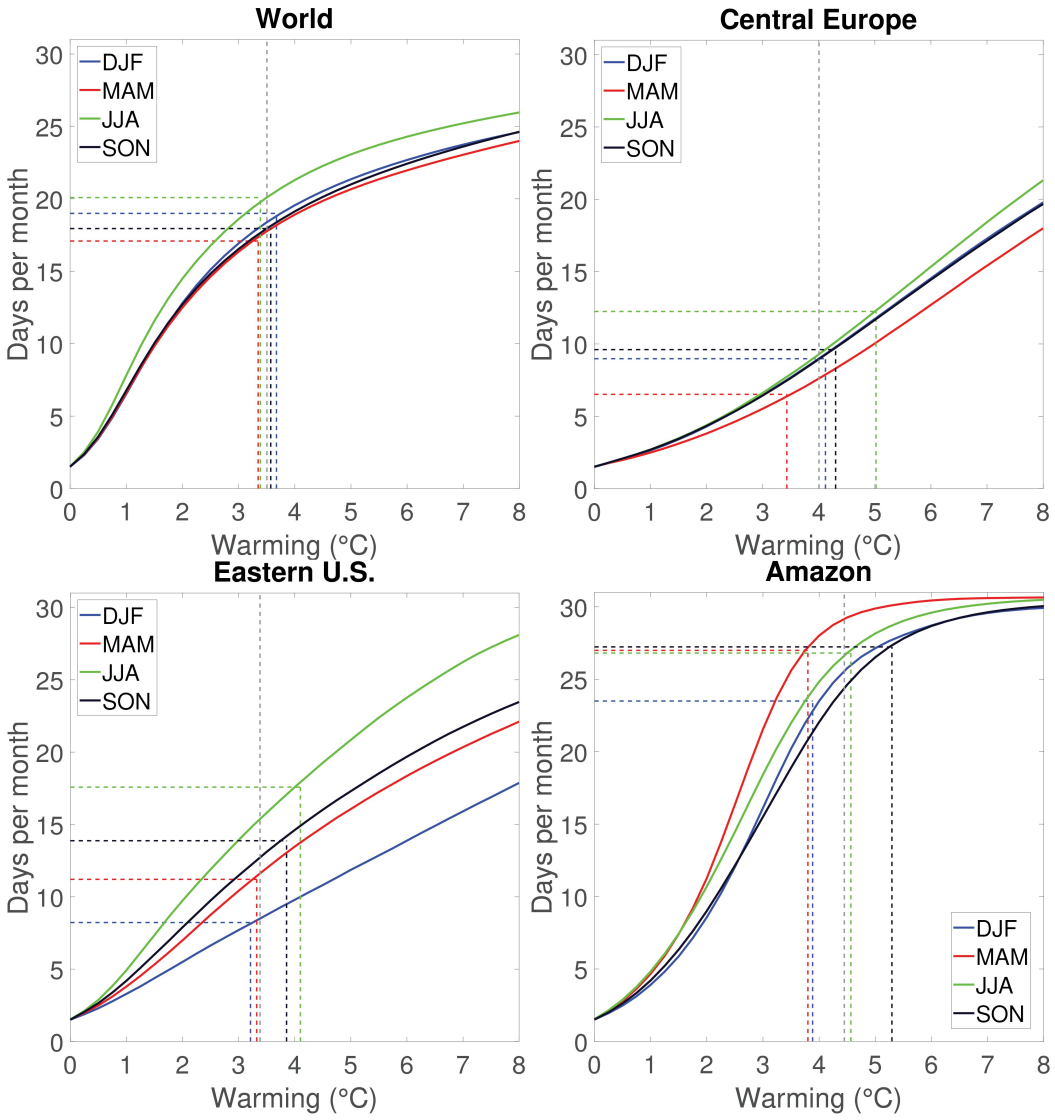


**Figure 1.14:** Multi-model mean projected number of days per month in 2060 – 2079 above the local historical (1981 – 2009) 95$^{th}$ percentile Tx (using the historical temperature distribution from the ERA-Interim reanalysis) as a function of seasonal mean Tx increase in December – February (DJF), March – May (MAM), June – August (JJA), and September – November (SON). Colored, dashed lines show the multi-model mean projected seasonal warming and corresponding recurrence frequency. Dashed gray line shows the multi-model mean projected regional, annual mean warming.

This chapter shows that TXx amplification is linked to reduced cloud cover and surface drying in all four selected regions. The projected reduction in cloud fraction leads to increased net surface shortwave radiation, increasing surface turbulent fluxes. This energy input is then

partitioned into sensible and latent heat fluxes according to the near-surface moisture content. In addition to the large-scale positive feedback between generally declining surface moisture and rising temperatures, short-term variations of this feedback may also occur. During heat waves, high temperatures increase evapotranspiration and dry the soil, which results in an increasing Bowen ratio and still higher temperatures[9]. It is likely this short term process contributes to TXx amplification and that it is made more likely by generally drier and less cloudy conditions.

The strength of warm-season land-atmosphere coupling is also observed to vary seasonally in both reanalysis and the CMIP5 models, with the eastern U.S., central Europe, and the Amazon experiencing a stronger relationship between soil moisture and the Bowen ratio during the warm months than during the rest of the year. Given the links that this chapter demonstrates between surface moisture content and TXx amplification, this uncertainty in model representation of the relationships between Bowen ratio, soil moisture, and temperature may have substantial effects on projected future heat risk. Models generally underestimate the correlation between soil moisture and Bowen ratio as compared to the NCEP II and ERA-Interim reanalyses (Figure 1.6), indicating that Bowen ratio and thus temperature response to surface drying may be greater than projected by most CMIP5 models. Similarly, reanalysis-based correlation between Bowen ratio and Tx is generally larger than in models globally and in the eastern U.S. (Figure 1.5), again suggesting that real-world temperature responses to rising Bowen ratios may be larger than anticipated.

TXx amplification, and warm season warming more generally, depend on changes in cloud cover and surface moisture availability. These variables are driven by small-scale processes which are parameterized in climate models and generally poorly constrained. In the four regions analyzed here, models robustly project a decline in cloud fraction and a

corresponding increase in net surface shortwave radiation, but model variability in the magnitude of the projected change is large and has a substantial impact on projected TXx amplification. These results show that extreme temperature projections cannot be separated from projections of hydrological change; the two are highly interdependent, and uncertainties in one translate into uncertainties in the other. Furthermore, the relation between extreme heat and surface moisture point to correlated climate risks – climate outcomes in these two variables are likely to be either both worse, or both better, than projected. If a region falls in the high range of projected drying, it is also likely to fall in the high range of TXx amplification. This fact underscores the importance of understanding the physical processes that are driving the projected TXx amplification as a way to evaluate model performance and constrain the uncertainties in projected warming and drying.

An unexplored factor in this chapter is vegetation cover and its response to climate change. Vegetation cover and type play a role in modulating regional evapotranspiration and thus Bowen ratios, soil moisture levels, and the strength of land-atmosphere coupling[94]. Models range from having no vegetation representation to incorporating sophisticated biosphere simulations that are coupled with their land-surface and atmosphere models[95,96]. Future research could analyze the extent to which vegetation affects monthly mean and daily extreme temperatures in observations and models, as well as the projected response of vegetation type and cover to warming and associated feedbacks. In addition, prior work has shown that intensive agriculture and irrigation can dampen the most extreme temperatures due to increased local evapotranspiration[97]; this process is not represented in models and could have an impact on TXx amplification in some regions.

Future work could also investigate whether there are regions which experience amplified warming of joint heat-humidity variables like the wet bulb temperature. Such metrics are relevant for human health, and may behave differently from temperature alone. In addition, the relative drying projected on the TXx day could be framed in terms of the rate of soil moisture depletion on dry days preceding the TXx event; due to higher background temperatures, this depletion rate will likely rise in the future, allowing heat waves to intensify more quickly and become more intense than in the historical climate.

Amplified warming of extreme cold temperatures is projected in regions that have historically had wintertime snow cover. This snow cover is projected to decline by 50% or more in much of the northern hemisphere, and the projected amplification is spatially correlated with this snow loss. Wintertime minimum temperatures are important for many ecosystems, as they act to control forest pests[62,78] and other invasive species in some areas. They also have significant implications for a variety of human activities.

Given the wide range of impacts on human activity and natural ecosystems caused by both extreme heat and decreased cold, TXx and TNn amplification may prove important in driving temperature-related climate impacts in the regions identified in this chapter. Constraining the uncertainty surrounding amplification will require improved understanding of hydrological change and its effects on cloud cover, vegetation, and land-atmosphere feedbacks.

# Chapter 2 Temperature and humidity based projections of a rapid rise in global heat stress exposure during the 21st century[98]

**Coffel, E. D.**, Horton, R. M., & de Sherbinin, A. (2018). Temperature and humidity based projections of a rapid rise in global heat stress exposure during the 21st century. *Environmental Research Letters*, *13*(1), 14001. https://doi.org/10.1088/1748-9326/aaa00e

## Introduction

The beginning of the 21st century has seen a variety of extreme heat impacts, from the 2003 European heat wave which was responsible for tens of thousands of additional deaths[36] to the 2010 Russian heat wave which was responsible for a rise in global food prices[99,100]. More recently, extreme temperatures occurred in Australia in 2012 and 2013, the U.S. Southwest in 2013, in India, Pakistan, and other parts of the Middle East in 2015 and 2016[101,102], and again in central Europe in the summer of 2017. Recent attribution studies have suggested that such extreme heat events have already been made more likely due to anthropogenic warming[2,3,103,104]. Furthermore, a large body of research now supports the expectation that as the climate continues to warm during the 21st century, the frequency, magnitude, and duration of extreme heat events will increase, as will population exposure to them[85,105,106]. In many parts of the world, seasonal warming variation may result in the hottest temperatures rising more than the annual mean[76,77,84], for reasons explored in Chapter 1, including declines in aerosols, changes in cloud cover and type, and surface drying[9]. Some research has also suggested that dynamical changes may affect the statistics of circulation regimes favorable to heat wave initiation[107]. A wide variety of studies show that extreme temperatures directly endanger human life[51], decrease agricultural yields[108], compromise ecosystems[62,78], damage infrastructure[46,69], and impair economic growth[47,59].

Human health impacts depend on both temperature and humidity. The human body is efficient at shedding heat through evaporative cooling, even in high air temperatures, if moisture levels are low. However, in hot and humid conditions the efficiency of evaporative cooling slows and the body may become unable to maintain a stable core temperature. A variety of heat stress indices are used to measure the potential impact of heat on humans. The most common index is the wet bulb globe temperature (WBGT), which is a weighted average of the dry bulb, wet bulb, and mean radiant (globe) temperatures and has a long history of use in the military, athletics, and workplace safety[109]. The WBGT has been shown to have increased along with temperature over the past four decades[110,111]. However, recent research has focused on the standard wet bulb temperature as an indicator of dangerous heat-humidity combinations, and that metric is used in this chapter. The wet bulb temperature is a physically relevant quantity defined as the temperature that an air parcel would reach through evaporative cooling once fully saturated. When the outside wet bulb temperature exceeds the body's skin temperature, about 35°C, evaporative cooling will be significantly less effective and the body will likely accumulate heat. Prior research has considered this wet bulb temperature threshold to be the limit of human tolerance to heat stress, as in theory a person would eventually suffer heat illness in the absence of artificial cooling[48–50].

Wet bulb temperatures approaching 35°C almost never occur in the current climate[112], and thus there is little real-world data on human health outcomes at the societal level during such extreme conditions. However, recent heat waves with lower wet bulb temperatures between 29°C and 31°C have caused tens of thousands of deaths[102,113], and empirical evidence suggests that most physical labor becomes unsafe at wet bulb temperatures above 32°C[60,114]. Morbidity and mortality can also increase in populations exposed to warm, but not extreme, temperature

conditions, as will be commonplace in many areas by the second half of the 21st century[115].The impact of heat stress on human society depends both on the severity of heat waves and the number and vulnerability of people exposed to them. Currently, some regions most at risk for extreme wet bulb temperatures – Northeast India, East China, West Africa, and the Southeast U.S. – are some of the world's most densely populated. In Northeast India and West Africa many people work outdoors and air conditioning, safe water, and medical treatment are not necessarily available. These factors make heat stress much more dangerous, especially for children, the elderly, and people with pre-existing health conditions. Population density is expected to rise dramatically in India and West Africa over the 21st century[116], increasing the number of people exposed to extreme heat at the same time as climate change makes high wet bulb temperature events more severe. In addition, continued urbanization will place more people in metropolitan areas affected by the urban heat island, which can raise air temperatures by several degrees Celsius[117]. As a result, regardless of whether wet bulb temperatures regularly reach 35°C, extreme heat is poised to become one of the most significant and directly observable impacts of climate change in the coming decades. Global economic impacts can be expected, affecting agriculture, construction, energy demand, emergency services, recreation, and the military[37,47,59,118].

Recent research has increasingly focused on heat stress as a human health risk[114]. The return period of high heat stress events has declined[119] and in the future the frequency of these events may increase the most in the tropics and parts of the mid latitudes that are already hot[110,120]. Two studies have shown that wet bulb temperatures could reach 35°C this century in some locations in the Middle East and India[49,50]. This chapter presents the first global analysis of population exposure to extreme wet bulb temperatures using 18 general circulation models

(GCMs) from the CMIP5[90] suite under two representative concentration pathways (RCP 4.5 & RCP 8.5) along with five spatially explicit population projections[121] from the shared socioeconomic pathways (SSP) project[122]. Future daily air and wet bulb temperatures are calculated by adding projected monthly changes from the CMIP5 GCMs onto a present-day air and wet bulb temperature distribution provided by the NCEP Reanalysis II[123]. The rise in exposure is partitioned into components driven by population increase, climate change, and a combination of the two, and the uncertainty associated with each is quantified.

**Data and methods**

In this chapter, the daily maximum wet bulb temperature is calculated for the NCEP Reanalysis II[123] and 18 CMIP5 GCMs using the daily maximum air temperature, daily mean specific humidity, and daily mean surface pressure using the algorithm described in Davies-Jones (2008)[124], implemented by Buzan (2015)[114], and ported to Matlab by Dr. Robert Kopp (Rutgers, 2016). Wet bulb temperature is normally estimated using a Skew-T diagram, and there is no analytical method to calculate it. Two primary empirical methods are used to estimate wet bulb temperature, one provided by Stull (2011)[125] and another provided by Davies-Jones (2008)[124]. This chapter uses the Davies-Jones method, as it is known to be more accurate at high wet bulb temperatures[114]. However, the simpler Stull (2011) empirical formula is reproduced here (Equation 2.1) to demonstrate the dependence of the wet bulb temperature on dry bulb temperature and relative humidity.

$$T_w = T\,\mathrm{atan}[0.151\,977(\mathrm{RH\%} + 8.313\,659)^{1/2}] + \mathrm{atan}(T + \mathrm{RH\%}) - \mathrm{atan}(\mathrm{RH\%} - 1.676\,331) + 0.003\,918\,38(\mathrm{RH\%})^{3/2}\,\mathrm{atan}(0.023\,101\mathrm{RH\%}) - 4.686\,035.$$

**Equation 2.1**: Calculation of wet bulb temperature ($T_W$) using relative humidity (RH) and dry bulb temperature (T). Taken from Stull (2011)[125].

The wet bulb temperature used here is different from the wet bulb globe temperature (WBGT) which is commonly used as a heat stress index. WBGT is defined as a weighted average of the wet bulb, dry bulb (standard air temperature), and globe temperature (mean radiative temperature, measured with a thermometer in the center of a black sphere). The heat index, commonly used to communicate heat stress in public weather reports, is also defined using an empirical formula and depends on temperature and relative humidity[126].

The reanalysis and GCM data are re-gridded using linear interpolation to a 2°x2° resolution to facilitate spatial comparison. Using the daily maximum temperature as opposed to a six-hourly time step in wet bulb temperature calculations prevents an underestimation of the daily maximum temperature due to it falling in between two of the time steps.

Future changes in monthly-mean daily maximum temperature and wet bulb temperature, relative to 1985 – 2005, are calculated at each grid cell for each GCM and emission scenario in each year between 2020 and 2080. These projected monthly changes are added to the historical daily maximum temperatures and wet bulb temperatures taken from the NCEP Reanalysis II for the period 1985 – 2005, generating a set of daily future projections which retain reanalysis-based historical daily variability and spatial patterns. This method eliminates GCM mean bias, although such mean biases may affect the warming simulated by GCMs and thus the projections used here. Variations in the spatial distribution, seasonality, or sub-monthly variability of warming could act to either increase or decrease projected future wet bulb temperatures. In addition, any errors in the original reanalysis will be retained. However, given the need for projections of absolute wet bulb temperature, this method may be preferable to bias-correcting GCM temperature and humidity data, as such corrections can produce non-physical results. The NCEP Reanalysis II is most accurate in regions with dense observational weather data; NCEP II

historical period wet bulb temperatures are compared with daily maximum wet bulb temperatures computed using observed station data in a variety of countries, some with dense station data networks (such as the U.S. or Germany) and others with sparse ground observations (such as Nigeria and parts of rural Brazil) (Figure 2.1). The bias between NCEP II and station data is between 0 and negative 3°C (indicating that the NCEP II is too cool), with most regions experiencing biases closer to negative 1°C. These negative biases suggest that the wet bulb temperature projections used in this chapter may be somewhat conservative in these regions. No bias correction is applied to the NCEP II dataset due to varying and uncertain quality and consistency in observed station data.

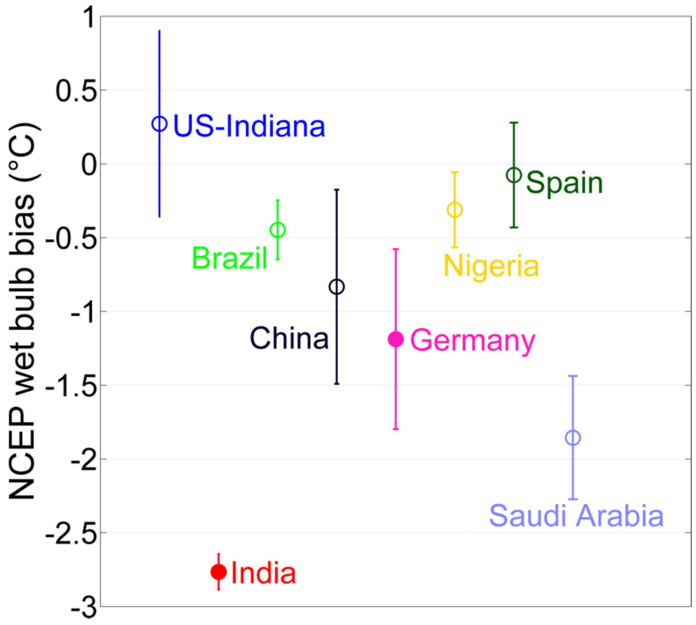


**Figure 2.1:** Mean bias in daily maximum wet bulb temperature between regionally-aggregated weather station data and the NCEP Reanalysis II. All available weather station records between 2010 and 2017 are used, and bias is calculated for each NCEP grid cell using the stations geographically contained within the grid cell region. Error bars show the mean difference in the standard deviation bias across daily wet bulb temperatures from each NCEP II grid cell and all corresponding stations, averaged across all grid cells in the specified country between each station's time series and that for the corresponding NCEP grid cell. Filled markers indicate a statistically significant mean bias (Student t-test, 95th percentile).

The relative frequency of future heat events for each GCM grid cell is calculated as the mean number of days per year during 2060 – 2080 which exceed the mean annual maximum temperature and wet bulb temperature for the same GCM during the modeled 1985 – 2005 period.

Spatially explicit population projections consistent with the SSP project[121] are up-scaled to a 2°x2° degree latitude/longitude grid to match the GCM resolution, and population exposure to wet bulb temperature thresholds are calculated for each GCM separately at a daily time resolution. If the GCM wet bulb temperature at a given grid cell exceeds a threshold value (e.g a wet bulb of 32°C or 35°C) on a given day, the grid cell is considered exposed, and the population total for that grid cell is added to the person-day exposure count. The annual exposure totals (in person-days) can count the same people multiple times, and indeed do as much of the exposure to high wet bulb temperatures occurs in the same grid cells repeatedly.

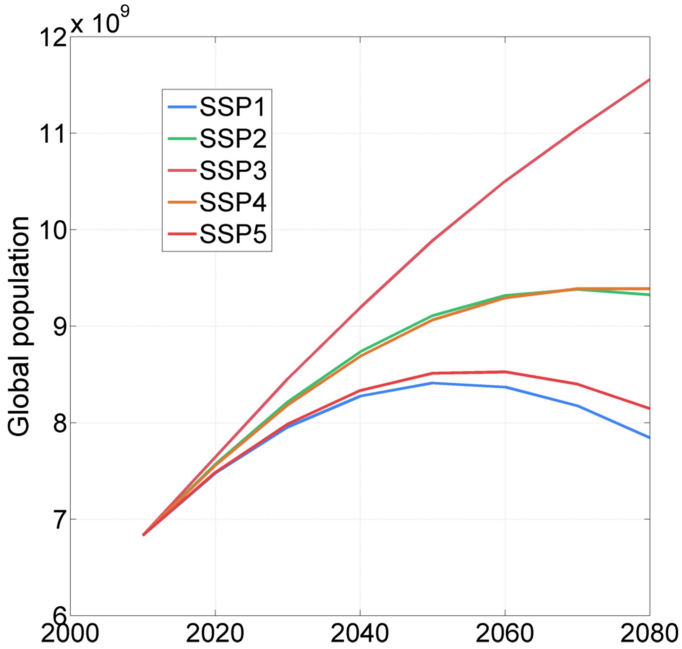


**Figure 2.2:** Projected global population through 2080 under the five shared socioeconomic pathway (SSP) scenarios.

The population exposure values are decomposed into three components: the population effect, the climate effect, and the combined effect. The population effect is calculated as the exposure in person-days that would result from a changing population under a constant climate. The historical daily maximum wet bulb temperatures (1985 – 2005) are used to select exposed grid cells, and mean population exposure for each decade is computed using decadal population means from the five SSP scenarios. Uncertainty in the population effect is estimated by taking the full range across the five SSPs, and this is displayed as the error bar on the population effect bars in Figure 2.7b-c. The climate effect is the exposure that results from rising temperatures alone, holding population constant (using SSP estimated population data from 2010). Uncertainty in the climate effect is calculated by taking the $10^{th}$ – $90^{th}$ percentile range across the 18 GCMs (so as to reduce the effect of outlier temperature change projections in several GCMs). The combined effect is calculated as the total population exposure minus the population and climate effects, and the uncertainty bars show the $10^{th}$ – $90^{th}$ percentile range across five SSPs and 18 GCMs. This represents the exposure that results from both rising populations and rising temperatures.

**Results and discussion**

The changes in wet bulb temperatures are expected to be smaller, more spatially uniform, and have less inter-GCM variation than for air temperatures, as GCMs that project the largest increases in air temperature also project the largest decreases in relative humidity (even with increases in specific humidity), producing a stabilizing effect on wet bulb temperature projections[127]. By 2070 – 2080, global multi-GCM mean increases in annual maximum wet bulb temperature across the tropics and mid-latitudes of 2 – 3°C are projected (Figure 2.3d-e), with an

inter-GCM range from 1 – 2.5°C under RCP 4.5 and 2 – 4.5°C under RCP 8.5. These projected increases are similar to those found in other studies focused on regional wet bulb temperature changes[49,50].

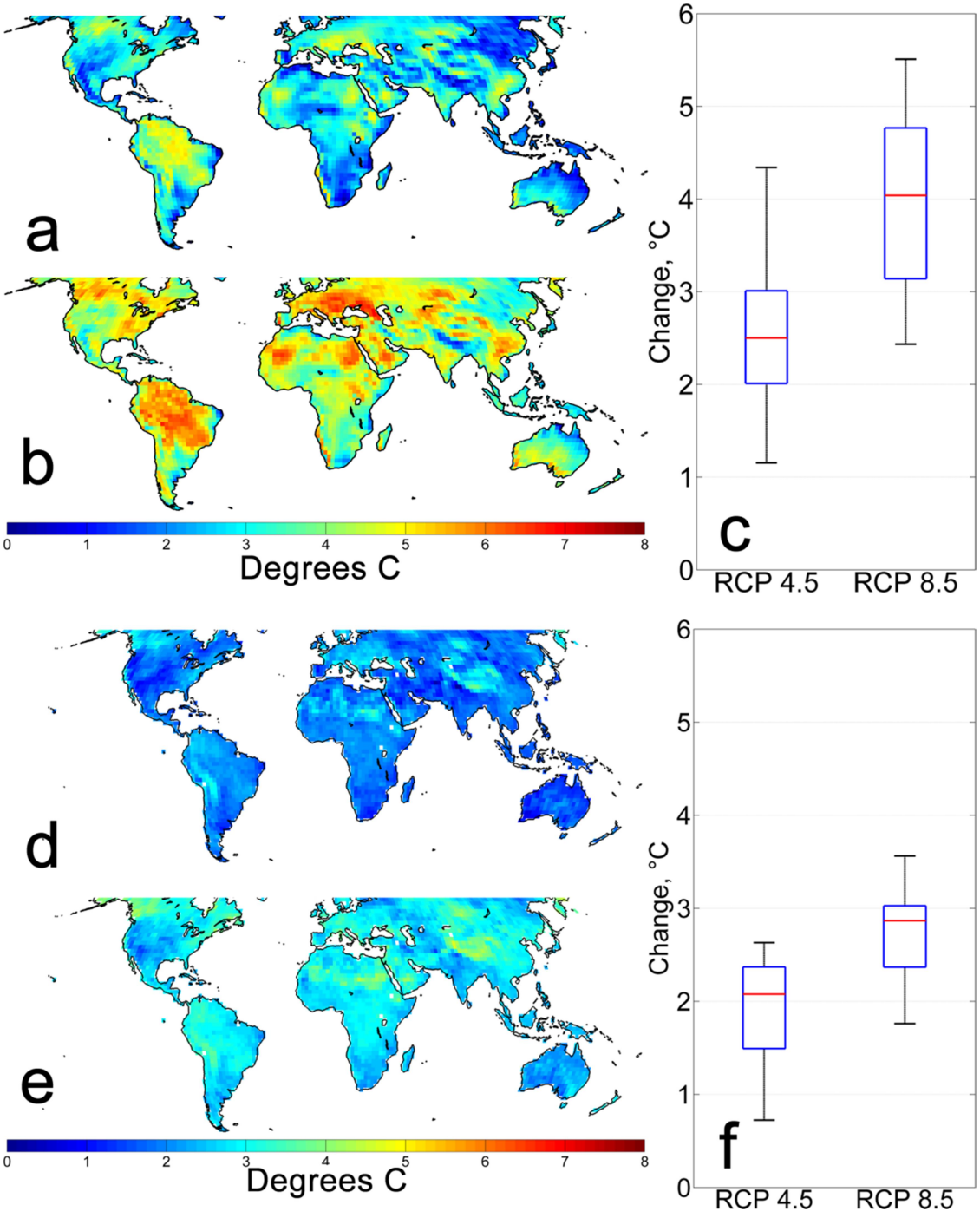


**Figure 2.3:** Top panel (a-c): changes in annual maximum air temperature in 2060 – 2080 relative to 1985 – 2005 under RCP 4.5 (a) and RCP 8.5 (b). Panel (c) shows the range in projected annual

maximum temperature increase spatially averaged over land for both emission scenarios over all 18 CMIP5 GCMs. Bottom panel (d-f): same as (a-c) except for annual maximum wet bulb temperature. Air temperatures increase at a faster rate and have more spatial variability than wet bulb temperatures, in part due to the dependence of wet bulb temperature on humidity.

Annual maximum wet bulb temperatures are projected to increase by approximately the same amount as mean daily maximum wet bulb temperatures across the tropics and mid-latitudes (Figure 2.4). This stands in contrast to annual maximum air temperatures, which are projected to increase by 1 – 2°C more than mean daily maximum temperatures in many regions, notably in the eastern U.S., much of Europe, parts of South America, and eastern China (see Chapter 1). This difference between changes in mean and extreme air temperatures aligns with previous research[76,77,84,128] and may be driven by land-atmosphere interactions and dynamical changes[9,85,107].

As global mean temperatures warm, it is expected, and has been observed, that atmospheric specific humidity levels will rise in accordance with the Clausius-Clapeyron relation[16], with the largest increases in specific humidity expected over the oceans. Four regions particularly vulnerable to heat stress, the eastern U.S., northeastern India, eastern China, and West Africa, have different climates and synoptic patterns during heat waves which affect the relative importance of temperature and humidity as contributors to extreme wet bulb temperatures. On the days with the highest wet bulb temperatures, specific humidity increases of 10 – 15% (relative to high wet bulb temperature days in the historical period) are projected across all four regions. However, increases in temperature on the days with the highest wet bulb temperatures range from 1 – 2°C in India to 3 – 4°C in the eastern U.S., West Africa, and eastern China (Figure 2.4), driving the regional differences in wet bulb temperature change.

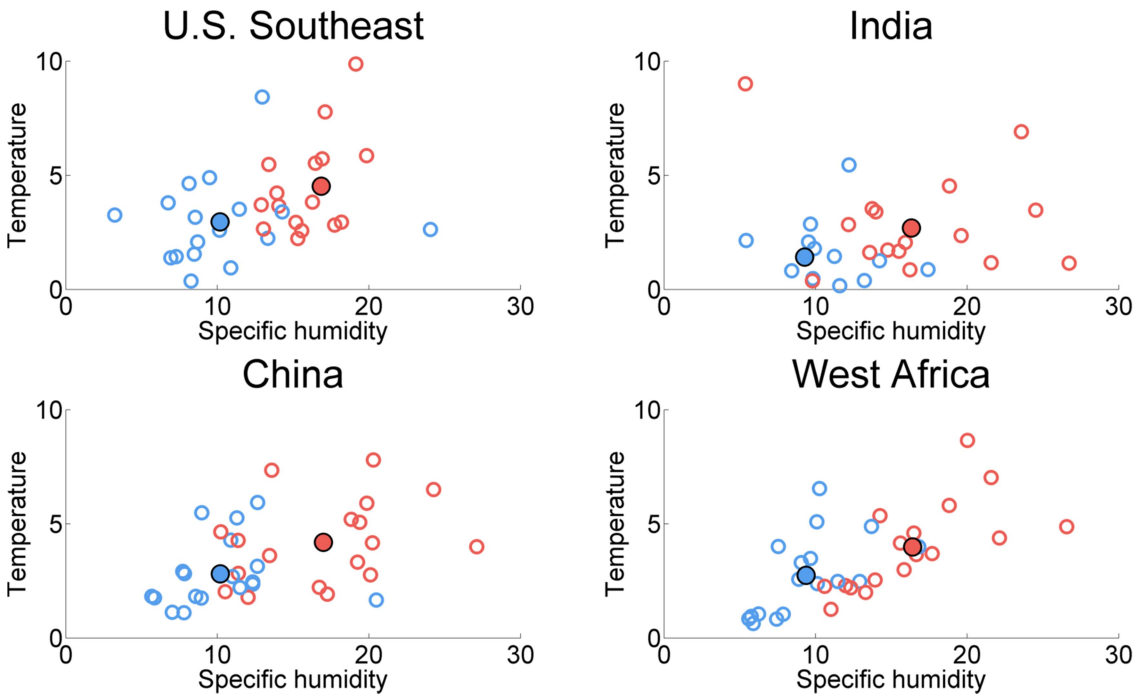


**Figure 2.4:** Projected change in air temperature (°C) and specific humidity (percent) on the 100 highest wet bulb days in 2060-2080 relative to 1985-2005 for each GCM (un-filled circles) and the multi-GCM mean (filled circles) for RCP 4.5 (blue) and RCP 8.5 (red). Multi-model mean temperature and specific humidity changes are relatively consistent in the four regions despite differences in geography and synoptic patterns during heat stress events.

Populations are to a large extent adapted to their local climates. To assess how wet bulb temperatures will change relative to historical conditions, the number of days per year that may exceed the historical annual maximum air and wet bulb temperatures are projected. By 2060 – 2080, most regions within 30° latitude of the equator may experience between 25 and 150 days per year that exceed the historical once-per-year maximum air temperature, and 25 – 250 days per year that exceed historical once-per-year maximum wet bulb temperature (Figure 2.5). In the mid-latitudes, these numbers are somewhat lower at 25 – 40 days per year for both air and wet bulb temperature, due to higher baseline variability. These results suggest a radical transformation of tropical and sub-tropical heat environments, with much of the year being spent above the highest historical wet bulb temperatures. As the duration of heat exposure is essential

in determining health impacts, more research is needed into the potential mortality response associated with long duration (months) heat exposure interspersed with unprecedented extreme heat waves.

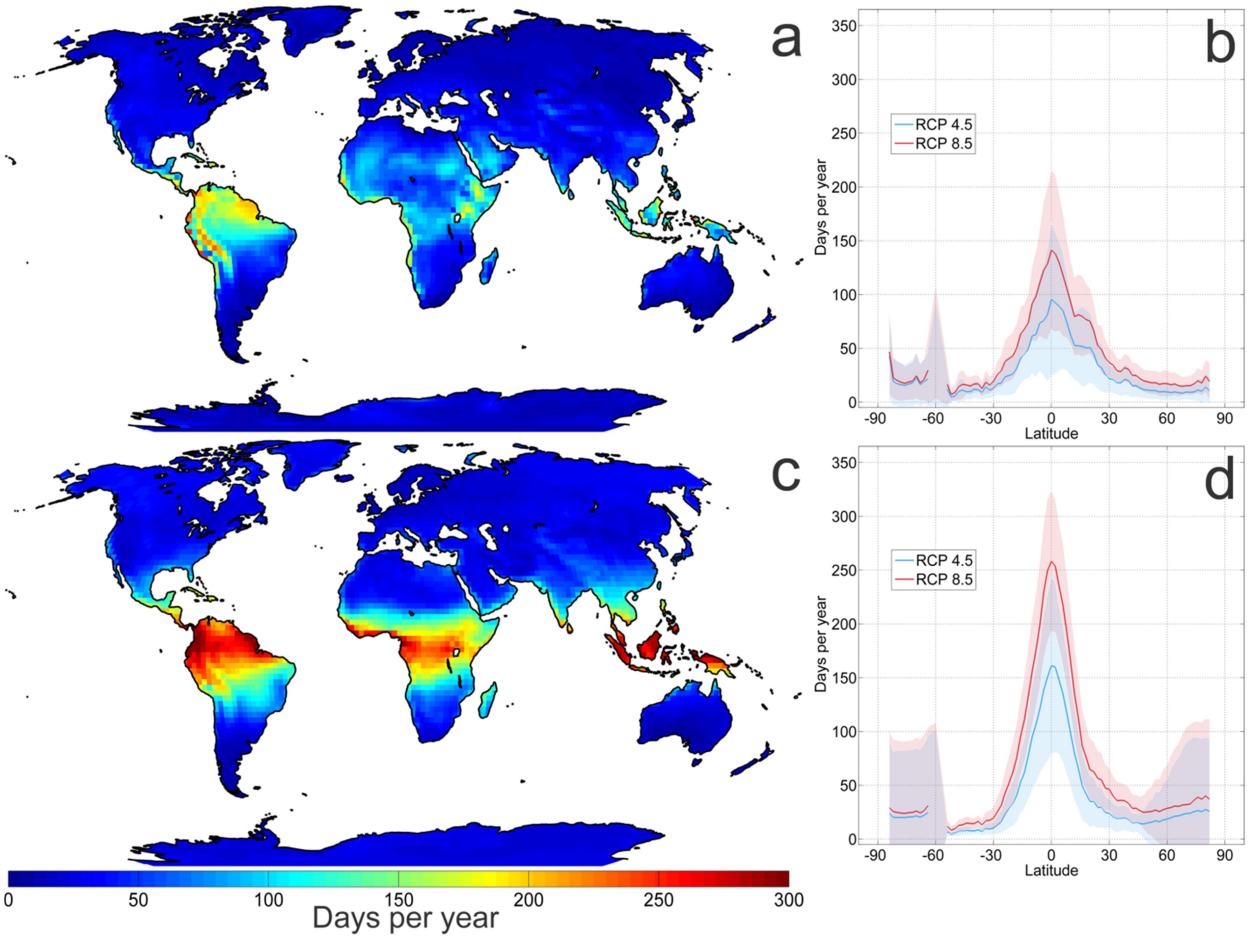


**Figure 2.5:** The number of days per year which exceed the historical (1985 – 2005) mean annual maximum temperature (top row) and wet bulb temperature (bottom row) in 2060 – 2080. Maps show results under RCP 8.5, and (b, d) show the variation with latitude of the number of days per year under both RCP 4.5 and RCP 8.5, excluding water grid cells. Wet bulb temperatures exceed the historical mean annual maximum more frequently than air temperatures due to lower variability, especially in the tropics.

Substantial population growth is expected throughout the 21st century, especially in the developing world (Figure 2.2). Much of this growth is anticipated to occur in regions that experience high wet bulb temperatures, resulting in large increases in the number of people

exposed to dangerous heat conditions. Annual exposure in person-days (one person exposed on one day) to high wet bulb temperatures in each decade through 2080 is estimated using the SSP population projections (Figure 2.7). The possible range of exposure outcomes is quantified by combining 18 GCMs and five SSPs under two emissions scenarios, assuming that the uncertainty resulting from GCM variability, future emissions trajectories, and population growth are equally irreducible in the context of present-day decision-making. These results include repeat exposures (see Figure 2.6 for the spatial distribution of exposure), and as the highest wet bulb temperatures are concentrated in a few regions, the same populations will likely bear the brunt of the world's most extreme heat.

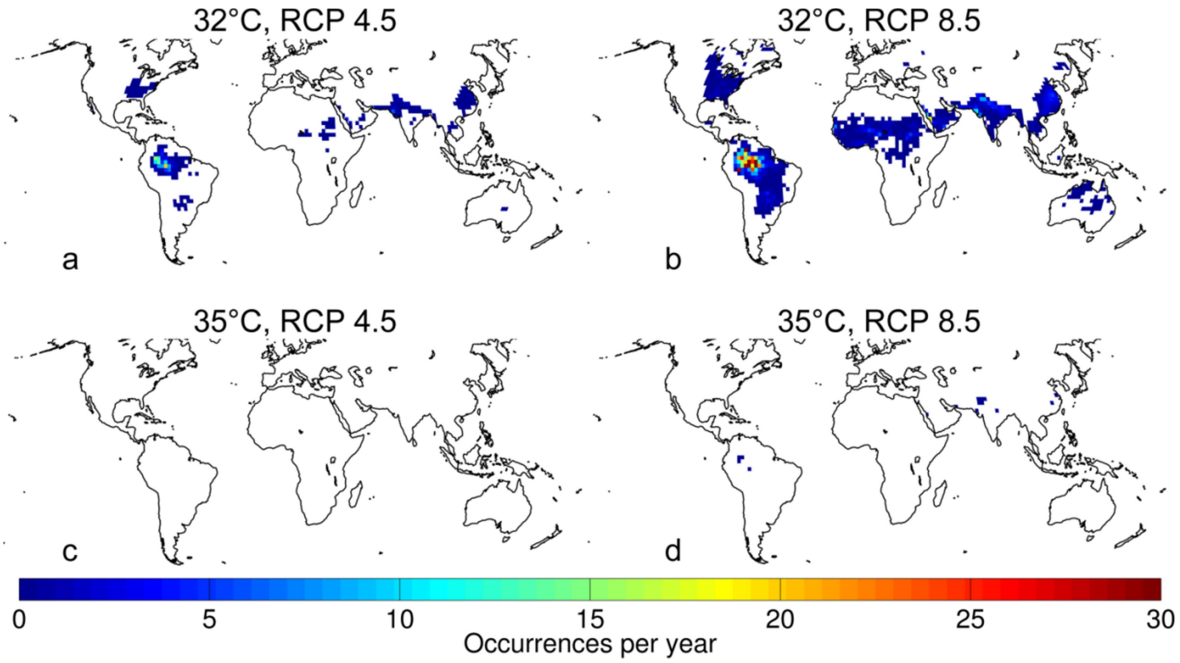


**Figure 2.6:** Multi-GCM mean number of days in 2070 – 2080 with wet bulb temperatures above 32°C (top row) and 35°C (bottom row). Left panels show results under RCP 4.5 and right panels under RCP 8.5. Wet bulb temperatures above 35°C are limited to small geographic areas, even under RCP 8.5, but some of these regions – in particular northeastern India and eastern China – are densely populated. RCP 4.5 completely avoids wet bulb temperatures of 35°C through 2080.

Exposure to extreme wet bulb temperatures depends heavily on future greenhouse gas emissions. Figure 2.7a shows the projected mean annual exposure to wet bulb temperatures from 30 – 35°C across 18 GCMs and five SSPs under RCP 4.5 and RCP 8.5. Projected exposure under the two emissions scenarios sharply diverges above wet bulb temperatures of approximately 32°C, the temperature above which most sustained labor becomes impossible[60,114], with differences in exposure person-days of several orders of magnitude. Figure 2.7b, c show projected exposure to wet bulb temperatures above 32°C, above the highest commonly experienced in the historical climate. By the 2070s annual exposure to wet bulb temperatures of at least 32°C may increase by a factor of 5 – 10 (relative to 2020; 32°C wet bulb temperatures are extremely rare in the 1985 – 2005 period) to around 750 million person days under RCP 8.5 and 250 million person days under RCP 4.5 (Figure 2.7b, c). Under the RCP 8.5 scenario, in any given year during the 2070s projections suggest that there is a greater than 33% chance of a wet bulb temperature above 34°C occurring in at least one model grid cell, and a greater than 15% chance for a wet bulb temperature above 35°C. These extreme wet bulb temperatures are concentrated in small parts of India, China, and the Amazon, but due to the high population densities in India and China, these results suggest multi-model mean annual exposure to wet bulb temperatures of 35°C or higher to be approximately a million person-days by the 2070s under RCP 8.5. The uncertainty range in exposure at all thresholds results mostly from differences in projected warming and moistening between GCMs and emissions scenarios, with a smaller contribution from population variation among SSPs.

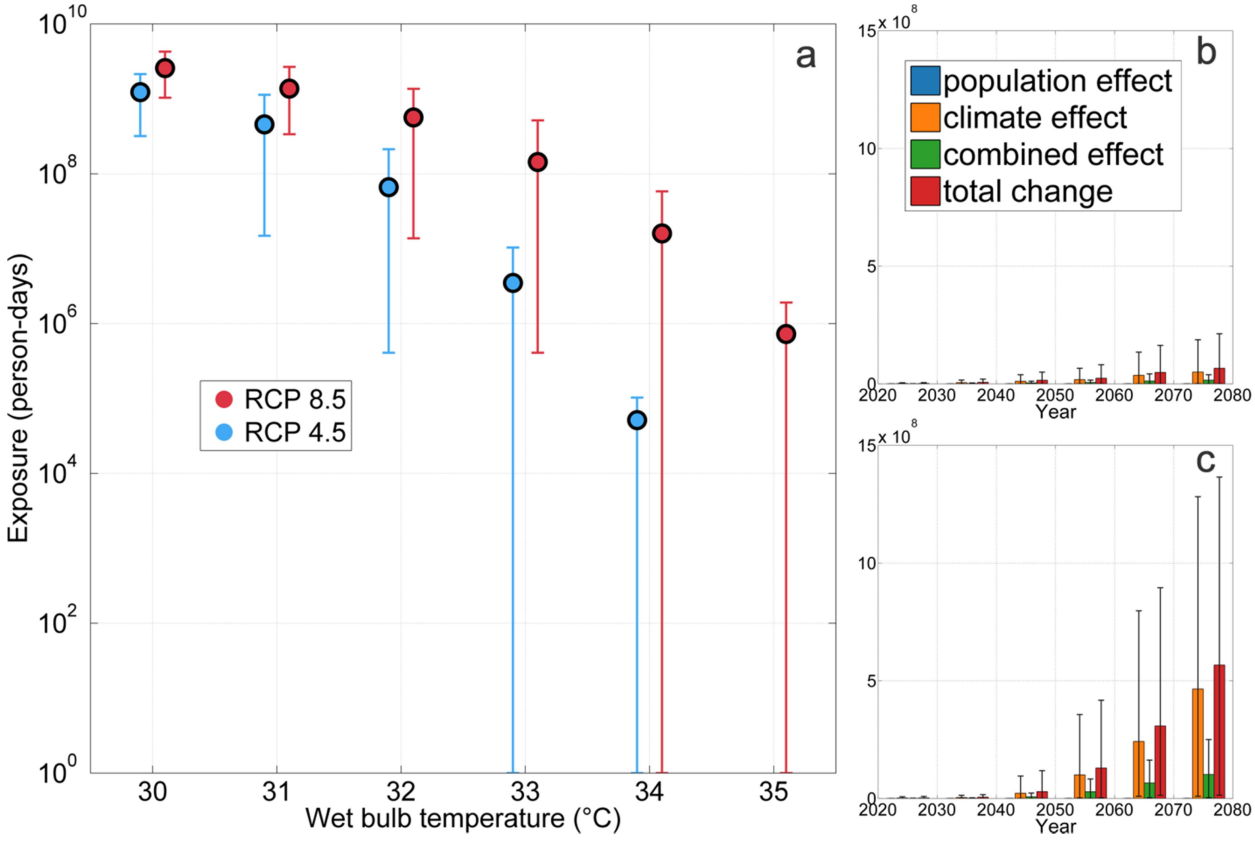


**Figure 2.7:** Global population exposure to varying wet bulb temperature thresholds, in mean number of person-days per year. (a): Global mean annual exposure under RCP 4.5 and RCP 8.5 in 2070 – 2080 to wet bulb temperatures from 30 – 35°C. Error bars show the full range across 18 GCMs and five SSPs. Exposure to wet bulb temperatures above 30°C is reduced by several orders of magnitude in RCP 4.5 as compared to RCP 8.5. Right: mean global annual exposure to wet bulb temperatures exceeding 32°C, approximately the upper limit at which sustained physical labor is possible[60] and above anything experienced in the historical climate. RCP 4.5 is shown on top (b), and RCP 8.5 on bottom (c). Exposure is separated into a population effect (constant climate but changing population), climate effect (constant population but changing climate), and a combined effect (result of changing population and changing climate). Total exposure is the sum of these three components. Error bars on total exposure show the 10$^{th}$ – 90$^{th}$ percentile range across 18 GCMs and five SSPs.

Global population exposure is divided into three components[106]: the population effect, or the additional exposure driven entirely by population growth (a constant climate but growing population); the climate effect, the exposure driven by climate change (constant population but changing climate); and the combined effect, or the exposure that results from changing population and changing climate in the same location (e.g. the additional exposure that results

from both population growth and climate change). The combined effect is equal to the total exposure minus the population and climate effects. Globally, the population effect is near zero as wet bulb temperatures of 31°C and higher are rare in the current climate and would remain so without warming. However, the combined effect comprises a substantial portion of increased exposure, indicating that while climate change is the dominant factor in increasing future exposure, population growth in hot regions also plays an important role. Increased heat stress may result in migration out of the hottest regions; the population projections used here do not consider this possibility.

Recent research suggests that there is no fundamental cap on wet bulb temperature[129–131]. However, further research into the development of convection at high wet bulb temperatures and tropical thermodynamics, including changes in vertical potential temperature profiles, extreme SSTs, and SST gradients, is warranted, as is further evaluation of GCM simulations of expected physical processes in a warmer future climate. It is possible that achieving high wet bulb temperatures may depend on strong local atmospheric subsidence inhibiting convection, but this process may not be well represented in GCMs; higher resolution, convection-resolving models could help resolve this question. Recent research has hinted at the possibility that shifts in dynamic (e.g. atmospheric blocking) and thermodynamic (e.g. soil moisture) processes poorly simulated by GCMs may be modifying the statistics of extreme temperatures, but the implications for extreme wet bulb temperatures remain unexplored. In general there is a negative correlation between warming and relative humidity change over interior continents[127] as dryer conditions result in more efficient warming of the air. However, research suggests that some localized heat stress hot spots, especially in the coastal Middle East, may result from the interaction of hot desert air masses with onshore moisture advection from warm bodies of

water[49]; these processes occur at too small a scale to be captured by GCMs, potentially adding a conservative bias to these results if they occur in other regions in the future. Further research is also needed into regional influences on heat, such as topography, local synoptic patterns, and the urban heat island effect, and whether variability of wet bulb temperatures may change on a daily timescale. In addition, given that small differences in wet bulb temperature can lead to large differences in population exposure to dangerous heat, GCM bias may have an important effect on projected results; advanced methods of GCM bias correction[132] could be tested and compared with the reanalysis-based projection method presented here.

This initial exploration of a potentially transformative risk factor for humans only considers population exposure. However, the impacts of heat on humans depend on both exposure and vulnerability, with the latter depending on many other factors including population age, degree and type of pre-existing health conditions, acclimatization, adaptive capacity, access to air conditioning, emergency response to severe heat waves, and economic and sociocultural factors that influence behavior[133]. In addition, research has shown that relatively simple adaptation strategies such as early warning of heat waves, public education campaigns on the dangers of heat, and social check-ups on vulnerable people can drastically reduce the death toll on hot days[113,134]. Each dimension of vulnerability will shape the impacts of heat stress events in distinct ways, pointing at the need for deeper epidemiological and economic analyses. This chapter also only considers heat stress at a 2° spatial resolution – the urban heat island and other localized climate effects could result in locally higher wet bulb temperatures than are represented by the grid cell-average.

There is high uncertainty in the population projections that we consider in this study, and the five SSPs are not independent from future emission scenarios (i.e. higher population is likely

associated with higher emissions). However, as a warming climate is by far the largest contributor to increasing heat exposure, changes in the future population trajectory are projected to have a second-order effect. The SSPs may offer a means of exploring potentially critical correlations between heat, population density, vulnerability, and the potential for adaptation. Furthermore, the potential for non-linear increases in impacts at the highest wet bulb temperatures suggest the need for further research into the characteristics of heat events, such as duration and potential correlation with co-hazards such as air pollution, dehydration, and sun exposure. The effects of rapid increases in wet bulb temperature on ecosystems and wildlife, especially large mammals, should also be considered.

The results presented in this chapter suggest that exposure to extreme wet bulb temperatures will rapidly increase throughout the 21$^{st}$ century and potentially beyond, depending on future greenhouse gas emissions. Given the number of people who may be exposed to dangerous heat across the world, failure to adopt both mitigation and adaptation measures is likely to result in suffering, economic damage, and increased heat-related mortality.

**Table 2.1:** CMIP5 models used to calculate wet bulb temperature.

| Model | Organization | Native Resolution |
|---|---|---|
| ACCESS1-0 | Commonwealth Scientific and Industrial Research Organisation | 1.25° x 1.875° |
| ACCESS1-3 | Commonwealth Scientific and Industrial Research Organisation | 1.25° x 1.875° |
| BCC-CSM1-1-M | Beijing Climate Center | 2.7906° x 2.8125° |
| BNU-ESM | College of Global Change and Earth System Science, Beijing, Normal University | 2.7906° x 2.8125° |
| CANESM-2 | Canadian Centre for Climate Modelling and Analysis | 2.7906° x 2.8125° |
| CSIRO-MK3-6-0 | Commonwealth Scientific and Industrial Research Organisation | 1.8653° x 1.875° |
| CNRM-CM5 | Centre National de Recherches Meteorologiques / Centre Europeen de Recherche et Formation Avancee en Calcul Scientifique | 1.4008° x 1.40625° |
| FGOALS-G2 | State Key Laboratory for Numerical Modeling for Atmospheric Science and Geophysical Fluid Dynamics | 2.7906° x 2.8125° |
| GFDL-CM3 | NOAA Geophysical Fluid Dynamics Laboratory | 2.0° x 2.5° |
| GFDL-ESM2G | NOAA Geophysical Fluid Dynamics Laboratory | 2.0225° x 2.0° |
| GFDL-ESM2M | NOAA Geophysical Fluid Dynamics Laboratory | 2.0225° x 2.5° |
| HADGEM2-CC | Met Office Hadley Center | 1.25° x 1.875° |
| HADGEM2-ES | Met Office Hadley Center | 1.25° x 1.875° |
| IPSL-CM5A-MR | Institut Pierre-Simon Laplace | 1.2676° x 2.5° |
| IPSL-CM5B-LR | Institut Pierre-Simon Laplace | 1.8947° x 3.75° |
| MIROC5 | International Centre for Earth Simulation | 1.4008° x 1.40625° |
| MRI-CGCM3 | Meteorological Research Institute | 1.12148° x 1.125° |
| NORESM1-M | Norwegian Climate Centre | 1.8947° x 2.5° |

# Chapter 3 The impacts of rising temperatures on aircraft takeoff performance[46,69]

**Coffel, E. D.**, & Horton, R. M. (2015). Climate Change and the Impact of Extreme Temperatures on Aviation. *Weather, Climate, and Society*, *7*(1), 94–102. https://doi.org/10.1175/WCAS-D-14-00026.1

**Coffel, E. D.**, Thompson, T. R., & Horton, R. M. (2017). The impacts of rising temperatures on aircraft takeoff performance. *Climatic Change*, *144*(2), 381–388. https://doi.org/10.1007/s10584-017-2018-9

## Introduction

Global mean surface temperatures have increased by approximately 1°C above pre-industrial levels, with most of that change occurring after 1980[135]. As air temperature increases at constant pressure, air expands and becomes less dense. The lift generated by an airplane wing is a function of the mass flux across the wing surface; at lower air densities, a higher airspeed is required to produce a given lifting force[136]. For a given runway and aircraft, there is a temperature threshold above which takeoff at the aircraft's maximum takeoff weight (MTOW) is impossible due to runway length or performance limits on tire speed or braking energy. Above this threshold temperature, a weight restriction – entailing the removal of passengers, cargo, and fuel – must be imposed to permit takeoff[69,137,138].

Weather is a leading cause of disruption to flight operations[139,140], either through direct impacts on airport capacity and flight routes or through cascading delays across the aviation system[141]. However, the study of the potential impacts of climate change on aviation is relatively recent[142]. Prior work has suggested that both turbulence[143,144] and trans-Atlantic flight times[145] may increase due to a strengthening and shifting mid-latitude jet stream. Climate change may also result in more extreme precipitation events[17,146], altered mid-latitude storm tracks[30,147], and changes in hurricane frequency and intensity[26,148], among other disruptions to prevailing weather

patterns. Sea-level rise is also likely to threaten low-lying coastal airports around the world[29,149,150]. Little work has explored these potential risks in detail in the context of the aviation sector, and they present fertile ground for future research.

This chapter focuses on one potential impact of climate change: an increase in weight restriction due to higher temperatures. The warming resulting from anthropogenic climate change to date (~1°C) has raised the mean airport density altitude (i.e. the altitude associated with air at a given pressure at standard atmospheric conditions) by approximately 100 feet, and expected additional warming of 1 – 3°C by the end of the century[39] will result in further increases of additional hundreds of feet. Prior work (Coffel and Horton, 2015) has shown that the frequency of days on which a Boeing 737-800 requires weight restriction is likely to increase by 100 – 300% at several airports in the U.S. in the coming decades[69]. This chapter expands on these results by building performance models for five common commercial aircraft, the Boeing 737-800, Airbus A320, Boeing 787-8, Boeing 777-300, and Airbus A380, and calculating the change in the magnitude and frequency of weight restriction events at 19 airports (see Table 3.1 and Table 3.2 for airport and aircraft information). Air traffic is heavily concentrated in a relatively small number of cities, and these selected locations represent the most common climates, elevations, and runway conditions found at the world's busiest airports. Here, weight restriction at a variety of takeoff weights (TOW) in both historical and future climate conditions is calculated. This analysis demonstrates a method which could be combined with aviation industry operational data to dynamically predict the weight restriction burden for an airline, taking into account fleets of diverse aircraft and daily schedules at different airports.

**Data and methods**

Future hourly airport temperatures are projected using 27 general circulation models (GCMs) from the CMIP5[90] model suite under both the RCP 4.5 and RCP 8.5 emissions scenarios[91], using the single grid cell that includes each selected airport. Sub-daily temperatures were approximated by linearly interpolating between the daily minimum and maximum temperatures. The resolution of the CMIP5 GCMs vary, but in most cases are approximately 200 km; this relatively large grid cell size results in local temperature bias, especially in coastal or mountainous areas where climate varies at small spatial scales. In addition, GCMs tend to compress the temperature distribution, making cold extremes too warm and hot extremes too cool. These biases are identified and corrected using airport station daily maximum and minimum temperature records from the NOAA-NCEI Global Historical Climatology Network (GHCN). Some airports do not have a full temperature record in the GHCN, and in some cities the stations with the longest and most reliable records are not at the airport. In these cases, all stations for the city are averaged for the time periods for which they are available.

Using raw GCM temperature data, the mean temperature bias as compared with observations across the 19 airport stations is -1.81°C. To correct the GCM bias, a decile-specific correction procedure is applied to the GCM data using the GHCN observations as a reference. Both the observed and the GCM temperature data for the full historical period are divided into deciles and then the mean bias between each GCM and the observed data is calculated for each decile. Then, the decile thresholds for the future GCM temperature distribution are calculated, and the bias correction is applied by subtracting the same decile bias for future GCM temperatures. This correction substantially reduces the error across the temperature distribution, including in the top two deciles of particular relevance for this study, with a resulting mean error of 0.38°C (see Figure 3.1).

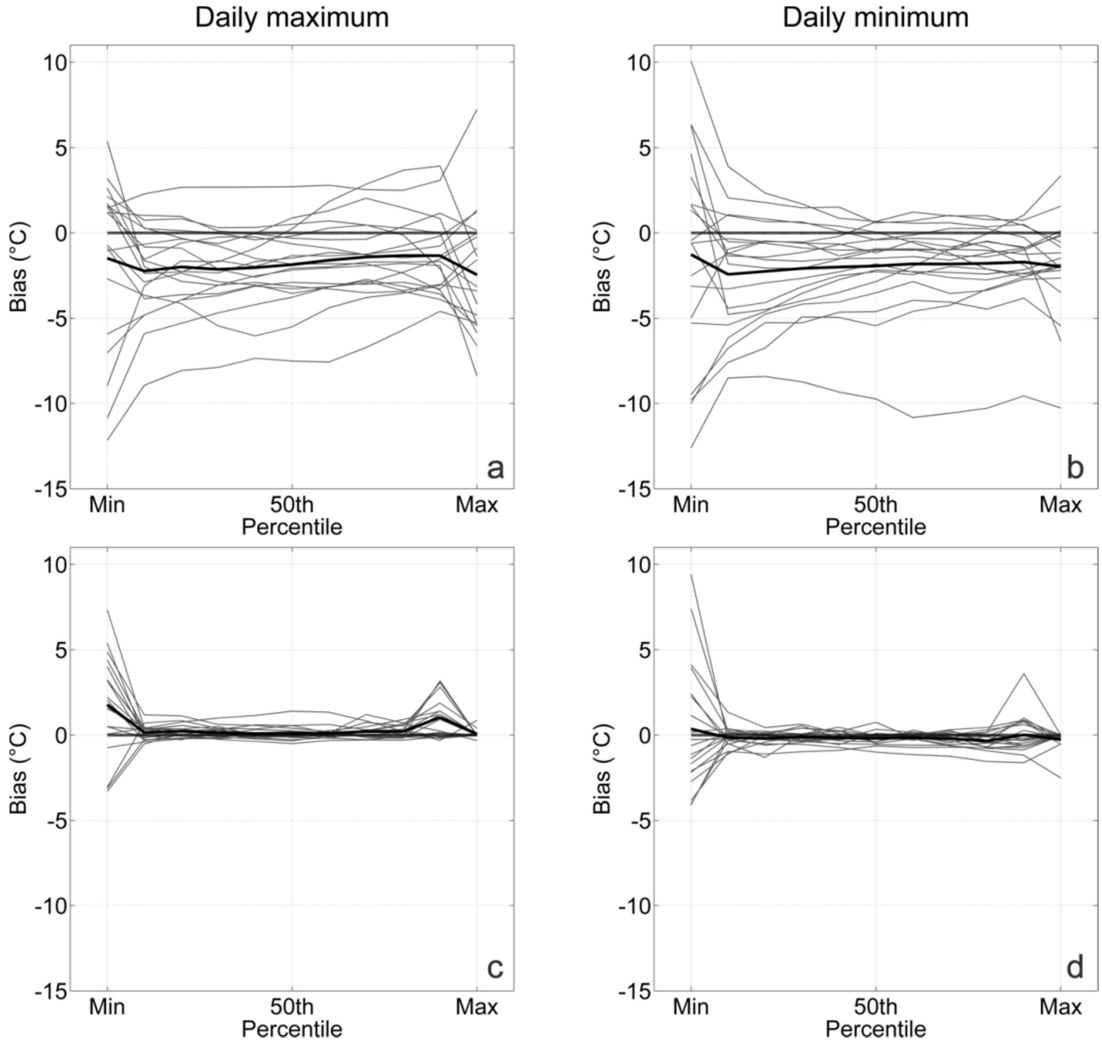


**Figure 3.1:** The GCM bias compared with airport station data at each decile in the daily maximum (left) and daily minimum (right) temperature distributions at each selected airport. All plots show data for the historical period from 1985 – 2005. The top row shows the multi-model mean across 27 un-corrected GCMs, and the bottom row shows bias-corrected GCM data. Each gray line represents an airport, and the solid black line represents the mean across all 19 airports.

While global mean temperatures are projected to rise by 2 – 4°C by 2100 relative to pre-industrial times, changes over land will be larger[39,151]. Changes in extremes may be larger still, with annual maximum airport temperatures projected to increase by 4 – 8°C[77] resulting in substantial fractions of the year being spent above the historical annual maximum temperature,

especially in the tropics where variability is lower[152]. The frequency and severity of extreme heat events have already increased due to climate change[99,153], and future mean warming and potential changes in temperature variability[77,84–86] are very likely to further enhance the risk of unprecedented heat waves.

Aircraft performance data is obtained from publicly available "Airplane characteristics for airport planning" documents which are produced by manufacturers for all commercial aircraft types[154]. These documents specify performance for several different outside air temperatures (starting at 15°C and reaching as high as 50°C) and for airport elevations of 0, 2,000, 4,000, 6,000, and 8,000 feet. To estimate performance curves for temperatures outside or between the ranges presented in the documents, the aviation-standard lapse rate of 2°C/1,000 feet is used with the higher elevation curves (e.g. if the highest presented temperature is 30°C, we estimate sea-level performance at 34°C using the curve for a 2,000 foot elevation at 30°C). Using these data, three-dimensional surfaces relating temperature and TOW to required takeoff runway length for each aircraft type and airport elevation are fitted; Figure 3.2 shows fitted surfaces and weight restriction characteristics. Using the appropriate surface for each aircraft and airport, weight restriction can be calculated at any air temperature and departure weight.

Weight restriction can be partitioned into payload reduction (i.e. passengers and/or cargo) and fuel weight reduction. When payload is reduced, less fuel is required to carry that payload, and less still is required to carry that reduced fuel load. Thus the required payload reduction is less than the total weight restriction. The Base Of Aircraft Data[155] (BADA) aircraft performance[155] model is used to estimate the mean partitioning of a weight restriction for a Boeing 737-800. The partitioning calculation involves three steps: (1) for different TOWs, the total trip fuel is calculated from the BADA equations for cruise and from BADA performance

tables for climb and descent; (2) from these values, the change in fuel required as the TOW varies is determined; and (3) the change in fuel per 10,000 kg (22,046 lbs) change in TOW is averaged over a range of TOWs to get an approximate value of the fuel added per unit change in TOW.

This method estimates that each pound of weight restriction translates into approximately 0.83 lbs of payload and 0.17 lbs of fuel. This relationship is non-linear and depends on the aircraft type, initial TOW, and the atmospheric temperature profile. For example, over trip distances of 1,000 – 3,000 nautical miles for the Boeing 737-800, the fuel portion may vary from 12% to 22% of the weight restriction, corresponding to payload portions of 88% to 78% of the weight restriction. The 83% / 17% aggregate estimate of the partition used in this chapter could be refined for more detailed analyses.

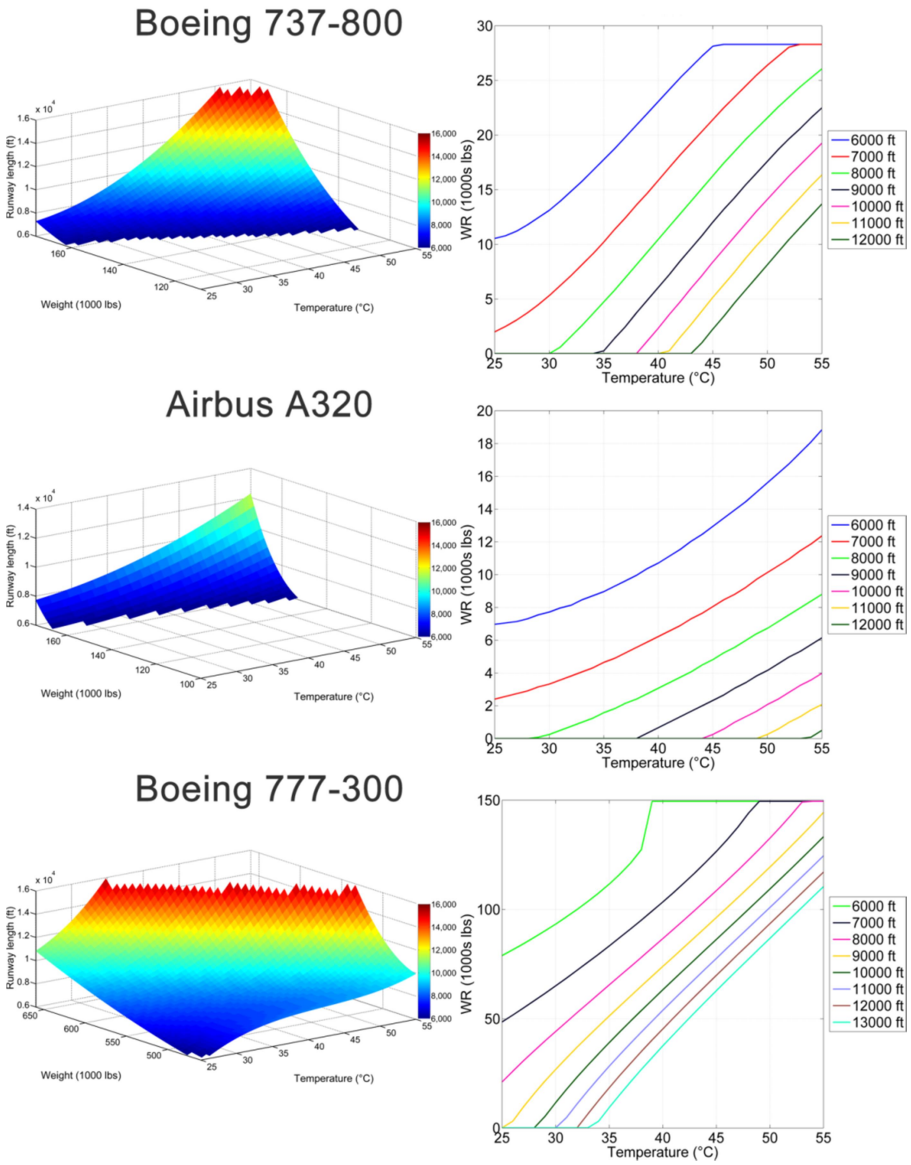


**Figure 3.2**: (left): Performance surfaces and weight restriction data for the Boeing 737-800, Airbus A320, and Boeing 777-300. Surface colors indicate runway length in feet required for takeoff. Data restricted to plausible runway lengths between 6,000 ft. and 16,000 ft. (right): Required weight restriction at a given temperature on a given runway. Similar models were constructed for all aircraft.

To calculate weight restriction for a given airport and aircraft at a specified TOW, the required takeoff runway length is first found using the appropriate fitted performance surface. If this runway length exceeds what is available at the departure airport, the aircraft must be weight restricted; the maximum allowable TOW can then be calculated by moving along the

performance surface at the departure-time air temperature until the required runway length is less than that of the airport's longest runway. The difference between the initial target TOW and the maximum TOW that allows for takeoff on the available runway at the departure-time air temperature is the required weight restriction.

**Results and discussion**

The aviation system, including aircraft and ground operations, has been developed largely based on the climate background of the 1920-1970 period. As temperatures begin to regularly exceed historical bounds, a variety of impacts are likely, from increased weight restrictions to a higher risk of heat stress for outdoor airport workers[48,49]. Figure 3.3 shows historical and projected annual maximum temperature trends as well as the projected mean number of days per year that exceed the historical average annual maximum temperature at two selected airports, New York's LaGuardia (LGA) and Dubai, UAE (DXB) under the RCP 4.5 and 8.5 scenarios. Similar projections were made for all 19 airports. Rising temperatures will result in rapid increases in the number of days that exceed the historical annual maximum temperature[156]; in most cities this frequency may rise to between 10 and 50 days per year by 2060 – 2080.

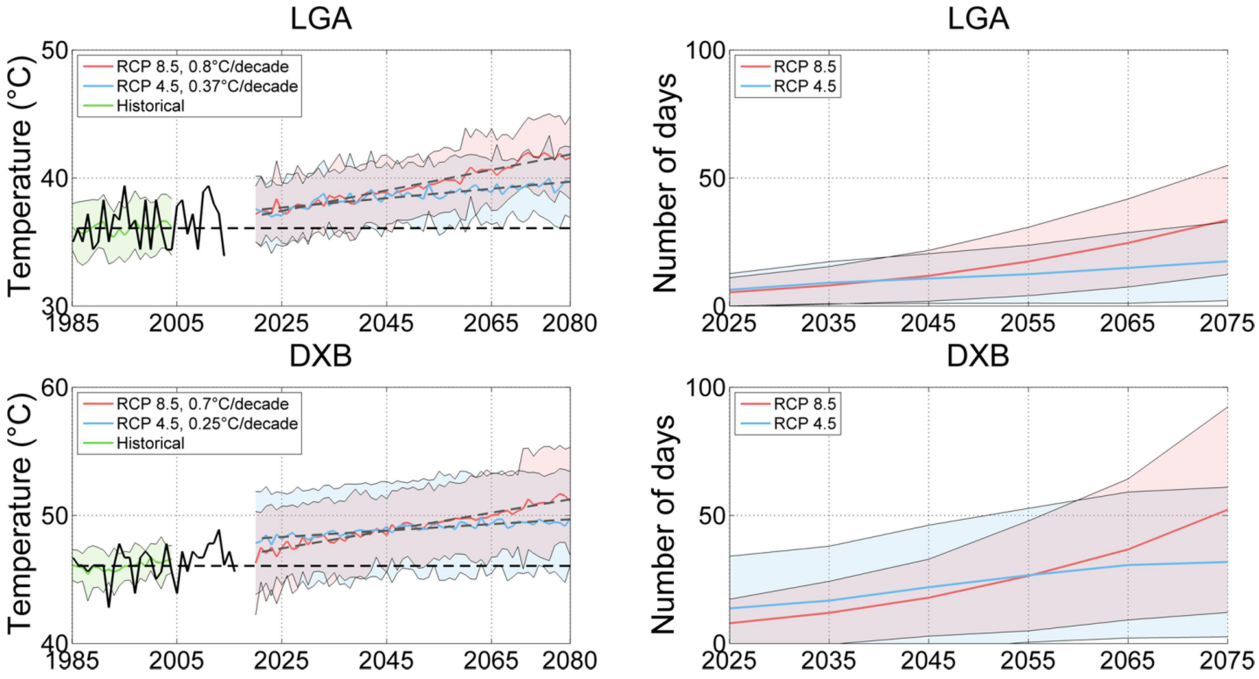


**Figure 3.3:** Left column: historical and projected annual maximum temperatures at New York's LaGuardia (LGA) and Dubai (DXB). The thick black line shows station data and the green line is the bias-corrected multi-GCM mean. The blue line shows bias-corrected multi-GCM mean projections under RCP 4.5, and the red line under RCP 8.5. The shaded regions show ±1 standard deviation across the 27 GCMs, and the dashed gray lines show linear temperatures trends. The thick horizontal dashed black line shows the historical annual maximum temperature based on historical GCM data. Right column: mean number of days per year that exceed the historical annual maximum temperature under the RCP 4.5 (blue) and RCP 8.5 (red) emissions scenarios. Shaded regions show ±1 standard deviation across the 27 GCMs. Similar projections were made for all airports.

Because air traffic volume varies across airports and may change in the future, weight restriction statistics are computed as if there were one takeoff of each aircraft type during each of the 24 hours in every day across all airports. In Figure 3.4, the mean payload reduction is calculated for several airport/aircraft pairs at the time of the daily maximum temperature on all days requiring some weight restriction from MTOW (Figure 3.4a). Figure 3.4b shows the change in the number of days per year exceeding a specified weight restriction threshold, and Figure 3.4c shows the change in the number of days per year experiencing various levels of weight restriction. The changes in mean payload shown in panel (a) vary considerably, but most

aircraft/airport pairs see 5 – 10% increases in payload reduction. Large changes are seen in the frequency of particular levels of weight restriction, with increases by a factor of 1.5 – 4 common by 2060 – 2080; the weight restriction threshold with the maximum frequency change is shown.

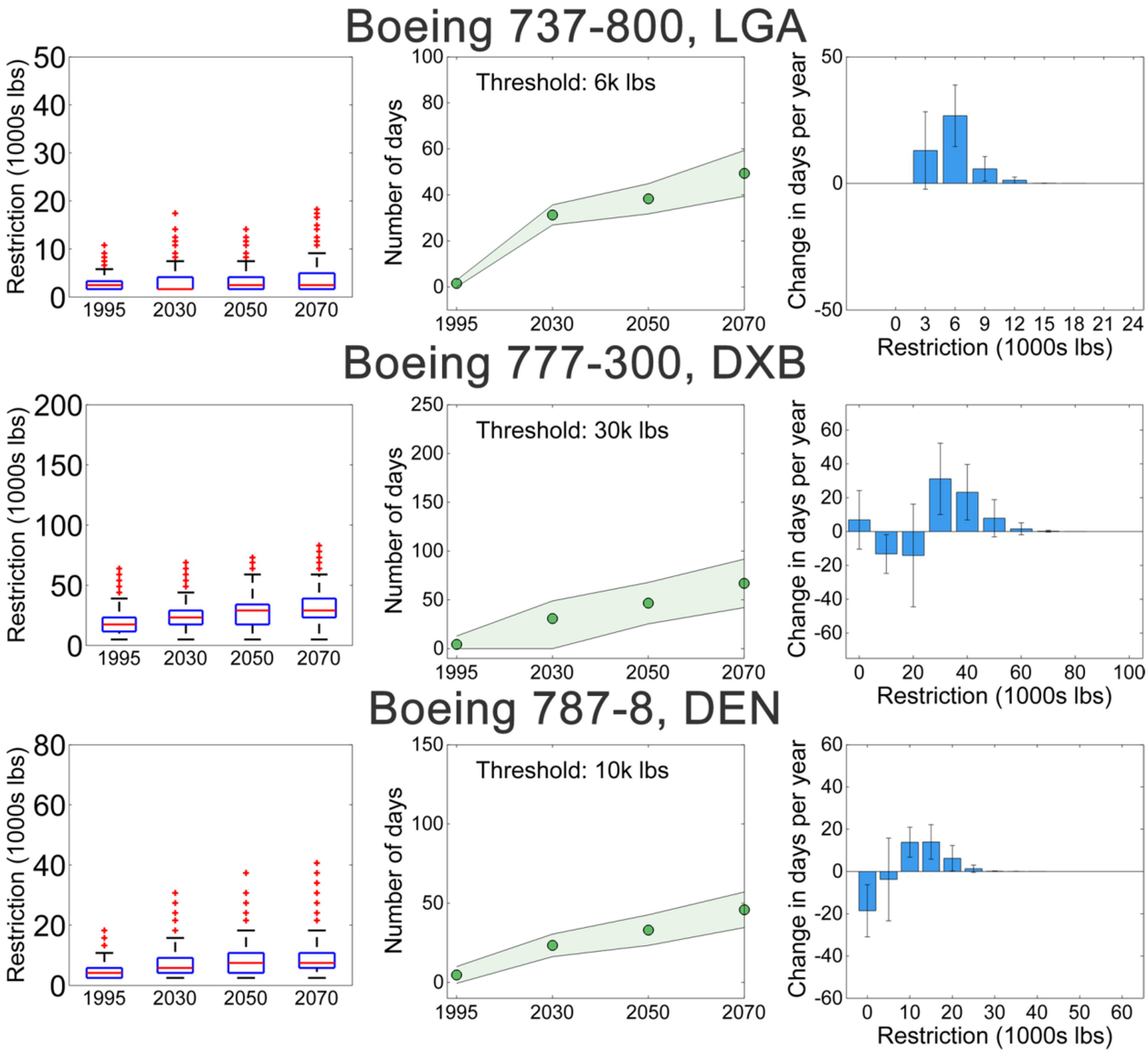


**Figure 3.4:** Weight restriction statistics for selected aircraft/airport pairs. The left panels show mean payload reduction on days requiring weight restriction; the black bars indicate the middle 99.3%, and red crosses indicate outliers. The middle column shows the mean number of days per year that require at least the specified payload restriction threshold; the green shaded region shows ±1 standard deviation across all 27 GCMs. The third column shows the change in the number of days per year requiring different amounts of payload reduction in 2060 – 2080 vs. 1985 – 2005; the error bars show ±1 standard deviation across all 27 GCMs. All projections are made using a combination of both the RCP 4.5 and RCP 8.5 emissions scenarios; weight

restriction projections under both scenarios are combined into one distribution, showing the full range of plausible future outcomes.

Weight restriction is heavily dependent on TOW. If a flight is scheduled to depart well below its MTOW, weight restriction will likely not be needed, even at high temperatures. The distribution of TOWs depends on the specifics of airline operations including route distance, cargo and passenger loads, and fuel reserves, and is difficult to estimate. Instead, weight restriction is modeled at TOW intervals spaced between each aircraft's operating empty weight (OEW, the weight of the airframe with no payload and limited fuel) and MTOW. Figure 3.6 shows weight restriction calculated at the time of the daily maximum temperature. The left panels show the percentage of flights requiring some restriction, and the right panels show the restriction magnitude as a percentage of total fuel and payload capacity. Both panels show the historical period (1985 – 2005) and RCP 8.5 in 2060 – 2080. Climate-related increases in the percentage of flights requiring some weight restriction range from 1 – 10 percentage points, with declines in total payload and fuel capacity of 0.5 – 1.5 percentage points. A small change in the total aircraft fuel and payload weight represents a large decrease in capacity when aggregated across an airline's fleet. For example, a 0.5% decrease from MTOW for a Boeing 737-800 equates to about 722 lbs, or 3 passengers using the airline-standard 220 lbs passenger mean weight. For a normal aircraft configuration of approximately 160 passengers this is nearly 2% of passenger capacity. Such a decrease can have a substantial impact on airline costs.

While the projected change in weight restriction is relatively consistent across aircraft, the total impact of restriction varies. The large Boeing 777-300 and 787-8 are projected to experience the greatest impacts from weight restriction; for an aircraft departing near MTOW, by mid- to late-century total fuel and payload capacity may be reduced by 3 – 5% with 30 – 40% of

flights experiencing some restriction. The Airbus A320 and Boeing 737-800 are less impacted; when departing near MTOW, approximately 5 – 10% of flights may experience some restriction, sacrificing on average 0.5% of their fuel and payload capacity. This is due in part to aircraft design characteristics as well as the fact that most of the world's commercial airports (and those simulated here) have far longer runways than are required by these mid-sized aircraft, even at high temperatures. The A380 is also expected to experience little weight restriction except at extremely high air temperatures, in part due to its exclusive operation at large airports.

The weight restriction burden varies significantly between airports (Figure 3.5).

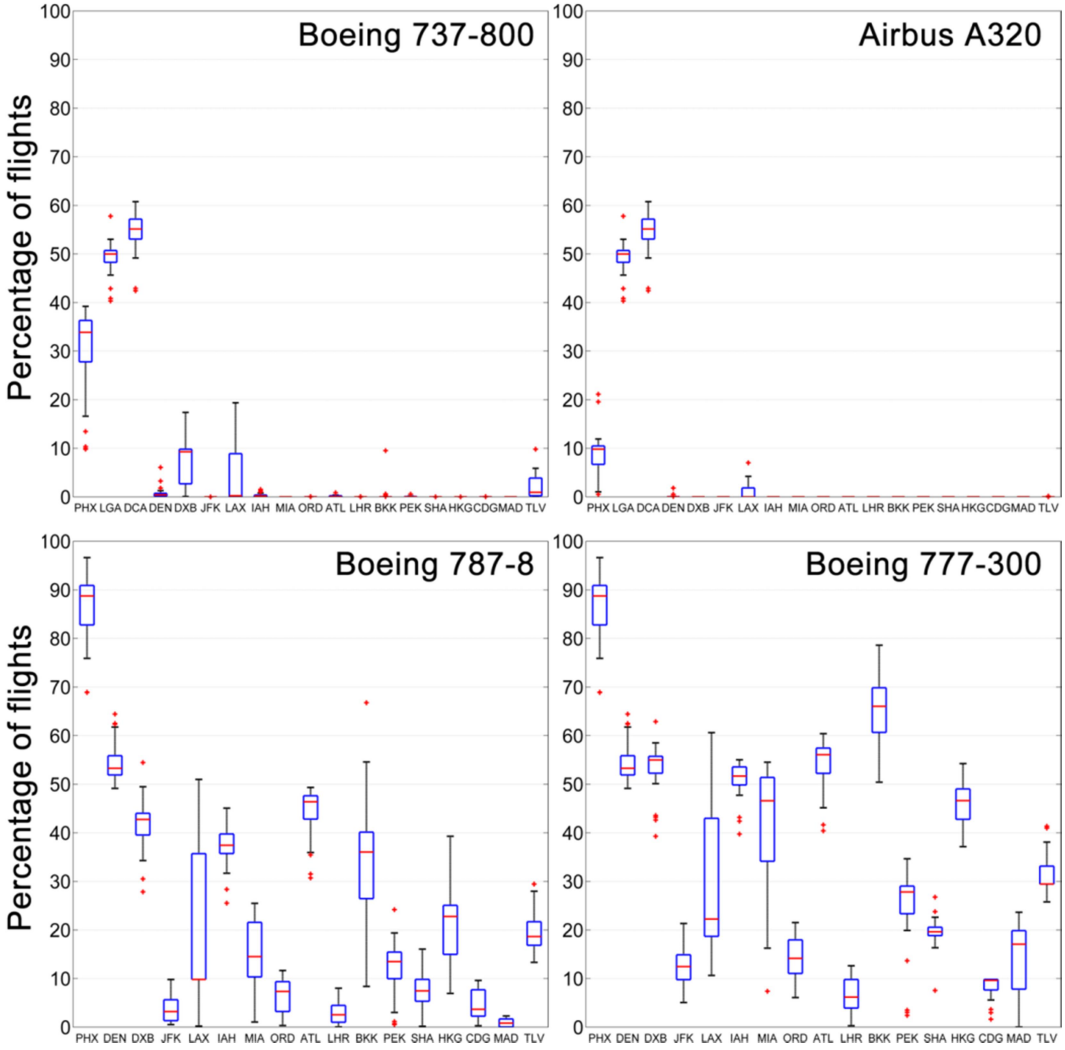


**Figure 3.5:** The percentage of total flights departing at the time of daily maximum temperature requiring some weight restriction at all selected airports. Data are shown for the future period,

2060 – 2080, under the RCP 8.5 emissions scenario. Different airports experience widely varying frequencies of weight restriction due to their runway length, elevation, and climate. The horizontal axis labels show airport codes; see Table 3.1 for corresponding airport information.

At New York's LaGuardia (LGA), a Boeing 737-800 near its MTOW may be weight-restricted approximately 50% of the time when departing at the time of the daily highest temperature and see weight reductions of close to 3.5% of fuel and payload capacity. Similarly, a Boeing 777-300 near MTOW departing from Dubai (DXB) at the time of the daily highest temperature may be weight-restricted about 55% of the time, with weight reductions of up to 6.5% of fuel and payload capacity. The averages over all 19 airports shown in Figure 3.6 are lower, as they demonstrate the system-wide impact of weight restriction, including airports which are minimally affected such as London (LHR), Paris (CDG), and New York (JFK).

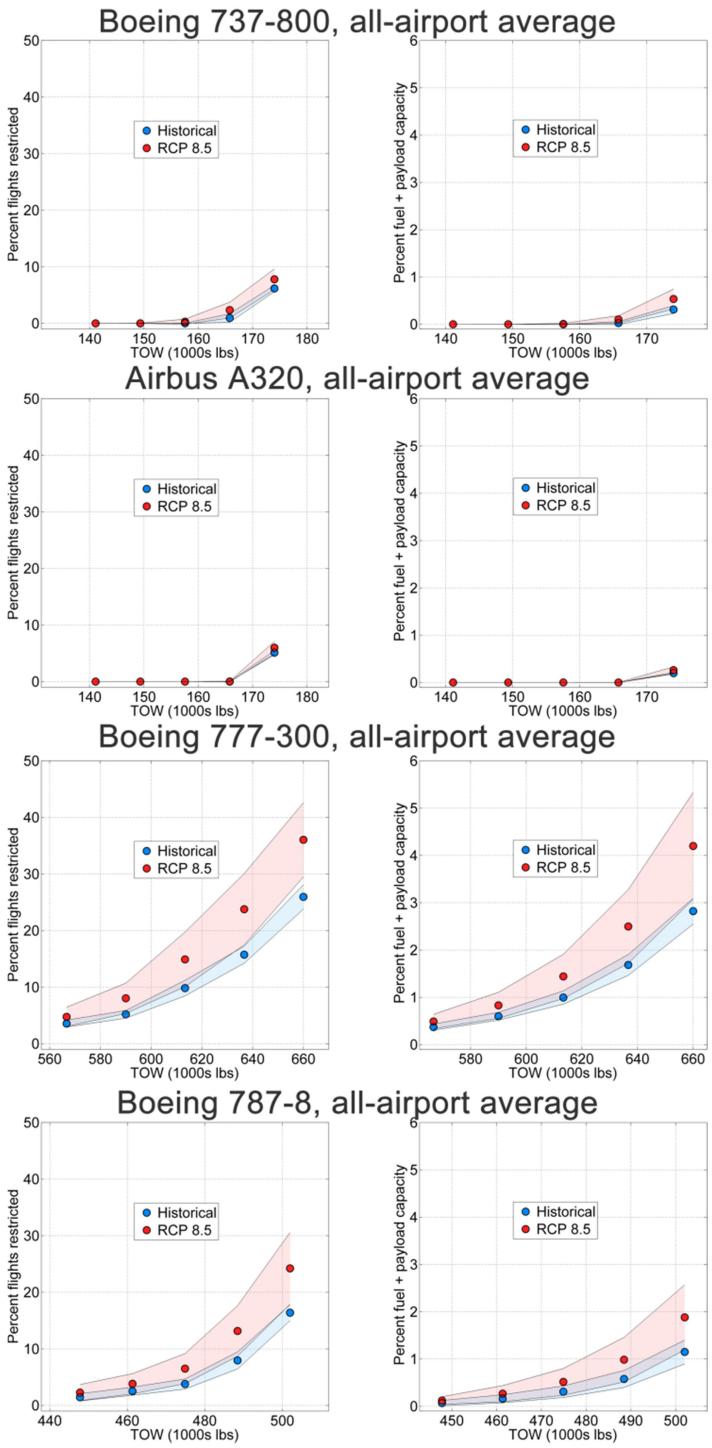


**Figure 3.6**: Weight restriction as a function of TOW in the historical period (blue, 1985 – 2005) and the future (red, 2060 – 2080) under RCP 8.5. Weight is restriction calculated at the time of highest daily air temperature at each of the 19 selected airports and then averaged. The left column shows the percentage of flights with some weight restriction, and the right column shows the restriction as a percentage of total fuel and payload capacity. The shaded region shows ±1 standard deviation across 27 GCMs.

Technological change, including improvements in engine performance and airframe efficiency, will likely ameliorate the effects of rising temperatures to some degree. In addition, the vast majority of weight restriction will occur near the time of highest temperature; in some locations, it may prove feasible to reschedule some flights, especially those with high TOWs, to cooler hours of the day (this is already done at some airports[157]). Airports could also lengthen runways, although such projects are expensive and politically difficult. However, even with adaptation, potentially including new aircraft designs, takeoff performance will still likely be lower than it would have been given no climate change due to both the effects of reduced air density and degraded engine performance and thrust at higher temperatures. This fact is true of all climate impacts: even if they can be adapted to, they still have a cost. A variety of climate impacts on the aviation industry are likely to occur in the coming decades, and the sooner climate change is incorporated into mid- and long-range plans the more effective adaptation efforts can be.

**Table 3.1**: Airport info using IATA codes, taken from official airport charts. Runway length and airport elevation are incorporated into weight restriction calculations.

| Airport code | Location | Maximum runway length(feet) | Elevation (feet) |
|---|---|---|---|
| PHX | Phoenix, AZ, U.S. | 11,489 | 1,111 |
| DEN | Denver, CO, U.S. | 16,000 | 5,321 |
| LGA | New York, NY, U.S. | 7,003 | 11 |
| DCA | Washington, DC, U.S | 7,170 | 11 |
| ORD | Chicago, IL, U.S. | 13,000 | 672 |
| ATL | Atlanta, GA, U.S. | 12,390 | 1,018 |
| JFK | New York, NY, U.S. | 14,511 | 12 |
| LAX | Los Angeles, CA, U.S. | 12,091 | 120 |
| IAH | Houston, TX, U.S. | 12,001 | 95 |
| MIA | Miami, FL, U.S. | 13,016 | 7 |
| DXB | Dubai, United Arab Emirates | 13,147 | 62 |
| LHR | London, UK | 12,800 | 83 |
| BKK | Bangkok, Thailand | 13,100 | 1 |
| PEK | Beijing, China | 12,400 | 116 |
| SHA | Shanghai, China | 13,100 | 13 |
| HKG | Hong Kong | 12,400 | 28 |
| CDG | Paris, France | 13,700 | 400 |
| MAD | Madrid, Spain | 14,200 | 2,000 |
| TLV | Tel Aviv, Israel | 12,000 | 135 |

**Table 3.2:** Weight and selected performance surface parameters for each aircraft. Operational empty weight (OEW) indicates the weight of the aircraft with no payload and minimal fuel. Maximum takeoff weight (MTOW) is the highest allowable weight at takeoff. Fuel and payload capacity is equal to MTOW minus OEW. Performance surfaces were fit using Matlab, and the fit selections for each dimension (temperature, TOW), were selected to best represent performance data within real-world temperatures and weights.

| Aircraft | Operational empty weight (1,000s lbs) | Maximum takeoff weight (1,000s lbs) | Fuel & payload capacity (1,000s lbs) | Surface model |
|---|---|---|---|---|
| Boeing 737-800 | 91 | 174 | 83 | $2^{nd}$ degree in temperature, $3^{rd}$ degree in TOW |
| Boeing 787-8 | 260 | 502 | 242 | $2^{nd}$ degree in temperature, $3^{rd}$ degree in TOW |
| Boeing 777-300 | 299 | 660 | 361 | $3^{rd}$ degree in temperature, $2^{rd}$ degree in TOW |
| Airbus A320 | 93 | 174 | 81 | $2^{nd}$ degree in temperature, $3^{rd}$ degree in TOW |
| Airbus A380 | 610 | 1,260 | 650 | $2^{nd}$ degree in temperature, $3^{rd}$ degree in TOW |

# Chapter 4 Adaptation to heat in urban areas[158]

**Coffel, E. D.**, Sherbinin, A. de, Horton, R. M., Lane, K., Kienberger, S., & Wilhelmi, O. (2017). The Science of Adaptation to Extreme Heat. In T. Frank & Z. Zommers (Eds.), *Resilience - The Science of Adaptation to Climate Change*. Elsevier. In press.

## Introduction

In recent years, research has focused on extreme heat as a serious risk to human health[51,61,159–161], agriculture[52,53,81,120], infrastructure[46,69,143–145], and economic performance[37,59,81]. Recent heat waves, which have been responsible for tens of thousands of additional deaths and damage to infrastructure and agriculture[99], have been linked to climate change[3,103–105,162], and the IPCC has concluded that the frequency, severity, and duration of extreme heat events is very likely to increase worldwide in the future[39]. The substantial impacts that result from present-day heat waves serves as a warning that future extreme temperatures are likely to cause increased harm to people around the world, in rural and urban areas, and in low- and high-income countries[163]. Adaptation to reduce these impacts is essential, and scientific research plays a key role in determining which strategies are most effective in varying climatic and societal conditions, as well the best methods of targeting adaptation to the most vulnerable populations. This chapter will review research surrounding adaptation strategies to extreme heat. It will not present new scientific research, but will address methods of reducing the impacts of the increased temperatures and heat stress that are described in Chapters 1 and 2. This chapter will first consider drivers of local variation in projections of future heat, the urban heat island effect, and urban microclimates, and then turn to population vulnerability, the health impacts of heat stress, and the interaction with air quality and infrastructure. Subsequent sections address adaptation strategies informed by science and human behavior, which is a critical element in responses to extreme heat. A concluding section addresses the importance of using evidence-

based adaptation strategies in developing heat-related adaptation initiatives so as to improve the cost-effectiveness and efficacy of these strategies and to reduce the risk of mal-adaptation.

**Heat projections**

Climate change resulting from greenhouse gas emissions is expected to result in a mean global temperature increase of 1.5 – 4°C by the end of the 21st century [39]. Warming will likely continue into the 22nd century depending on how rapidly net emissions of greenhouse gases and other radiatively important agents like aerosols are reduced, as well as the success of potential negative emissions technology. Temperature changes over land will be larger than the global mean[151], with more warming expected over high latitude land masses than tropical ones. There is also evidence that the most extreme temperatures may increase more than the mean in some regions[77,84,85].

Climate change has already resulted in 0.8 – 1°C of warming as compared with pre-industrial times[135]. This upward shift in the temperature distribution has been manifest as increases in the frequency, duration, and intensity of heat waves[164–166], as well as a rise in the global land area coverage of above average temperatures[156]. Extreme heat events have intensified due to changes in the mean temperature alone[128]; there is some evidence, however, that temperature variability may also increase in the future due to a variety of physical processes[27,86,107], although this has not yet been observed on a global scale[88] and may be accounted for by varied rates of mean temperature change[76].

Climate change will intensify the hottest heat events, but an equally serious effect will be to drastically increase the frequency of temperatures that are currently considered severe[167,168]. In the tropics, where temperature variability is lowest, by mid- to late-century a large portion of the

year may be spent above the current average annual maximum temperature[85], resulting in significant increases in exposure to extreme heat events such as the heat wave that struck India in 2015[102]. The mid-latitudes too will see significant changes; recent research projects that the number of days exceeding the annual maximum temperature could increase by a factor of 10 – 20 in cities across the United States[77] by mid-century (2050 – 2070). As an example, this means that Baltimore, MD, could potentially experience 15 – 20 days above the current average once-per-year hottest temperature of 37°C. These changes in the frequency of extreme events will occur rapidly in the coming decades, regardless of emissions reductions.

While many impacts of heat depend on temperature alone, human health and wellbeing also depend on humidity. The human body is highly efficient at controlling its core temperature through evaporative cooling as long as relative humidity is low. However, as relative humidity rises, thermal regulation becomes difficult and the risk of physiological stress is amplified. A variety of metrics are used to estimate the combined impacts of temperature and humidity. The most commonly reported heat stress indicator is the heat index, or the "feels like" temperature, which is widely presented in weather reports in the United States, for example. There are many variations of the heat index algorithm[169], but all are based on empirical formulae calibrated to relate temperature and humidity conditions to physiological impacts[170]. This task requires that the index include assumptions about body type, clothing, wind, and activity level – varying these parameters can have a substantial impact on potential heat risk, making the heat index a problematic general heat stress index.

The wet-bulb globe temperature (WBGT) is the most widely used heat stress index in workplace safety, athletics, and the military[109]. It is a weighted average of the dry bulb, wet bulb, and globe (also known as the mean radiant temperature and is measured using a thermometer

inside of a black sphere) temperatures, and can be measured directly or estimated using an empirical model. There is extensive calibration data relating WBGT thresholds to levels of heat risk; however, as with the heat index, differences in clothing, activity level, and other individual factors can substantially degrade its ability to predict heat illness. Research suggests that most heat stress indices perform similarly in predicting heat-related mortality, likely due to their strong correlation with temperature[171].

Other, less widely used indices exist, such as the apparent temperature[172], HUMIDEX[173], the environmental stress index (ESI)[174], and the human thermal comfort index (HTCI)[175]. A more physically based measure is the wet bulb temperature, which represents the lowest temperature that can be achieved through evaporative cooling alone. While there is little empirical evidence relating wet bulb temperature to heat stress impacts, the direct relationship between wet bulb temperature and evaporative cooling makes it relevant to human health since the body sheds heat through the evaporation of sweat. Recent research has posited that when the wet bulb temperature exceeds the skin temperature, the body will no longer lose heat through evaporative cooling, and heat illness will occur with prolonged exposure. This wet bulb temperature threshold, about 35°C, may pose a fundamental limit to heat adaptation[48], although in practice those exerting themselves outdoors, exposed to sunlight, and those more vulnerable to heat would be unable to tolerate the heat at much lower temperature and humidity combinations.

Climate change has been linked to a rise in the WBGT since the 1970s[111], and there is evidence that wet bulb temperatures could regularly approach the 35°C limit by late century in certain densely populated regions[49,50]. Thus far, the literature on heat stress and heat-induced mortality has focused on the effects of high air temperatures[176], which in many locations are strongly correlated with high wet bulb temperatures and other measures of heat stress. However,

the possibility of reaching wet bulb temperatures of 35°C indicates an urgent need for research into the effects of extreme heat and humidity on human health, and whether temperature alone may not be a sufficient predictor of heat illness in the future if mortality begins to respond non-linearly to extreme heat and humidity. In addition, livestock and other large animals may be severely affected by rising temperatures, potentially with impacts on agriculture and food supply.

**Microclimates and the urban heat island**

Temperatures can vary across small spatial scales, resulting in different levels of heat exposure between neighborhoods within a city or, to a lesser extent, between localized regions in rural areas. These microclimates have a variety of causes, including land cover[177], vegetation, material use, local air quality[178], and localized weather associated with topography and coastal effects. In addition, development patterns and socioeconomic conditions can result in large differences in heat stress vulnerability between or within neighborhoods[179]. In many high-income cities, dense development, lack of vegetation, and scarce open space are linked to higher temperatures. These areas also are often occupied by people with fewer economic and social resources to cope with heat[175]. By focusing on both climate and social microenvironments, heat adaptation strategies can be targeted to the most at-risk populations.

The urban heat island (UHI) effect is a long studied phenomena[180] which can amplify temperatures in metropolitan areas by 1-4°C during the day and up to 10°C at night. The UHI is observed in long term temperature records and is large enough to necessitate a correction factor in calculations of global mean temperature[181]. There are five key physical causes of the UHI, the most important of which is the loss of convective efficiency between the surface and the lower atmosphere[117] in urban areas due to the reduced surface friction over smooth, paved city

landscapes. Other drivers of the UHI are reduced evaporative cooling in cities due to lower levels of vegetation cover, enhanced energy absorption due to reduced albedo, increased energy storage by artificial materials, and direct waste heat release from buildings, industry, and vehicles.

Approximately 50% of the world's population lives in urban areas[182]; given the strong warming effect of the UHI – especially with regard to nighttime temperatures – mitigating urban warming could substantially reduce global heat exposure[179]. Effective mitigation of the UHI will require localized adaptation, as the relative importance of the physical drivers listed above depends on the background climate and the characteristics of the city, and each physical driver can be combated through different adaptation strategies. Most research on the UHI to date has focused on high-income cities; more work is needed to quantify the effect and causes of the UHI in low- and middle-income countries, as well as the influence of local air pollution on urban temperatures[183]. A first-ever global estimate of the UHI across all major cities using land surface temperature data found that the biggest factor in determining the degree of UHI is the size of city, and that many tropical cities experience more than a 3°C nighttime temperature differential between urban and surrounding rural areas[184].

**Population vulnerability**

Vulnerability to heat stress and mortality during heat waves varies widely among populations[185,186]. The elderly[187] and those with pre-existing health conditions – especially limited mobility, obesity, and serious mental illness[134] – are more susceptible to heat illness and death. However, the young (including infants[188]), too, are vulnerable to heat. Early heat stress research focused on military training and athletics[109,189], and those performing rigorous physical labor or wearing confining clothes can experience heat illness, no matter their age[190]. Some

classes of medications, such as antipsychotics, can impair thermoregulation, potentially increasing risk during hot weather[191]. Research also suggests that heat illness can have profound and long-lasting health impacts, contributing to a higher risk of future illness and early mortality[192].

Experience from recent heat waves has shown that social isolation is a major risk factor for heat illness; in the 1995 Chicago heat wave, many deaths occurred in single-person households in neighborhoods without convenient public transportation or strong community structures[193]; these regions also have decreased community cohesiveness, with higher crime rates, declining population levels, more empty housing stock, and reduced levels of business and other street activities[194]. Many studies in the United States have also found that African-Americans are at higher risk of heat illness[195], likely reflecting lower access to air conditioning and greater baseline health challenges due to higher rates of poverty.

A consensus is emerging that large scale heat-related mortality events are primarily social disasters, which can be ameliorated through behavioral adaptation. Evidence of reduced heat risk can be found in France: during the 2003 European heat wave, an estimated 15,000 people died of heat-related illness[196]. After that event, heat adaptation measures were put into place at the national and local levels including opening cooling centers – free public spaces with air conditioning and water – and promoting public heat-safety awareness; in 2006, another heat wave occurred, and statistical comparisons to the 2003 event suggest that adaptation measures reduced heat-related mortality by approximately two-thirds[113].

Exposure to high temperatures during a heat wave can vary across a population due to socioeconomic factors[197]. A variety of mapping studies have helped to identify those neighborhoods most likely to be vulnerable to extreme heat, which can help in targeting

adaptation activities[179,182,198]. Air conditioning is the most effective way to prevent heat-related illness and death, and lack of air conditioning, which is closely tied to income, is a major vulnerability factor[199]. Cities in the United States with higher air conditioning prevalence have been found to have lower rates of heat-related mortality[200], and the long-term decline in heat-related mortality may largely be due to the increasing prevalence of air conditioning[160,201]. However, as long as electricity is supplied by fossil fuel sources, increased air conditioner use will worsen the underlying problem of greenhouse gas emissions.

Housing and neighborhood characteristics also play a role in risk; during the 2003 heat wave in France, those living on the top floor of a building or those in buildings with little nearby vegetation were more likely to die, likely due to exposure to localized higher temperatures[134]. People in more vulnerable housing are often those with the least social resources, concentrating risk in marginalized groups of society[193]. In addition, areas with higher poverty levels may be home to more people with multiple chronic health conditions and fewer resources to prevent and treat illness[202]. These neighborhoods may also have more physical vulnerabilities. In New York City, for example, neighborhoods with less green space, higher surface temperatures, and more people needing financial assistance were associated with more excess deaths during and after heat waves[203].

In many urban heat events, existing resources such as cooling centers have not been utilized by vulnerable people for a variety of reasons including inability to get to the center, concerns about theft, personal safety, and the well-being of pets[204], as well as concern about the stigma of accepting public assistance[205] and preference for staying home[199]. Research and experience show that awareness of a heat warning does not necessarily translate into an individual taking protective action[206]. Close attention to public perception of heat adaptation

strategies and awareness of behavioral tendencies, along with effective risk communication, is essential to effective urban adaptation. Simply providing the opportunity to seek shelter from heat isn't enough; people must be aware of the danger of heat, willing to admit their personal risk, and be able and motivated to seek help when they need it.

Less research has been conducted on vulnerability in lower- and middle-income countries, but it is likely that similar factors apply: the elderly, those with pre-existing health conditions, and those without access to air conditioning or safe water are at high risk during heat waves. Other factors likely are important as well, especially the relationship between heat, drought, and water/food insecurity in low-income regions. In addition, in many low-income rural areas, a high proportion of the population works outdoors, making occupational exposure to heat stress a major concern[207].

## Health impacts of heat stress

### Physiology

Humans must maintain an extremely narrow core temperature range to live, but the body is capable of tolerating temporary high levels of heat stress[208]. Heat illness (hyperthermia) results from the body's failure to maintain its normal core temperature, and exposure to extreme heat can result in a range of health impacts. Heat illness can range from fatigue, syncope, and cramps to heat exhaustion, which is generally reversible given prompt medical treatment, and finally to heat stroke, a medical emergency which can cause long-term organ damage and rapid death through multi-organ failure[209].

Acclimatization to a wide variety of climates is possible through technology and behavioral adaptation, and to some extent, physiological[210] changes. Physiological adjustment to

heat, however, happens slowly over the course of repeated exposures, as when one relocates to a warmer climate; physiological change is unlikely to protect against infrequent extreme heat events[211]. The degree of acclimatization varies in different regions and for different climatic variables. Research has suggested that in the United States acclimatization to cold is more spatially uniform than for heat, as suggested by the relatively similar levels of temperature-induced mortality in cold weather across the country. Heat has been found to produce more varied mortality responses, with some regions – like the hot U.S. Southwest – seeing smaller changes in mortality during heat waves than cooler regions under similar departures from the local mean temperature (e.g. a hot day reaching the 90$^{th}$ percentile relative to the local temperature distribution)[200]. This difference is due to different baseline temperatures and also may be due in part to better air conditioning coverage in hotter regions, as opposed to the Northeast United States or Europe, where coverage varies[176]. In addition, the risk of widespread heat illness may be greatest when temperatures rise far above the local climatologically normal range, which is most likely to occur in the mid-latitudes where temperature variability is greatest.

Emergency room visits and hospital admissions for certain cardiovascular, respiratory, renal, and mental health[212,213] conditions have been observed to spike during heat waves[214,215]. Similarly, on days with extremely high temperatures, overall mortality from natural causes is generally greater than what would be expected during summer. For example, a 2010 heat wave in Ahmedabad, Gujarat, India, a city that routinely deals with hot temperatures, resulted in 1,344 excess deaths, or a 43% increase in all-cause mortality[216]. In 2015 a heat wave in India resulted in over 2,300 deaths[217], and the severe June 2015 heat wave in Pakistan resulted in 17-fold increase in heat-related mortality in Karachi; this is likely an underestimate due to the challenges

of tracking and recording deaths in an under-resourced area[101]. Mortality often falls after heat waves end, as vulnerable people may die earlier than they would have absent the heat.

The World Health Organization (WHO) estimates that only four countries in Africa – Algeria, Mauritius, Seychelles and South Africa – have high quality daily death data[218]. In countries lacking enough death data for analysis, heat-related mortality and morbidity may go unrecorded. Excess mortality associated with heat also occurs during hot, but not extreme, summer conditions[219]. Because there are more of these days in any given summer, substantial mortality may occur outside of extreme events. Rising average temperatures due to climate change may lead to increases in this non-extreme excess mortality as well.

**Historical trends and future projections of heat wave mortality**

Many studies have quantified the excess deaths attributable to heat across the world and have projected how these mortality rates may change in the future[51,80,159–161,176,220,221]. Heat-related mortality in the United States is found to have declined throughout the 21st century[160], likely due to the spread of air conditioning throughout the country and generally improving health[201]; however, some studies indicate that the decline has stopped[222]. Almost all research concludes that heat-related mortality is likely to substantially increase in the future[196,223], due to both higher temperatures and much higher levels of exposure[106], and that this increase will not be offset by declining cold-related mortality[221].

Most projections of future mortality rely on statistical models fit to historical daily mortality data. It is difficult to estimate the impacts of adaptation on future mortality, and there is some evidence that aggressive strategies to protect the most vulnerable populations can have a large impact[113]. However, there is also evidence that heat stress may begin to approach

fundamental limits for prolonged human tolerance[48,49]; it is unknown how mortality will respond to such thresholds, but it is reasonable to expect substantial increases without aggressive adaptation measures. More research into the relationship between extremely high wet bulb temperatures and mortality is urgently needed, as some of the world's most densely populated regions in India, Africa, and the Middle East could experience wet bulb temperatures approaching the theoretical limit for human tolerance – 35°C – by mid- to late-century[50]. More research is also needed on the relationship between heat and other stressors outside the scope of this chapter such as drought, food and water insecurity, political instability, and conflict.

The UHI results in urban populations suffering greater exposure to extreme heat, but research does not necessarily find that urban areas experience the highest rates of heat-related mortality[80]. While temperatures are higher in cities, urban residents may also have more access to air conditioning, water, and social support, especially in low-income countries with substantial income divides between rural and urban areas. More research is needed on mortality in rural areas, especially in low-income regions.

## Urban heat, air quality, and infrastructure

### Air quality

Air pollution is estimated to result in the premature deaths of approximately three million people each year, far more than from heat directly, mostly in low- and middle-income countries and in both urban and rural areas[224]. The main emission sources that contribute to air pollution are electricity generation, heavy industry, vehicle engines, both natural and human biomass burning, and agriculture. Like heat, air pollution is a physiological stressor which can both cause acute illness – especially respiratory and cardiovascular conditions – as well as exacerbate

existing health problems. In addition, heat stress and poor air quality are often coincident, amplifying their impact; a substantial proportion of the deaths attributed to the 2003 European heat wave may have been caused by or related to air pollution[225]. Future particulate emissions are highly uncertain, but under a business as usual scenario premature air quality-related mortality could double by mid-century[224] due to a rise in both population and emissions, especially in Asia and Africa.

High air temperatures can worsen local air pollution in some cases even without additional emissions[226]. Regional ground-level ozone ($O_3$) pollution in already polluted areas is correlated with temperature. High temperatures accelerate the photochemical processes that generate $O_3$, and they may also increase natural biomass burning (e.g. wildfires) which may generate $O_3$ precursors (possibly only when combined with anthropogenic $NO_x$ emissions)[227]. However, precipitation and humidity tend to reduce pollution through wet deposition and convective atmospheric venting. Most models project increases in warm-season $O_3$ levels in already polluted regions and more intense $O_3$ pollution during heat waves[228], a phenomena known as the "climate penalty"[229]. However, global background $O_3$ is projected to decrease due to increased atmospheric water vapor content. The effect of climate change on particulate matter is more uncertain[230], but some studies suggest that if global aridity increases, dust and wildfire emissions could contribute to at least localized increases in particulate and aerosol pollution[226].

There is also evidence that climate change may increase the frequency of meteorological conditions favorable to poor air quality in some regions[231,232]. Air pollution episodes are associated with calm winds, low humidity, and temperature inversions, where the atmospheric lapse rate becomes negative near the surface, causing temperature to increase with height and acting as a block on vertical convective air movement. In some regions, notably China, these

conditions are expected to become more likely in the future due to circulation changes[232]. Precipitation helps to clear the air of particulate matter[226]; while more of the globe is projected to see precipitation increase than decrease under climate change due to increasing atmospheric water vapor[16], even regions with more overall precipitation may see longer dry spells with a larger fraction of precipitation falling in a smaller number of events[2,17], allowing pollution to accumulate. It is also possible that pollen production could increase in some regions due to a lengthened growing season, potentially worsening allergies and asthma for some populations[233].

**Infrastructure**

High temperatures have strongly negative effects on urban infrastructure, affecting electricity generation[82,234] and transportation[235,236], both of which can contribute to human health impacts by reducing the availability of air conditioning, medical treatment, and in low-income countries, food and safe water. In severe heat waves, the loss of electricity due to excessive demand or heat-induced equipment failure can result in the potentially dangerous loss of air conditioning and refrigeration[83]. For vulnerable populations, air conditioning can be a life-saving necessity during the most extreme heat, and thus maintaining electricity supply can be critical. Electricity demand is expected to rapidly rise due to development and population increase, especially in Asia and Africa[237]. Many of these regions are also prone to extreme heat, and since peak electricity load is strongly correlated with temperature (largely due to air conditioning)[234,238], it will be important to consider resilience to increasing temperatures in the design of electricity transmission grids and generation equipment.

Transportation infrastructure, including roads, railroads, and the aviation system[46,69,143,145], can experience performance loss or failure in hot conditions[239]. In addition, the

large spatial extent of heat waves means that there is the potential for significant disruption to transportation networks during severe heat events. Since even localized failures can result in cascading delays throughout a transportation network, it will be important to consider changing extreme temperature events in the design of future infrastructure.

## Adaptation Strategies

A variety of adaptation strategies exist to mitigate the impacts of extreme heat and the UHI. Some of these practices are standard in high-income cities around the world, such as air conditioning access, public cooling centers, and weather forecasts warning of the dangers of heat waves and air pollution. Other techniques require architectural or urban design changes and are not yet widely used. This section presents the evidence supporting some of the most prominent methods to both cool urban areas and reduce the human impacts of heat.

### Green spaces

Green spaces, from large parks to trees and grass, can reduce local temperatures by 1 – 6°C during the day, in both the sun and shade, through albedo change, reduced surface heat storage, and increased evapotranspiration[102,240–245]. Trees, plants, and green spaces can also reduce local air pollution, improve human wellbeing in dense urban areas[246,247], and increase property values[248]. Due to increased evapotranspiration, it is possible that wet bulb temperatures could be higher in vegetated areas; more work is needed to quantify the tradeoff between reduced temperatures and more humidity.

The amount of cooling that a green space provides depends on its design, the characteristics of the surrounding urban area, and the local climate. Case studies of specific green

spaces have found some provide the strongest cooling effect during the day[241], while others are most effective at night[249] especially in regions with high building height-to-street-width ratios. Research in an arid city in China found that small but densely-spaced green patches were more efficient at reducing surface temperature than sparse but large spaces; this may be especially relevant in water-constrained regions[250]. While green spaces are generally cooler than their surroundings, they have been found to have little or no impact on ambient temperatures outside of their boundaries[240,241,244]. The effectiveness of a green space may be enhanced in dry climates, as low relative humidity allows for evaporative cooling of water transpired by plants; studies in humid regions have generally shown less of a green-space cooling effect[251].

The type of greenery has an impact on the effectiveness of a green space at reducing urban temperatures. Parks with trees may have a stronger cooling effect than those without[252]. Even single trees can reduce energy costs by providing shade on buildings; a study in Sacramento, CA in the United States found that each residential tree providing shade to a house reduces air conditioning energy use by 7% while increasing winter heating energy use by only 2%[253]. However, the impact of street trees on ambient temperatures is uncertain; some studies have found reduced temperatures near trees, while others have found little effect[241].

Current research suggests that green spaces and urban parks are essential for wellbeing in dense cities and can reduce air pollution and provide limited cooling, but they are unlikely to substantially reduce the average temperature across large urban areas.

**Cool roofs**

Modifying roof color can raise the albedo and thus lower the energy absorption of a large building, providing a cost effective method of reducing cooling energy use in warm climates;

recent research has suggested that cool roofs, whether white (in color) or green (e.g. vegetation-covered), be adopted in warm climates[245,254,255]. A large fraction – perhaps up to 10% – of urban air conditioning energy use goes towards cooling the heat added by the UHI[256], and air conditioning units also produce substantial waste heat. A dark colored roof, the standard in the U.S., absorbs up to 80% of incoming solar radiation, where as a white roof reflects 50 – 80%[256], potentially reducing building energy consumption by up to 20%[257,258]. Modeling studies, backed by empirical tests, suggest that white and green roofs applied across a city could reduce urban temperatures by 1 – 2°C, substantially countering the UHI[259–262]. Green roofs reduce ambient temperature mainly through evapotranspiration, while white and reflective roofs cool by raising the mean albedo of an urban area. The effect of both is greatest during the day, with limited night-time cooling[260]. When applied globally, one study suggests white and green roofs could provide the cooling equivalent of removing 1 – 4 years of current human $CO_2$ emissions from the atmosphere (approximately 0.05°C in global mean cooling)[263]. In metropolitan regions, these temperature reductions account for a substantial fraction of the current UHI and could offset a portion of the heat effects of future climate change for large populations[264].

Green roofs are more expensive than white roofs and are less effective at raising albedo; however, they can reduce storm water runoff[265] and can provide localized evaporative cooling[259]. Green roofs may also improve ecological connectivity, and can provide public green space if so configured[266,267]. Their cost effectiveness depends on the climate; energy savings may be outweighed by irrigation costs in arid regions, and by installation costs in temperate zones[268]. Green roofs may also necessitate structural modifications in some buildings, while white roofs may require frequent cleaning and re-painting to maintain strong albedo benefits.

Overall, research suggests that cool roofs are a promising approach to reducing urban energy use and ambient temperature, and most research suggests that white roofs are the most effective and cost efficient option.

**Building design**

The geometry and material used in urban structures affect their thermal properties. Many common building materials, especially those with a low albedo like concrete and asphalt, store heat and contribute to UHI.

The geometry of urban streets can affect the strength of the UHI; urban canyons, or streets with tall buildings on each side, have reduced ventilation and generally higher temperatures[269,270] than more open areas. The building height-to-street-width (H/W) ratio is correlated with the strength of the UHI; when this ratio is higher, meaning tall buildings surrounding narrow streets, temperature tends to drop more slowly at night. This effect is likely due to a decrease in radiative cooling, as more outgoing long-wave radiation is absorbed by surrounding buildings rather than escaping into the atmosphere[270].

New materials with retro-reflective properties offer a method of reducing radiation absorption by closely-spaced buildings. Retro-reflective materials reflect incoming radiation in the same direction from which it came; this means that incoming solar radiation can be reflected back to the atmosphere instead of reflecting off a surface and then being absorbed by the ground or a nearby building[255].

Green facades – usually implemented with climbing plants and vines on the side of a building – can be an effective way of reducing local near-surface temperatures by 10°C or more[269]. In general, green facades are generally not as effective as cool roofs at reducing ambient

temperatures, as the sides of buildings receive less direct sunlight and thus changing their albedo has less thermal effect. However, as a part of a comprehensive urban-greening strategy, green facades can play a significant role in reducing thermal absorption by man-made structures.

### Urban water bodies

Urban water bodies, whether nearby oceans, lakes, rivers, or even small ponds and creeks, can provide a cooling effect. The air over a body of water can be 2 – 6°C cooler than over the surrounding city landscape[177], and regions downwind of the water body will experience some cooling, with many studies suggesting 1 – 2°C as a common temperature reduction[271]. The spatial extent of the cooling effect depends heavily on the size of the water body, the prevailing winds, and the local humidity conditions; as evaporative cooling is the dominant mechanism for temperature reduction, water bodies will have less effect in humid conditions[272]. Moving or spraying water has a stronger cooling effect than stationary water bodies, and even small fountains can substantially cool nearby areas[273]. Water provides increased latent and decreased sensible heat fluxes, which are likely to reduce air temperature during the daytime, but less so at night – and it should be noted that when air temperature drops below water temperature, bodies of water serve as strong warming influences, in some cases canceling out their daytime cooling effect and making them a net contributor to mean UHI[274]. In addition, increased evaporation can raise local relative humidity, and depending on the balance between temperature reduction and humidity increase, measures of heat stress may rise or fall near bodies of water[275].

## Behavior

### Early warning systems

In recent years as the public health impacts of major heat waves have become more widely understood, countries have begun implementing heat wave early warning systems (HEWS) in an attempt to reduce heat-related mortality and prepare for climate change[276,277]. Early warning systems generally consist of a trigger, usually some combination of predicted extreme heat and humidity lasting for a specified duration, and a response plan once the trigger occurs. For early warning systems to be effective, they must be accompanied by active and targeted warnings for high-risk individuals[278], as well as advice on what protective measures people should take.

As climate change continues to intensify heat waves, early warning systems may need to be updated[279] to reflect the changing characteristics of heat waves or changing public responses to extreme temperatures. Temperature-health relationships must also be monitored, especially if non-linear responses of mortality to heat begin to appear at extremely high temperatures. Heat wave early warning systems can also be improved by monitoring their performance in past heat waves and adapting their trigger thresholds accordingly[280].

**Personalized heat monitoring**

Increased recognition of the localized nature of heat stress and the difficulty of predicting individual heat risk based on environmental conditions has spurred research into personalized heat exposure monitoring[190,281,282]. Tests of such devices have found substantial variation in exposure between individuals in the same neighborhood due to differences in activity level, clothing, and access to air conditioning[197,283]. Most devices have been used only to measure heat exposure, but some have attempted to predict heat illness. These types of monitors usually take the form of wearable body temperature or heart rate sensors which can alert the user when their

physiological parameters indicate unsafe heat exposure. More research is needed to identify and calibrate these physiological predictors of heat illness, as well as to test the efficacy of this adaptation approach in improving overall health outcomes during extreme heat events. As with many adaptation strategies, adopting the monitoring device is only the first step; users need to be trained in the proper response to a heat stress alert, and they must have the ability to seek air conditioning, water, and rest.

Most research thus far has focused on high-income countries, and has generally found personal heat exposure to be strongly correlated with but generally less than outside air temperature, likely due to air conditioning. Implementing personalized monitoring in low-income regions will likely prove more challenging, especially in rural areas where electricity access may be limited and equipment delivery and maintenance costs more expensive.

**Encouraging protective action**

Recent heat waves have shown that making cooling centers, water, and other services available to vulnerable populations isn't enough; there are often a variety of reasons that people choose not to take protective action without active encouragement. The use of air conditioning is considered to be the most effective protection against heat-related illness, but many at-risk individuals either do not have access or are reluctant to use it due to cost or personal preference[199]. Many at-risk elderly people report checking on their friends or family during heat waves, a practice that may provide some protection by encouraging individuals to take protective actions[284]. In urban areas, most heat-related deaths occur at home[194,199]; more research is needed on the most effective methods of encouraging vulnerable populations to seek water and cooler

spaces during heat waves. Several jurisdictions have programs to check on vulnerable residents; however, more research to evaluate and optimize these efforts is needed.

Optimizing interior spaces for hot weather can have significant impacts on heat exposure[285]. Shutters and blinds can be closed on windows during the day. If air conditioning is available, it can be used to cool a small area of the indoor space, and set to a low-cool setting to protect health while reducing energy use and costs. The use of fans to remove hot air during the day and to inject cool air during the night, as well as using shades to block sunlight during the hottest hours of the day, can reduce indoor temperatures in the absence of air conditioning. However, during periods of extreme heat, there is no evidence that fans help prevent illness and death among vulnerable individuals[286]. Informing the public about strategies to mitigate indoor temperatures may be an effective way to reduce heat risk in some communities. In addition, frequent cool showers and baths may help to provide relief[287].

**Conclusions**

Heat is a serious health risk in the current climate and will likely impose a greater burden on both urban and rural populations as heat waves intensify in the future. Experience in recent heat waves has shown that targeted intervention strategies, especially centered around alerting at-risk individuals to the risk of heat stress and providing them with the resources to protect themselves, can be highly effective at reducing mortality. Many of the heat wave adaptation strategies presented here have thus far been tested primarily in high-income countries; more research is needed on the most effective and efficient ways of implementing these and other evidence-based adaptation methods in low- and middle-income regions. In addition, most adaptation strategies thus far have focused on urban areas; while urban regions have a higher

heat burden due to the urban heat island, rural regions face extreme heat as well, and often have less access to air conditioning, safe water, and social support. More research is needed into rural adaptation, especially for agricultural workers in low-income countries, who may face an increasingly high heat risk in the future.

It is essential that adaptation measures be scientifically tested before being implemented on a large scale, especially where resources are limited. Some adaptations are much more effective than others, and many effective methods are not expensive. More research is also needed on implementation, barriers to adaptation, and the potential for co-benefits and costs of heat-related adaptation. Increasingly severe heat is poised to be one of the most directly observable impacts of climate change, as well as one with significant health impacts. Governments, both national and local, can reduce the burden of heat on their populations by implementing well-designed and tested adaptation strategies.

# Conclusions & future work

This dissertation has focused on extreme heat, the processes driving increasing heat wave risk, and some of the potential adaptation strategies to reduce the impacts on society. As exposure to extreme heat grows in the future, it will be increasingly essential to understand what regions are at highest risk and how confident we can be in assessing the full range of potential future climate outcomes. While the research community has made great progress in recent years in analyzing the impacts of climate change, there is still more work to do to assess the specific effects of changing extremes on ecosystems and human society. Climate impacts research is likely to play an increasingly important role in shaping adaptation policy around the world. Identifying the most serious climate risks and evaluating both the effectiveness and the efficiency of potential adaptation strategies will be crucial to reducing the impacts of climate change in the coming decades.

The amplified warming of extreme temperatures as compared to the mean significantly increases projected heat wave statistics, especially in Europe. Most models agree that this amplification will occur, but they differ in magnitude, and the variation is linked to the projected change in warm season sensible heat flux and net surface shortwave radiation. These variables, in turn, depend on both the availability of surface moisture which controls the partitioning of incoming energy into sensible or latent heat flux, as well as on changes in cloud cover, aerosol emissions, and greenhouse gas forcing which control how much incoming radiation reaches the surface. The dependence of extreme temperature change on model representation of clouds and moisture introduces substantial projection uncertainty. In climate impact studies, it is often assumed that model-projected temperature changes are more reliable than for precipitation, soil moisture, or metrics of land-atmosphere coupling. This work suggests that projections of the

most extreme temperatures cannot be separated from these hydrological processes. In addition, it shows that somewhat different processes are driving the projected amplification of extreme temperature warming in different regions. While Chapter 1 suggests that surface drying is related to the projected TXx amplification, there are regions (e.g. southern Africa) that are projected to dry but not experience amplification. More work is necessary to identify the regional differences that lead to this result. Prior work has demonstrated that intensive agriculture can reduce the occurrence of extreme temperatures by increasing the near-surface evaporative fraction[97], and it is possible that this, other land-cover changes, and/or larger scale processes are affecting projected amplification in some regions. In addition, it will be important to assess the interaction of TXx amplification with the urban heat island, as recent evidence has suggested that in some situations temperatures can warm more in cities than in surrounding areas[288]. As Chapter 1 also demonstrates, the coldest daily minimum temperatures are projected to increase by at least 3°C more than mean daily minimum temperatures in snow-covered parts of the Northern Hemisphere. The initial analyses presented in this dissertation suggest that this wintertime amplification is spatially correlated with snow decline, but more work is necessary to confirm whether the snow-albedo feedback is the driving process at work.

Warmer temperatures are increasing the moisture content of the atmosphere, leading to rapid rises in human health-relevant joint heat-humidity metrics. Annual maximum wet bulb temperatures are projected to rise by 1.5 – 3.5°C by the 2070s, putting some regions at risk of experiencing occasional values above a theoretical limit for human tolerance. More research is needed to understand the health implications of such extreme levels of heat stress. Recent heat waves – which have resulted in thousands of heat-related deaths – have had maximum wet bulb temperatures of 31 to 32°C, and isolated locations have experienced values as high as 34°C.

However, there has never been widespread and prolonged exposure to 32°C or higher wet bulb temperatures, which appears likely in India, the Middle East, and parts of West Africa by the second half of the 21st century even under RCP 4.5. Experimental evidence suggests that physical labor will become difficult and dangerous at these heat stress levels[60], and it is likely that unexpected heat-related illnesses[61] will occur. A more fundamental question is whether wet bulb temperatures of 35°C will indeed prove to be fatal for humans after six hours of exposure, as proposed by Sherwood and Huber (2010)[48]. If so, hot and low-income regions in India, Africa, and the Middle East may experience larger increases in heat-related mortality and economic impacts than are predicted by historical heat-health relationships. Chapter 2 of this dissertation assesses future population exposure to dangerous heat stress. The population projections used in this chapter do not take into account the ways in which climate change could influence migration; it is plausible that in some regions heat stress or other climate impacts could discourage population growth, leading to lower exposure values than estimated.

Better understanding the sources of uncertainty surrounding extreme wet bulb temperature events will also prove crucial. High heat stress values depend on a combination of extreme temperatures and high humidity levels, and small differences in wet bulb temperature can have large implications for the impacts of heat stress. Models vary significantly in the projections of wet bulb temperature change; a better understanding of the processes leading to this variation will help build confidence in future heat stress projections. Similarly, several regions – notably northern India, the coastal Middle East, eastern China, and coastal West Africa – emerge as particularly vulnerable to high wet bulb temperatures. Thus far little work has assessed the mechanisms driving extreme heat stress in these regions, whether they differ, and how models represent them.

Another important factor in any analysis of heat exposure is the urban heat island (UHI). The UHI can increase air temperatures by more than 2°C, and given the increasing urbanization of the global population, makes a large and growing contribution to heat exposure. There has thus far been little analysis of the urban heat island's effect on wet bulb temperature. This effect will likely depend mostly on urban humidity levels, which may be elevated due to human activity but also reduced by the lack of evapotranspiration over paved areas. It is unknown how the temperature effect of the UHI interacts with modified urban humidity to change heat stress in cities. Agricultural intensification may also affect local heat stress levels through increases in evapotranspiration. Prior work has shown that agriculture has reduced temperature extremes in some regions[97] by increasing evapotranspiration; as in urban areas, the balance between increased humidity and decreased temperature will determine whether heat stress rises or falls. The answer may prove significant for heat stress exposure in densely populated agricultural regions in India and China, for example.

Heat stress is a joint hazard, in that it depends on changes in two climate variables, temperature and humidity. Other joint hazards include hot drought (combining temperature and precipitation) and coastal flooding (combining sea level rise, rainfall, and wave activity). In some cases, the factors involved in a joint hazard are correlated, increasing the risk of extremes in both variables occurring simultaneously. The best example is temperature and precipitation; in much of the world, higher temperatures are correlated with less precipitation. This correlation results in a higher risk of a season being both hot and dry than would be expected if the variables were independent. Coupled with the expected increase in global precipitation variability[19], the risk of hot and dry seasons is likely to increase worldwide. Attempts to assess the impacts of joint

hazards and correlated extremes are relatively recent, but deserve substantial research attention in the coming years.

Chapter 3 of this dissertation showed the potential impacts of rising temperatures on aviation operations. The aviation industry is a substantial contributor to climate change but also faces climate risks. In addition to the potential for increasingly frequent aircraft weight restrictions, clear air turbulence is increasing in intensity, and sea-level rise is likely to threaten many coastal airports. The impacts of climate change on specific industries, such as aviation, have just begun to be analyzed. There is likely substantial unreported climate risk, which in many cases results in financial risk, spread across the economy. As the understanding of climate impacts becomes more widespread, this risk will likely come under scrutiny by investors and governments. Developing assessment methods to quantify the potential impacts of climate change on infrastructure, transportation, logistics, and supply chains will be essential. Climate adaptation is often considered at the national level, but much adaptation work will be done within industries, encouraged both by regulation and financial interest. Clearly and robustly estimating climate impacts may encourage adaptation efforts to begin sooner rather than later, reducing both physical and economic impacts.

Adaptation strategies require robust analysis to ensure that they are in fact efficient and effective methods of reducing climate risk. As Chapter 4 reviewed, heat adaptation techniques vary widely in efficacy, and often the best strategies – such as providing social support and access to water and air conditioning to the most vulnerable – are among the least costly. The analysis of adaptation strategies has mostly been conducted in high-income countries. Adaptation in places with less capacity and higher societal vulnerability may be more challenging, and in these regions it will also be even more essential to focus on strategies that are cost- and resource-

efficient. In addition to efficiency, it is vitally important that adaptation strategies be proven effective, and that they are tested in small-scale implementations before being widely adopted. It is always difficult to anticipate the effects of any adaptation strategy, and mal-adaptation – where an intervention creates a new problem or makes other, existing problems worse – is a real possibility. For example, building sea walls could in the short term reduce coastal flooding risk, but if coastal ecosystems are damaged in the process, the loss of natural flood defenses could outweigh the benefits of the adaptation.

The most effective strategy for reducing urban temperatures appears to be the large-scale implementation of white or (in dry climates) green roofs. By increasing the albedo of urban areas, and in the case of green roofs increasing evapotranspiration, cool roofs substantially lower the amount of radiation absorbed by buildings, reducing both the energy required to cool them as well as the ambient air temperature. Modeling studies have found urban temperature reductions of 2°C or more are possible with white roofs, potentially offsetting a significant portion of climate change-driven temperature rise. Green roofs also produce substantial, but somewhat smaller, temperature reductions, as does extensive tree cover within an urban area. However, due to increased humidity, green roofs could increase local wet bulb temperatures; this effect has thus far not been studied but deserves research attention if green roofs are to be widely implemented. The existing analyses of the benefits of cool roofs are based on a limited number of modeling studies and less empirical testing. Due to the potentially large benefits of cool roofs, much more research and tests of large-scale implementation strategies are warranted in the near future.

Since the 2003 European heat wave, which was responsible for tens of thousands of excess deaths, many countries and cities have implemented heat wave response plans. The

centerpiece of these plans is generally education, early warning, and social and behavioral intervention for at-risk populations. The best predictor of heat related death both in Europe and the United States is social isolation. By providing assistance and support to isolated people and encouraging them to seek shelter from heat in public cooling centers, the death toll can be dramatically reduced. In France, a statistical analysis found that post-2003 policy changes may have reduced the heat-related death toll during a similar event by up to two-thirds. These results show the importance of cultural adaptation in responding to climate change. For some climate threats, education and behavior modification can prove cheaper and more effective at reducing the risk from climate extremes than physical adaptation.

This dissertation has investigated some of the processes driving amplified warming of the most extreme temperatures as compared to the mean, and assessed potential impacts of future extreme heat. Much work remains to understand the ways in which extreme events are changing, the processes driving these changes, and how human activities and natural ecosystems will be impacted in the coming decades. As the impacts of climate change become more widespread and damaging, climate impacts work will increasingly be called upon to understand the changes that are occurring and the processes driving them. Methods of rapidly assessing specific, regional changes in climate will be needed, as will a rigorous focus on the uncertainty surrounding climate projections. By analyzing the full range of possible climate outcomes simulated by a range of climate models, understanding the physical mechanisms driving these outcomes, and clearly communicating the sources and magnitudes of uncertainty, climate impacts science will facilitate clearly evaluating the climate risks that we face now and in the future. By understanding these risks, science will be able to inform policy more accurately.

**References**


1. U.S. Billion-Dollar Weather and Climate Disasters (2018). *NOAA National Centers for Environmental Information (NCEI)* (2018). Available at: https://www.ncdc.noaa.gov/billions/.
2. Rahmstorf, S. & Coumou, D. Increase of extreme events in a warming world. *Proc. Natl. Acad. Sci.* **109,** 4708–4708 (2012).
3. Christidis, N., Jones, G. S. & Stott, P. A. Dramatically increasing chance of extremely hot summers since the 2003 European heatwave. *Nat. Clim. Chang.* **5,** 3–7 (2015).
4. van Oldenborgh, G. J. *et al.* Attribution of extreme rainfall from Hurricane Harvey, August 2017. *Environ. Res. Lett.* **12,** 124009 (2017).
5. Diffenbaugh, N. S. *et al.* Quantifying the influence of global warming on unprecedented extreme climate events. *Proc. Natl. Acad. Sci.* **114,** 4881–4886 (2017).
6. Horton, D. E. *et al.* Contribution of changes in atmospheric circulation patterns to extreme temperature trends. *Nature* **522,** 465–469 (2015).
7. Coumou, D., Lehmann, J. & Beckmann, J. The weakening summer circulation in the Northern Hemisphere mid-latitudes. **348,** (2015).
8. Coumou, D., Petoukhov, V., Rahmstorf, S., Petri, S. & Schellnhuber, H. J. Quasi-resonant circulation regimes and hemispheric synchronization of extreme weather in boreal summer. *Proc. Natl. Acad. Sci.* **111,** 12331–12336 (2014).
9. Miralles, D. G., Teuling, A. J., van Heerwaarden, C. C. & Vilà-Guerau de Arellano, J. Mega-heatwave temperatures due to combined soil desiccation and atmospheric heat accumulation. *Nat. Geosci.* **7,** 345–349 (2014).
10. Dai, A. Drought under global warming: A review. *Wiley Interdiscip. Rev. Clim. Chang.* **2,**

45–65 (2011).

11. Sanchez-Lorenzo, A. *et al.* Fewer clouds in the Mediterranean: Consistency of observations and climate simulations. *Sci. Rep.* **7,** 1–10 (2017).

12. Vavrus, S., Walsh, J. E., Chapman, W. L. & Portis, D. The behavior of extreme cold air outbreaks under greenhouse warming. *Int. J. Climatol.* **26,** 1133–1147 (2006).

13. Kretschmer, M. *et al.* More-Persistent Weak Stratospheric Polar Vortex States Linked to Cold Extremes. *Bull. Am. Meteorol. Soc.* BAMS-D-16-0259.1 (2017). doi:10.1175/BAMS-D-16-0259.1

14. Horton, R. M., Coffel, E. D., Winter, J. M. & Bader, D. A. Projected changes in extreme temperature events based on the NARCCAP model suite. *Geophys. Res. Lett.* **42,** (2015).

15. Mankin, J. S. & Diffenbaugh, N. S. Influence of temperature and precipitation variability on near-term snow trends. *Clim. Dyn.* **45,** 1099–1116 (2015).

16. Willett, K. M., Gillett, N. P., Jones, P. D. & Thorne, P. W. Attribution of observed surface humidity changes to human influence. *Nature* **449,** 710–712 (2007).

17. O'Gorman, P. A. & Schneider, T. The physical basis for increases in precipitation extremes in simulations of 21st-century climate change. *Proc. Natl. Acad. Sci.* **106,** 14773–14777 (2009).

18. Trenberth, K. E. Changes in precipitation with climate change. *Clim. Res.* **47,** 123–138 (2011).

19. Seager, R., Naik, N. & Vogel, L. Does global warming cause intensified interannual hydroclimate variability? *J. Clim.* **25,** 3355–3372 (2012).

20. Singh, D., Tsiang, M., Rajaratnam, B. & Diffenbaugh, N. S. Precipitation extremes over the continental United States in a transient, high-resolution, ensemble climate model

experiment. *J. Geophys. Res. Atmos.* **118,** 7063–7086 (2013).

21. Williams, a. P. *et al.* Contribution of anthropogenic warming to California drought during 2012 – 2014. *Geophys. Res. Lett.* 1–10 (2015). doi:10.1002/2015GL064924.Received

22. Seager, R. *et al.* Causes of the 2011–14 California Drought. *J. Clim.* **28,** 6997–7024 (2015).

23. Mankin, J. S., Viviroli, D., Singh, D., Hoekstra, A. Y. & Diffenbaugh, N. S. The potential for snow to supply human water demand in the present and future. *Environ. Res. Lett.* **10,** (2015).

24. Ault, T. R., Cole, J. E., Overpeck, J. T., Pederson, G. T. & Meko, D. M. Assessing the risk of persistent drought using climate model simulations and paleoclimate data. *J. Clim.* **27,** 7529–7549 (2014).

25. Cook, B. I., Ault, T. R. & Smerdon, J. E. Unprecedented 21st century drought risk in the American Southwest and Central Plains. *Sci. Adv.* **1,** e1400082–e1400082 (2015).

26. Knutson, T. R. *et al.* Tropical cyclones and climate change. *Nat. Geosci.* **3,** 157–163 (2010).

27. Cohen, J. *et al.* Recent Arctic amplification and extreme mid-latitude weather. *Nat. Geosci.* **7,** 627–637 (2014).

28. Woollings, T., Gregory, J. M., Pinto, J. G., Reyers, M. & Brayshaw, D. J. Response of the North Atlantic storm track to climate change shaped by ocean-atmosphere coupling. *Nat. Geosci.* **5,** 313–317 (2012).

29. Hinkel, J. *et al.* Coastal flood damage and adaptation costs under 21st century sea-level rise. *Proc. Natl. Acad. Sci.* **111,** 3292–3297 (2014).

30. Yin, J. H. A consistent poleward shift of the storm tracks in simulations of 21st century

climate. *Geophys. Res. Lett.* **32,** 1–4 (2005).

31. Bengtsson, L., Hodges, K. I. & Roeckner, E. Storm tracks and climate change. *J. Clim.* **19,** 3518–3543 (2006).

32. Simpson, I. R., Shaw, T. A. & Seager, R. A Diagnosis of the Seasonally and Longitudinally Varying Midlatitude Circulation Response to Global Warming*. *J. Atmos. Sci.* **71,** 2489–2515 (2014).

33. Kelley, C. P., Mohtadi, S., Cane, M. A., Seager, R. & Kushnir, Y. Climate change in the Fertile Crescent and implications of the recent Syrian drought. *Proc. Natl. Acad. Sci.* **112,** 3241–3246 (2015).

34. Bohra-Mishra, P., Oppenheimer, M. & Hsiang, S. M. Nonlinear permanent migration response to climatic variations but minimal response to disasters. *Proc. Natl. Acad. Sci.* **111,** 9780–9785 (2014).

35. Missirian, A. & Schlenker, W. Asylum applications respond to temperature fluctuations. *Science (80-. ).* **358,** 1610–1614 (2017).

36. Haines, A., Kovats, R. S., Campbell-Lendrum, D. & Corvalan, C. Climate change and human health: Impacts, vulnerability and public health. *Public Health* **120,** 585–596 (2006).

37. Burke, M., Hsiang, S. M. & Miguel, E. Global non-linear effect of temperature on economic production. *Nature* **527,** 235–239 (2015).

38. Hay, C. C., Morrow, E., Kopp, R. E. & Mitrovica, J. X. Probabilistic reanalysis of twentieth-century sea-level rise. *Nature* **517,** 481–484 (2015).

39. IPCC & Press, C. U. The Physical Science Basis. Contribution of Working Group I to the Fifth Assessment Report of the Intergovernmental Panel on Climate Change. in

*Intergovernmental Panel on Climate Change, Working Group I Contribution to the IPCC Fifth Assessment Report (AR5)(Cambridge Univ Press, New York)* (eds. Stocker, T. F. et al.) 1535 (Cambridge University Press, 2013).

40. Rahmstorf, S. A Semi-empirical Approach to Projecting Future Sea Level Rise. *Science (80-. ).* **315,** 368–370 (2006).

41. Overpeck, J. T. *et al.* Paleoclimatic evidence for future ice-sheet instability and rapid sea-level rise. *Science (80-. ).* **311,** 1747–1750 (2006).

42. Joughin, I., Smith, B. E. & Medley, B. Marine Ice Sheet Collapse Potentially Under Way for the Thwaites Glacier Basin, West Antarctica. *Science (80-. ).* **344,** 735–738 (2014).

43. Ritz, C. *et al.* Potential sea-level rise from Antarctic ice-sheet instability constrained by observations. *Nature* **528,** 115–118 (2015).

44. Hino, M., Field, C. B. & Mach, K. J. Managed retreat as a response to natural hazard risk. *Nat. Clim. Chang.* **7,** 364–370 (2017).

45. Götz, L., Djuric, I. & Nivievskyi, O. Regional Price Effects of Extreme Weather Events and Wheat Export Controls in Russia and Ukraine. *J. Agric. Econ.* **67,** 741–763 (2016).

46. Coffel, E. D., Thompson, T. R. & Horton, R. M. The impacts of rising temperatures on aircraft takeoff performance. *Climatic Change* 1–8 (2017). doi:10.1007/s10584-017-2018-9

47. Dunne, J. P., Stouffer, R. J. & John, J. G. Reductions in labour capacity from heat stress under climate warming. *Nat. Clim. Chang.* **3,** 563–566 (2013).

48. Sherwood, S. C. & Huber, M. An adaptability limit to climate change due to heat stress. *Proc. Natl. Acad. Sci.* **107,** 9552–9555 (2010).

49. Pal, J. S. & Eltahir, E. A. B. Future temperature in southwest Asia projected to exceed a

threshold for human adaptability. *Nat. Clim. Chang.* **18203,** 1–4 (2015).

50. Im, E.-S., Pal, J. S. & Eltahir, E. A. B. Deadly heat waves projected in the densely populated agricultural regions of South Asia. *Sci. Adv.* **3,** 1–8 (2017).

51. Petkova, E. P., Horton, R. M., Bader, D. A. & Kinney, P. L. Projected heat-related mortality in the U.S. Urban Northeast. *Int. J. Environ. Res. Public Health* **10,** 6734–6747 (2013).

52. Ray, D. K., Gerber, J. S., MacDonald, G. K. & West, P. C. Climate variation explains a third of global crop yield variability. *Nat. Commun.* **6,** 5989 (2015).

53. Schlenker, W. & Roberts, M. J. Nonlinear temperature effects indicate severe damages to U.S. crop yields under climate change. *Proc. Natl. Acad. Sci.* **106,** 15594–15598 (2009).

54. Lobell, D. B. *et al.* The critical role of extreme heat for maize production in the United States. *Nat. Clim. Chang.* **3,** 497–501 (2013).

55. Anderson, W., Seager, R., Baethgen, W. & Cane, M. Life cycles of agriculturally relevant ENSO teleconnections in North and South America. *Int. J. Climatol.* **37,** 3297–3318 (2017).

56. Leng, G. & Huang, M. Crop yield response to climate change varies with crop spatial distribution pattern. *Sci. Rep.* **7,** 1–10 (2017).

57. Moore, F. C., Baldos, U. L. C. & Hertel, T. Economic impacts of climate change on agriculture: A comparison of process-based and statistical yield models. *Environ. Res. Lett.* **12,** (2017).

58. Hsiang, S. M., Burke, M. & Miguel, E. Quantifying the influence of climate on human conflict. *Science* **341,** 1235367 (2013).

59. Kjellstrom, T., Kovats, R. S., Lloyd, S. J., Holt, T. & Tol, R. S. J. The Direct Impact of

Climate Change on Regional Labor Productivity. *Arch. Environ. Occup. Health* **64,** 217–227 (2009).

60. Liang, C. *et al.* A new environmental heat stress index for indoor hot and humid environments based on Cox regression. *Build. Environ.* **46,** 2472–2479 (2011).

61. Glaser, J. *et al.* Climate change and the emergent epidemic of CKD from heat stress in rural communities: The case for heat stress nephropathy. *Clin. J. Am. Soc. Nephrol.* **11,** 1472–1483 (2016).

62. Lesk, C., Coffel, E., D'Amato, A. W., Dodds, K. & Horton, R. Threats to North American forests from southern pine beetle with warming winters. *Nat. Clim. Chang.* **7,** (2017).

63. Moore, F. C. & Diaz, D. B. Temperature impacts on economic growth warrant stringent mitigation policy. *Nat. Clim. Chang.* **5,** 127–131 (2015).

64. Solomon, S., Plattner, G.-K., Knutti, R. & Friedlingstein, P. Irreversible climate change due to carbon dioxide emissions. *Proc. Natl. Acad. Sci. U. S. A.* **106,** 1704–9 (2009).

65. Christensen, J. H., Boberg, F., Christensen, O. B. & Lucas-Picher, P. On the need for bias correction of regional climate change projections of temperature and precipitation. *Geophys. Res. Lett.* **35,** (2008).

66. Teutschbein, C. & Seibert, J. Bias correction of regional climate model simulations for hydrological climate-change impact studies: Review and evaluation of different methods. *J. Hydrol.* **456–457,** 12–29 (2012).

67. Ehret, U., Zehe, E., Wulfmeyer, V., Warrach-Sagi, K. & Liebert, J. HESS Opinions 'should we apply bias correction to global and regional climate model data?' *Hydrol. Earth Syst. Sci.* **16,** 3391–3404 (2012).

68. Feser, F., Rockel, B., von Storch, H., Winterfeldt, J. & Zahn, M. Regional Climate Models

Add Value to Global Model Data: A Review and Selected Examples. *Bull. Am. Meteorol. Soc.* **92,** 1181–1192 (2011).

69. Coffel, E. & Horton, R. Climate Change and the Impact of Extreme Temperatures on Aviation. *Weather. Clim. Soc.* **7,** 94–102 (2015).

70. Haerter, J. O., Hagemann, S., Moseley, C. & Piani, C. Climate model bias correction and the role of timescales. *Hydrol. Earth Syst. Sci.* **15,** 1065–1079 (2011).

71. Kay, J. E. *et al.* The Community Earth System Model (CESM) Large Ensemble Project: A Community Resource for Studying Climate Change in the Presence of Internal Climate Variability. *Bull. Am. Meteorol. Soc.* **96,** 1333–1349 (2014).

72. Coffel, E. D., Mankin, J. S., Winter, J. M. & Horton, R. M. The amplified warming of extreme temperatures. *Geophys. Res. Lett.* (2017).

73. Screen, J. A. Arctic amplification decreases temperature variance in northern mid- to high-latitudes. *Nat. Clim. Chang.* **4,** 577–582 (2014).

74. Mascioli, N. R., Previdi, M., Fiore, A. M. & Ting, M. Timing and seasonality of the United States 'warming hole'. *Environ. Res. Lett.* **12,** 34008 (2017).

75. Meehl, G. A., Arblaster, J. M. & Branstator, G. Mechanisms contributing to the warming hole and the consequent U.S. East-west differential of heat extremes. *J. Clim.* **25,** 6394–6408 (2012).

76. Argüeso, D., Di Luca, A., Perkins-Kirkpatrick, S. E. & Evans, J. P. Seasonal mean temperature changes control future heat waves. *Geophys. Res. Lett.* **43,** 7653–7660 (2016).

77. Horton, R. M., Coffel, E. D., Winter, J. M. & Bader, D. A. Projected changes in extreme temperature events based on the NARCCAP model suite. *Geophys. Res. Lett.* **42,** 7722–7731 (2015).

78. Kurz, W. A. *et al.* Mountain pine beetle and forest carbon feedback to climate change. *Nature* **452,** 987–990 (2008).

79. Berg, E. E., David Henry, J., Fastie, C. L., De Volder, A. D. & Matsuoka, S. M. Spruce beetle outbreaks on the Kenai Peninsula, Alaska, and Kluane National Park and Reserve, Yukon Territory: Relationship to summer temperatures and regional differences in disturbance regimes. *For. Ecol. Manage.* **227,** 219–232 (2006).

80. Chen, K. *et al.* Impact of climate change on heat-related mortality in Jiangsu Province, China. *Environ. Pollut.* **224,** 317–325 (2017).

81. Lobell, D. B. & Gourdji, S. M. The Influence of Climate Change on Global Crop Productivity. *Plant Physiol.* **160,** 1686–1697 (2012).

82. Franco, G. & Sanstad, A. H. Climate change and electricity demand in California. *Clim. Change* **87,** 139–151 (2008).

83. Auffhammer, M., Baylis, P. & Hausman, C. H. Climate change is projected to have severe impacts on the frequency and intensity of peak electricity demand across the United States. *Proc. Natl. Acad. Sci. U. S. A.* **114,** 1886–1891 (2017).

84. Kodra, E. & Ganguly, A. R. Asymmetry of projected increases in extreme temperature distributions. *Sci. Rep.* **4,** 5884 (2014).

85. Horton, R. M., Mankin, J. S., Lesk, C., Coffel, E. & Raymond, C. A Review of Recent Advances in Research on Extreme Heat Events. *Curr. Clim. Chang. Reports* **2,** 242–259 (2016).

86. Schär, C. *et al.* The role of increasing temperature variability in European summer heatwaves. *Nature* **427,** 332–336 (2004).

87. Fischer, E. M., Rajczak, J. & Schär, C. Changes in European summer temperature

variability revisited. *Geophys. Res. Lett.* **39,** 1–8 (2012).

88. Huntingford, C., Jones, P. D., Livina, V. N., Lenton, T. M. & Cox, P. M. No increase in global temperature variability despite changing regional patterns. *Nature* **500,** 327–330 (2013).

89. Mearns, L. O. *et al.* The north american regional climate change assessment program overview of phase i results. *Bull. Am. Meteorol. Soc.* **93,** 1337–1362 (2012).

90. Taylor, K. E., Stouffer, R. J. & Meehl, G. A. An overview of CMIP5 and the experiment design. *Bull. Am. Meteorol. Soc.* **93,** 485–498 (2012).

91. Moss, R. H. *et al.* The next generation of scenarios for climate change research and assessment. *Nature* **463,** 747–756 (2010).

92. Kanamitsu, M. *et al.* NCEP-DOE AMIP-II reanalysis (R-2). *Bull. Am. Meteorol. Soc.* **83,** 1631–1643+1559 (2002).

93. Katz, R. W. & Brown, B. G. Extreme events in changing climate variability is more important than average. *Clim. Change* **21,** in (1992).

94. Friedlingstein, P. *et al.* Climate–carbon cycle feedback analysis: results from the C4MIP model intercomparison. *J. Clim.* **19,** 3337–3353 (2006).

95. Quillet, A., Peng, C. & Garneau, M. Toward dynamic global vegetation models for simulating vegetation–climate interactions and feedbacks: recent developments, limitations, and future challenges. *Environ. Rev.* **18,** 333–353 (2010).

96. Mankin, J. S., Smerdon, J. E., Cook, B. I., Williams, A. P. & Seager, R. The curious case of projected 21st-century drying but greening in the American West. *J. Clim.* JCLI-D-17-0213.1 (2017). doi:10.1175/JCLI-D-17-0213.1

97. Mueller, N. D. *et al.* Cooling of US Midwest summer temperature extremes from cropland

intensification. *Nat. Clim. Chang.* **6,** 317–322 (2016).

98. Coffel, E. D., Horton, R. M. & de Sherbinin, A. Temperature and humidity based projections of a rapid rise in global heat stress exposure during the 21st century. *Environ. Res. Lett.* **13,** 14001 (2018).

99. Dole, R. *et al.* Was there a basis for anticipating the 2010 Russian heat wave? *Geophys. Res. Lett.* **38,** (2011).

100. Welton, G. The Impact of Russia' s 2010 Grain Export Ban. *Oxfam Res. Reports* 32 (2011).

101. Ghumman, U. & Horney, J. Characterizing the Impact of Extreme Heat on Mortality, Karachi, Pakistan, June 2015. *Prehosp. Disaster Med.* **31,** 263–6 (2016).

102. UNEP. *Loss and Damage: The Role of Ecosystem Services*. (United National Environment Programme, 2016).

103. Stott, P. A., Stone, D. A. & Allen, M. R. Human contribution to the European heatwave of 2003. *Nature* **432,** 610–614 (2004).

104. Black, E., Blackburn, M., Harrison, R. G., Hoskins, B. J. & Methven, J. Factors contributing to the summer 2003 European heatwave. *Weather* **59,** 217–223 (2004).

105. Meehl, G. A. & Tebaldi, C. More Intense, More Frequent, and Longer Lasting Heat Waves in the 21st Century. *Science (80-. ).* **305,** 994–997 (2004).

106. Jones, B. *et al.* Future population exposure to US heat extremes. *Nat. Clim. Chang.* **5,** 652–655 (2015).

107. Coumou, D., Petoukhov, V., Rahmstorf, S., Petri, S. & Schellnhuber, H. J. Quasi-resonant circulation regimes and hemispheric synchronization of extreme weather in boreal summer. *Proc. Natl. Acad. Sci.* **111,** 12331–12336 (2014).

108. Hatfield, J. *et al.* Ch. 6: Agriculture. in *Climate Change Impacts in the United States: The Third National Climate Assessment* (eds. Melillo, J. M., (T.C.), T. R. & Yohe, G. W.) 150–174 (U.S. Global Change Research Program, 2014).

109. Budd, G. M. Wet-bulb globe temperature (WBGT)-its history and its limitations. *J. Sci. Med. Sport* **11,** 20–32 (2008).

110. Willett, K. M. & Sherwood, S. Exceedance of heat index thresholds for 15 regions under a warming climate using the wet-bulb globe temperature. *Int. J. Climatol.* **32,** 161–177 (2012).

111. Knutson, T. R. & Ploshay, J. J. Detection of anthropogenic influence on a summertime heat stress index. *Clim. Change* **138,** 25–39 (2016).

112. Schar, C. Climate extremes: The worst heat waves to come. *Nat. Clim. Chang.* **6,** 128–129 (2016).

113. Fouillet, A. *et al.* Has the impact of heat waves on mortality changed in France since the European heat wave of summer 2003? A study of the 2006 heat wave. *Int. J. Epidemiol.* **37,** 309–317 (2008).

114. Buzan, J. R., Oleson, K. & Huber, M. Implementation and comparison of a suite of heat stress metrics within the Community Land Model version 4.5. *Geosci. Model Dev.* **8,** 151–170 (2015).

115. Kjellstrom, T., Gabrysch, S., Lemke, B. & Dear, K. The 'hothaps' programme for assessing climate change impacts on occupational health and productivity: An invitation to carry out field studies. *Glob. Health Action* **2,** 10.3402/gha.v2i0.2082 (2009).

116. *World Population Prospects The 2012 Revision Volume I : Comprehensive Tables*. **1,** (United Nations Population Division, 2013).

117. Zhao, L., Lee, X., Smith, R. B. & Oleson, K. Strong contributions of local background climate to urban heat islands. *Nature* **511,** 216–219 (2014).

118. Kjellstrom, T., Holmer, I. & Lemke, B. Workplace heat stress, health and productivity – an increasing challenge for low and middle-income countries during climate change. *Glob. Health Action* **2,** 10.3402/gha.v2i0.2047 (2009).

119. Sippel, S. & Otto, F. E. L. Beyond climatological extremes - assessing how the odds of hydrometeorological extreme events in South-East Europe change in a warming climate. *Clim. Change* **125,** 381–398 (2014).

120. Battisti, D. S. & Naylor, R. L. Historical Warnings of Future Food Insecurity with Unprecedented Seasonal Heat. *Science (80-. ).* **323,** 240–244 (2009).

121. Jones, B. *et al.* Spatially explicit global population scenarios consistent with the Shared Socioeconomic Pathways. *Environ. Res. Lett.* **11,** 84003 (2016).

122. O'Neill, B. C. *et al.* A new scenario framework for climate change research: The concept of shared socioeconomic pathways. *Clim. Change* **122,** 387–400 (2014).

123. Kanamitsu, M. *et al.* NCEP–DOE AMIP-II Reanalysis (R-2). *Bull. Am. Meteorol. Soc.* **83,** 1631–1643 (2002).

124. Davies-Jones, R. An Efficient and Accurate Method for Computing the Wet-Bulb Temperature along Pseudoadiabats. *Mon. Weather Rev.* **136,** 2764–2785 (2008).

125. Stull, R. Wet-bulb temperature from relative humidity and air temperature. *J. Appl. Meteorol. Climatol.* **50,** 2267–2269 (2011).

126. Rothfusz, L. P. *The Heat Index 'Equation'. Fort Worth, Texas: National Oceanic and Atmospheric Administration, National Weather Service, Office of Meteorology* (1990).

127. Fischer, E. M. & Knutti, R. Robust projections of combined humidity and temperature

extremes. *Nat. Clim. Chang.* **3,** 126–130 (2012).

128. Ballester, J., Rodó, X. & Giorgi, F. Future changes in Central Europe heat waves expected to mostly follow summer mean warming. *Clim. Dyn.* **35,** 1191–1205 (2010).

129. Williams, I. N., Pierrehumbert, R. T. & Huber, M. Global warming, convective threshold and false thermostats. *Geophys. Res. Lett.* **36,** 2–6 (2009).

130. Frieling, J. *et al.* Extreme warmth and heat-stressed plankton in the tropics during the Paleocene-Eocene Thermal Maximum. *Sci. Adv.* **3,** e1600891 (2017).

131. Korty, R. L., Emanuel, K. A., Huber, M. & Zamora, R. A. Tropical cyclones downscaled from simulations with very high carbon dioxide levels. *J. Clim.* **30,** 649–667 (2017).

132. Levy, A. A. L. *et al.* Can correcting feature location in simulated mean climate improve agreement on projected changes? *Geophys. Res. Lett.* **40,** 354–358 (2013).

133. Luber, G. & McGeehin, M. Climate Change and Extreme Heat Events. *Am. J. Prev. Med.* **35,** 429–435 (2008).

134. Vandentorren, S. *et al.* August 2003 heat wave in France: Risk factors for death of elderly people living at home. *Eur. J. Public Health* **16,** 583–591 (2006).

135. Walsh, J. *et al.* Chapter 2: Our Changing Climate. *Third US Natl. Clim. Assess.* (2014).

136. Anderson, J. D. *Introduction to Flight*. (McGraw-Hill Education, 2015).

137. Coffel, E. D. & Horton, R. M. Reply to ‘“Comment on ‘Climate Change and the Impact of Extreme Temperatures on Aviation’””. *AMS Weather. Clim. Soc.* **8,** 207–208 (2016).

138. Hane, F. T. Comment on ‘Climate Change and the Impact of Extreme Temperatures on Aviation’. *Weather. Clim. Soc.* **8,** 205–206 (2015).

139. Lan, S., Clarke, J.-P. & Barnhart, C. Planning for Robust Airline Operations: Optimizing Aircraft Routings and Flight Departure Times to Minimize Passenger Disruptions. *Transp.*

*Sci.* **40,** 15–28 (2006).

140. Koetse, M. J. & Rietveld, P. The impact of climate change and weather on transport: An overview of empirical findings. *Transp. Res. Part D Transp. Environ.* **14,** 205–221 (2009).

141. Fleurquin, P., Ramasco, J. J. & Eguiluz, V. M. Systemic delay propagation in the US airport network. *Sci. Rep.* **3,** 1159 (2013).

142. Thompson, T. R. Aviation and the Impacts of Climate Change · Climate Change Impacts Upon the Commercial Air Transport Industry: An Overview. *Carbon Clim. Law Rev.* **10,** 105–112 (2016).

143. Williams, P. D. & Joshi, M. M. Intensification of winter transatlantic aviation turbulence in response to climate change. *Nat. Clim. Chang.* **3,** 644–648 (2013).

144. Williams, P. D. Increased light, moderate, and severe clear-air turbulence in response to climate change. *Adv. Atmos. Sci.* **34,** 576–586 (2017).

145. Bhaduri, A. Climate Change. *Econ. Labour Relations Rev.* **23,** 3–12 (2012).

146. Kharin, V. V., Zwiers, F. W., Zhang, X. & Hegerl, G. C. Changes in temperature and precipitation extremes in the IPCC ensemble of global coupled model simulations. *J. Clim.* **20,** 1419–1444 (2007).

147. Coumou, D., Lehmann, J. & Beckmann, J. The weakening summer circulation in the Northern Hemisphere mid-latitudes. *Science (80-. ).* **348,** 324–327 (2015).

148. Webster, P. J. Changes in Tropical Cyclone Number, Duration, and Intensity in a Warming Environment. *Science (80-. ).* **309,** 1844–1846 (2005).

149. Parris, A. *et al. Global Sea Level Rise Scenarios for the US National Climate Assessment*. *NOAA Tech Memo OAR CPO* (2012).

150. Burbidge, R. Adapting European Airports to a Changing Climate. *Transp. Res. Procedia* **14,** 14–23 (2016).

151. Karl, T. R. *et al.* Possible artifacts of data biases in the recent global surface warming hiatus. *Science (80-. ).* **348,** 1469–1472 (2015).

152. Mora, C. *et al.* The projected timing of climate departure from recent variability. *Nature* **502,** 183–187 (2013).

153. Joughin, I., Tulaczyk, S., Bindschadler, R. & Price, S. F. Changes in west Antarctic ice stream velocities: Observation and analysis. *J. Geophys. Res. Solid Earth* **107,** EPM 3-1-EPM 3-22 (2002).

154. Boeing. *Airplane characteristics for airport planning - 747*. *Boeing Commerical Airplanes* (2011). doi:10.2307/2230120

155. EUROCONTROL Experimental Centre. *User Manual for the Base of Aircraft Data (BADA)*. (2004).

156. Hansen, J., Sato, M. & Ruedy, R. Perception of climate change. *Proc. Natl. Acad. Sci.* **109,** E2415–E2423 (2012).

157. *ICAO Environmental Report*. (2016).

158. Coffel, E. D. *et al.* The Science of Adaptation to Extreme Heat. in *Resilience - The Science of Adaptation to Climate Change* (eds. Frank, T. & Zommers, Z.) (Elsevier, 2017).

159. Hayhoe, K., Sheridan, S., Kalkstein, L. & Greene, S. Climate change, heat waves, and mortality projections for Chicago. *J. Great Lakes Res.* **36,** 65–73 (2010).

160. Petkova, E. P., Gasparrini, A. & Kinney, P. L. Heat and Mortality in New York City Since the Beginning of the 20th Century. *Epidemiology* **25,** 1 (2014).

161. Kalkstein, L. S. & Greene, J. S. An evaluation of climate/mortality relationships in large U.S. cities and the possible impacts of a climate change. *Environ. Health Perspect.* **105,** 84–93 (1997).

162. Barriopedro, D., Fischer, E. M., Luterbacher, J., Trigo, R. M. & Garcia-Herrera, R. The Hot Summer of 2010: Redrawing the Temperature Record Map of Europe. *Science (80-. ).* **332,** 220–224 (2011).

163. Donat, N. H. and L. A. and D. G. and M. Greater increases in temperature extremes in low versus high income countries. *Environ. Res. Lett.* **12,** 34007 (2017).

164. Easterling, D. R. *et al.* Climate Extremes: Observations, Modeling, and Impacts. *Science (80-. ).* **289,** 2068–2074 (2000).

165. Donat, M. G. *et al.* Updated analyses of temperature and precipitation extreme indices since the beginning of the twentieth century: The HadEX2 dataset. *J. Geophys. Res. Atmos.* **118,** 2098–2118 (2013).

166. Alexander, L. V. *et al.* Global observed changes in daily climate extremes of temperature and precipitation. *J. Geophys. Res. Atmos.* **111,** D05109 (2006).

167. Mora, C. *et al.* Global risk of deadly heat. *Nat. Clim. Chang.* **7,** 501–506 (2017).

168. Forzieri, G., Cescatti, A., e Silva, F. B. & Feyen, L. Increasing risk over time of weather-related hazards to the European population: a data-driven prognostic study. *Lancet Planet. Heal.* **1,** e200–e208 (2017).

169. Brooke Anderson, G., Bell, M. L. & Peng, R. D. Methods to calculate the heat index as an exposure metric in environmental health research. *Environ. Health Perspect.* **121,** 1111–1119 (2013).

170. Rothfusz, L. P. & Headquarters, N. S. R. *The heat index equation (or, more than you ever*

*wanted to know about heat index)*. *Fort Worth, Texas: National Oceanic and Atmospheric Administration, National Weather Service, Office of Meteorology* (1990).

171. Barnett, A. G., Tong, S. & Clements, A. C. A. What measure of temperature is the best predictor of mortality? *Environ. Res.* **110,** 604–611 (2010).

172. Steadman, R. G. A Universal Scale of Apparent Temperature. *Journal of Climate and Applied Meteorology* **23,** 1674–1687 (1984).

173. Masterton;, J. M. & Richardson, F. A. Humidex: A Method of Quantifying Human Discomfort due to Excessive Heat and Humidity. *Environ. Canada, Atmos. Environ. Serv.* (1979).

174. Moran, D. S. *et al.* An environmental stress index (ESI) as a substitute for the wet bulb globe temperature (WBGT). *J. Therm. Biol.* **26,** 427–431 (2001).

175. Harlan, S. L., Brazel, A. J., Prashad, L., Stefanov, W. L. & Larsen, L. Neighborhood microclimates and vulnerability to heat stress. *Soc. Sci. Med.* **63,** 2847–2863 (2006).

176. Brooke Anderson, G. & Bell, M. L. Heat waves in the United States: Mortality risk during heat waves and effect modification by heat wave characteristics in 43 U.S. communities. *Environ. Health Perspect.* **119,** 210–218 (2011).

177. Manteghi, G., Bin Limit, H. & Remaz, D. Water bodies an urban microclimate: A review. *Mod. Appl. Sci.* **9,** 1–12 (2015).

178. Karner, A. A., Eisinger, D. S. & Niemeier, D. A. Near-roadway air quality: Synthesizing the findings from real-world data. *Environ. Sci. Technol.* **44,** 5334–5344 (2010).

179. Weber, S., Sadoff, N., Zell, E. & de Sherbinin, A. Policy-relevant indicators for mapping the vulnerability of urban populations to extreme heat events: A case study of Philadelphia. *Appl. Geogr.* **63,** 231–243 (2015).

180. Oke, T. R. City size and the urban heat island. *Atmos. Environ.* **7,** 769–779 (1973).

181. McKitrick, R. R. & Michaels, P. J. Quantifying the influence of anthropogenic surface processes and inhomogeneities on gridded global climate data. *J. Geophys. Res. Atmos.* **112,** 1–14 (2007).

182. Sidiqui, P., Huete, A. & Devadas, R. Spatio-temporal mapping and monitoring of Urban Heat Island patterns over Sydney, Australia using MODIS and Landsat-8. *Earth Obs. Remote Sens. Appl. (EORSA), 2016 4th Int. Work.* 217–221 (2016). doi:10.1109/EORSA.2016.7552800

183. Cao, C. *et al.* Urban heat islands in China enhanced by haze pollution. *Nat. Commun.* **7,** 12509 (2016).

184. Center for International Earth Science Information Network (CIESIN), C. U. *Global Urban Heat Island (UHI) Data Set*. (2013).

185. Hondula, D. M. *et al.* Fine-scale spatial variability of heat-related mortality in Philadelphia County, USA, from 1983-2008: a case-series analysis. *Environ. Heal. A Glob. Access Sci. Source* **11,** 1–11 (2012).

186. Medina-Ramón, M., Zanobetti, A., Cavanagh, D. P. & Schwartz, J. Extreme temperatures and mortality: Assessing effect modification by personal characteristics and specific cause of death in a multi-city case-only analysis. *Environ. Health Perspect.* **114,** 1331–1336 (2006).

187. Ellis, F. P. & Nelson, F. Mortality in the elderly in a heat wave in New York City, August 1975. *Environ. Res.* **15,** 504–512 (1978).

188. Berko, J., Ingram, D. D., Saha, S. & Parker, J. D. Deaths attributed to heat, cold, and other weather events in the United States, 2006-2010. *Natl. Health Stat. Report.* 1–15 (2014).

189. Kerr, Z. Y., Casa, D. J., Marshall, S. W. & Comstock, R. D. Epidemiology of Exertional Heat Illness Among U.S. High School Athletes. *Am. J. Prev. Med.* **44,** 8–14 (2013).

190. Jay, O. & Kenny, G. P. Heat exposure in the Canadian workplace. *Am. J. Ind. Med.* **53,** 842–853 (2010).

191. Cuddy, M. L. S. The effects of drugs on thermoregulation. *AACN Clin. Issues* **15,** 238–53 (2004).

192. Wallace, R. F., Kriebel, D., Punnett, L., Wegman, D. H. & Amoroso, P. J. Prior heat illness hospitalization and risk of early death. *Environ. Res.* **104,** 290–295 (2007).

193. Klinenberg, E. Dying Alone. *Ethnography* **2,** 501–531 (2001).

194. Klinenberg, E. *Heat Wave: A Social Autopsy of Disaster in Chicago*. (University of Chicago Press, 2002).

195. Gronlund, C. J. Racial and socioeconomic disparities in heat-related health effects and their mechanisms: a review. *Curr. Epidemiol. reports* **1,** 165–173 (2014).

196. Kovats, R. S. & Hajat, S. Heat Stress and Public Health: A Critical Review. *Annu. Rev. Public Health* **29,** 41–55 (2008).

197. Kuras, E. R., Hondula, D. M. & Brown-Saracino, J. Heterogeneity in individually experienced temperatures (IETs) within an urban neighborhood: insights from a new approach to measuring heat exposure. *Int. J. Biometeorol.* **59,** 1363–1372 (2015).

198. Wolf, T. & McGregor, G. The development of a heat wave vulnerability index for London, United Kingdom. *Weather Clim. Extrem.* **1,** 59–68 (2013).

199. Lane, K. *et al.* Extreme Heat Awareness and Protective Behaviors in New York City. *J. Urban Heal.* **91,** 403–414 (2014).

200. Medina-Ramon, M. & Schwartz, J. Temperature, temperature extremes, and mortality: a

study of acclimatisation and effect modification in 50 US cities. *Occup. Environ. Med.* **64,** 827–833 (2007).

201. Bobb, J. F., Peng, R. D., Bell, M. L. & Dominici, F. Heat-related mortality and adaptation to heat in the United States. *Environ. Health Perspect.* **122,** 811–816 (2014).

202. Krieger, N., Chen, J. T., Waterman, P. D., Rehkopf, D. H. & Subramanian, S. V. Painting a truer picture of US socioeconomic and racial/ethnic health inequalities: The public health disparities geocoding project. *Am. J. Public Health* **95,** 312–323 (2005).

203. Madrigano, J., Ito, K., Johnson, S., Kinney, P. L. & Matte, T. A Case-Only Study of Vulnerability to Heat Wave – Related Mortality. *Environ. Health Perspect.* **672,** 672–678 (2015).

204. Hall, M. J. *et al.* Psychological impact of the animal-human bond in disaster preparedness and response. *J. Psychiatr. Pract.* **10,** 368–374 (2004).

205. Sampson, N. R. *et al.* Staying cool in a changing climate: Reaching vulnerable populations during heat events. *Glob. Environ. Chang.* **23,** 475–484 (2013).

206. Bassil, K. L. & Cole, D. C. Effectiveness of public health interventions in reducing morbidity and mortality during heat episodes: A structured review. *Int. J. Environ. Res. Public Health* **7,** 991–1001 (2010).

207. Srinivasan, K., Maruthy, K., Venugopal, V. & Ramaswamy, P. Research in occupational heat stress in India: Challenges and opportunities. *Indian J Occup Env. Med* **20,** 73–78 (2016).

208. Périard, J. D., Racinais, S. & Sawka, M. N. Adaptations and mechanisms of human heat acclimation: Applications for competitive athletes and sports. *Scand. J. Med. Sci. Sport.* **25,** 20–38 (2015).

209. Hess, J. J., Saha, S. & Luber, G. Summertime Acute Heat Illness in U . S . Emergency Departments from 2006 through 2010 : Analysis of a Nationally Representative Sample. *Environ. Health Perspect.* **122,** 1209–1215 (2014).

210. Nielsen, B. *et al.* Human circulatory and thermoregulatory adaptations with heat acclimation and exercise in a hot, dry environment. *J. Physiol.* **460,** 467–485 (1993).

211. Chalmers, S., Esterman, A., Eston, R., Bowering, K. J. & Norton, K. Short-Term Heat Acclimation Training Improves Physical Performance: A Systematic Review, and Exploration of Physiological Adaptations and Application for Team Sports. *Sport. Med.* **44,** 971–988 (2014).

212. Peng, Z., Wang, Q., Kan, H., Chen, R. & Wang, W. Effects of ambient temperature on daily hospital admissions for mental disorders in Shanghai, China: A time-series analysis. *Sci. Total Environ.* **590–591,** 281–286 (2017).

213. Hansen, A. *et al.* The effect of heat waves on mental health in a temperate Australian City. *Environ. Health Perspect.* **116,** 1369–1375 (2008).

214. Fletcher, B. A., Lin, S., Fitzgerald, E. F. & Hwang, S. A. Association of summer temperatures with hospital admissions for renal diseases in New York state: A case-crossover study. *Am. J. Epidemiol.* **175,** 907–916 (2012).

215. Lin, S. *et al.* Extreme high temperatures and hospital admissions for respiratory and cardiovascular diseases. *Epidemiology* **20,** 738–746 (2009).

216. Azhar, G. S. *et al.* Heat-related mortality in India: Excess all-cause mortality associated with the 2010 Ahmedabad heat wave. *PLoS One* **9,** (2014).

217. NRDC. *Expanding Heat Resilient Cities Across India*. (2016).

218. WHO. Civil registration and vital statistics systems. (2017). Available at:

http://www.aho.afro.who.int/profiles_information/index.php/AFRO:Civil_registration_and_vital_statistics_systems.

219. Gasparrini, A. *et al.* Mortality risk attributable to high and low ambient temperature: a multicountry observational study. *Lancet* **386,** 369–375 (25AD).

220. Samet, J. M., Dominici, F., Zeger, S. L., Schwartz, J. & Dockery, D. W. The National Morbidity, Mortality, and Air Pollution Study. Part I: Methods and methodologic issues. *Res. Rep. Health. Eff. Inst.* 5-14-84 (2000). doi:PubMed ID: 11354823

221. Staddon, P. L., Montgomery, H. E. & Depledge, M. H. Climate warming will not decrease winter mortality. *Nat. Clim. Chang.* **4,** 190–194 (2014).

222. Sheridan, S. C., Kalkstein, A. J. & Kalkstein, L. S. Trends in heat-related mortality in the United States, 1975-2004. *Nat. Hazards* **50,** 145–160 (2009).

223. Peng, R. D. *et al.* Toward a Quantitative Estimate of Future Heat Wave Mortality under Global Climate Change. *Environ. Health Perspect.* **119,** 701–706 (2011).

224. Lelieveld, J., Evans, J. S., Fnais, M., Giannadaki, D. & Pozzer, A. The contribution of outdoor air pollution sources to premature mortality on a global scale. *Nature* **525,** 367–371 (2015).

225. Fischer, P. H., Brunekreef, B. & Lebret, E. Air pollution related deaths during the 2003 heat wave in the Netherlands. *Atmos. Environ.* **38,** 1083–1085 (2004).

226. Fiore, A. M. *et al.* Global air quality and climate. *Chem. Soc. Rev.* **41,** 6663 (2012).

227. Jacobson, M. Z. & Streets, D. G. Influence of future anthropogenic emissions on climate, natural emissions, and air quality. *J. Geophys. Res. Atmos.* **114,** 1–21 (2009).

228. Rieder, H. E., Fiore, A. M., Polvani, L. M., Lamarque, J.-F. & Fang, Y. Changes in the frequency and return level of high ozone pollution events over the eastern United States

following emission controls. *Environ. Res. Lett.* **8,** 14012 (2013).

229. Rasmussen, D. J., Hu, J., Mahmud, A. & Kleeman, M. J. The Ozone–Climate Penalty: Past, Present, and Future. *Environ. Sci. Technol.* **47,** 14258–14266 (2013).

230. Tai, A. P. K., Mickley, L. J. & Jacob, D. J. Correlations between fine particulate matter (PM2.5) and meteorological variables in the United States: Implications for the sensitivity of PM2.5 to climate change. *Atmos. Environ.* **44,** 3976–3984 (2010).

231. Horton, D. E., Skinner, C. B., Singh, D. & Diffenbaugh, N. S. Occurrence and persistence of future atmospheric stagnation events. *Nat. Clim. Chang.* **4,** 698–703 (2014).

232. Horton, D. E., Harshvardhan & Diffenbaugh, N. S. Response of air stagnation frequency to anthropogenically enhanced radiative forcing. *Environ. Res. Lett.* **7,** 44034 (2012).

233. Beggs, P. J. & Bambrick, H. J. Is the global rise of asthma an early impact of anthropogenic climate change? *CiÃ\textordfemeninencia & SaÃ\textordmasculinede Coletiva* **11,** 745–752 (2006).

234. Sathaye, J. A. *et al.* Estimating impacts of warming temperatures on California's electricity system. *Glob. Environ. Chang.* **23,** 499–511 (2013).

235. Schweikert, A., Chinowsky, P., Kwiatkowski, K. & Espinet, X. The infrastructure planning support system: Analyzing the impact of climate change on road infrastructure and development. *Transp. Policy* **35,** 146–153 (2014).

236. Meyer, M. D., Amekudzi, A. & Patrick, J. Transportation Asset Management Systems and Climate Change. *Transp. Res. Rec. J. Transp. Res. Board, No. 2160, Transp. Res. Board Natl. Acad. Washington, D.C.* **2160,** 12–20 (2010).

237. Isaac, M. & van Vuuren, D. P. Modeling global residential sector energy demand for heating and air conditioning in the context of climate change. *Energy Policy* **37,** 507–521

(2009).

238. Deschênes, O. & Greenstone, M. Climate change, mortality, and adaptation: Evidence from annual fluctuations in weather in the US. *Am. Econ. J. Appl. Econ.* **3,** 152–185 (2011).

239. Smoyer-Tomic, K. E., Kuhn, R. & Hudson, A. Heat Wave Hazards: An Overview of Heat Wave Impacts in Canada. *Nat. Hazards* **28,** 465–486 (2003).

240. Bowler, D. E., Buyung-Ali, L., Knight, T. M. & Pullin, A. S. Urban greening to cool towns and cities: A systematic review of the empirical evidence. *Landsc. Urban Plan.* **97,** 147–155 (2010).

241. Oliveira, S., Andrade, H. & Vaz, T. The cooling effect of green spaces as a contribution to the mitigation of urban heat: A case study in Lisbon. *Build. Environ.* **46,** 2186–2194 (2011).

242. Georgi, N. J. & Zafiriadis, K. The impact of park trees on microclimate in urban areas. *Urban Ecosyst.* **9,** 195–209 (2006).

243. Solecki, W. D. *et al.* Mitigation of the heat island effect in urban New Jersey. *Environ. Hazards* **6,** 39–49 (2005).

244. Chen, X. *et al.* Study on the cooling effects of urban parks on surrounding environments using Landsat TM data: a case study in Guangzhou, southern China. *Int. J. Remote Sens.* **33,** 5889–5914 (2012).

245. Susca, T., Gaffin, S. R. & Dell'Osso, G. R. Positive effects of vegetation: Urban heat island and green roofs. *Environ. Pollut.* **159,** 2119–2126 (2011).

246. Givoni, B. Impact of planted areas on urban environmental quality: A review. *Atmos. Environ. Part B, Urban Atmos.* **25,** 289–299 (1991).

247. Bertram, C. & Rehdanz, K. The role of urban green space for human well-being. *Ecol. Econ.* **120,** 139–152 (2015).

248. Bolitzer, B. & Netusil, N. R. The impact of open spaces on property values in Portland, Oregon. *J. Environ. Manage.* **59,** 185–193 (2000).

249. Zoulia, I., Santamouris, M. & Dimoudi, A. Monitoring the effect of urban green areas on the heat island in Athens. *Environ. Monit. Assess.* **156,** 275 (2008).

250. Maimaitiyiming, M. *et al.* Effects of green space spatial pattern on land surface temperature: Implications for sustainable urban planning and climate change adaptation. *ISPRS J. Photogramm. Remote Sens.* **89,** 59–66 (2014).

251. Hamada, S. & Ohta, T. Seasonal variations in the cooling effect of urban green areas on surrounding urban areas. *Urban For. Urban Green.* **9,** 15–24 (2010).

252. Shashua-Bar, L., Potchter, O., Bitan, A., Boltansky, D. & Yaakov, Y. Microclimate modelling of street tree species effects within the varied urban morphology in the Mediterranean city of Tel Aviv, Israel. *Int. J. Climatol.* **30,** 44–57 (2010).

253. Simpson, J. R. & McPherson, E. G. Simulation of tree shade impacts on residential energy use for space conditioning in Sacramento. *Atmos. Environ.* **32,** 69–74 (1998).

254. Gaffin, S. R., Khanbilvardi, R. & Rosenzweig, C. Development of a Green Roof Environmental Monitoring and Meteorological Network in New York City. *Sensors* **9,** 2647–2660 (2009).

255. Rossi, F., Pisello, A. L., Nicolini, A., Filipponi, M. & Palombo, M. Analysis of retro-reflective surfaces for urban heat island mitigation: A new analytical model. *Appl. Energy* **114,** 621–631 (2014).

256. Akbari, H., Pomerantz, M. & Taha, H. Cool surfaces and shade trees to reduce energy use

and improve air quality in urban areas. *Sol. Energy* **70,** 295–310 (2001).

257. Akbari, H., Menon, S. & Rosenfeld, A. Global cooling: increasing world-wide urban albedos to offset CO2. *Clim. Change* **94,** 275–286 (2009).

258. Touchaei, A. G., Hosseini, M. & Akbari, H. Energy savings potentials of commercial buildings by urban heat island reduction strategies in Montreal (Canada). *Energy Build.* **110,** 41–48 (2016).

259. Santamouris, M. Cooling the cities - A review of reflective and green roof mitigation technologies to fight heat island and improve comfort in urban environments. *Sol. Energy* **103,** 682–703 (2014).

260. Li, D., Bou-Zeid, E. & Oppenheimer, M. The effectiveness of cool and green roofs as urban heat island mitigation strategies. *Environ. Res. Lett.* **9,** 55002 (2014).

261. Zhang, J., Zhang, K., Liu, J. & Ban-Weiss, G. Revisiting the climate impacts of cool roofs around the globe using an Earth system model. *Environ. Res. Lett.* **11,** 84014 (2016).

262. Synnefa, A., Dandou, A., Santamouris, M., Tombrou, M. & Soulakellis, N. On the Use of Cool Materials as a Heat Island Mitigation Strategy. *J. Appl. Meteorol. Climatol.* **47,** 2846–2856 (2008).

263. Akbari, H., Damon Matthews, H. & Seto, D. The long-term effect of increasing the albedo of urban areas. *Environ. Res. Lett.* **7,** 24004 (2012).

264. Georgescu, M., Morefield, P. E., Bierwagen, B. G. & Weaver, C. P. Urban adaptation can roll back warming of emerging megapolitan regions. *Proc. Natl. Acad. Sci. U. S. A.* **111,** 2909–14 (2014).

265. Sproul, J., Wan, M. P., Mandel, B. H. & Rosenfeld, A. H. Economic comparison of white, green, and black flat roofs in the United States. *Energy Build.* **71,** 20–27 (2014).

266. Braaker, S., Ghazoul, J., Obrist, M. K. & Moretti, M. Habitat connectivity shapes urban arthropod communities: the key role of green roofs. *Ecology* **95,** 1010–1021 (2014).

267. Berardi, U., GhaffarianHoseini, A. & GhaffarianHoseini, A. State-of-the-art analysis of the environmental benefits of green roofs. *Appl. Energy* **115,** 411–428 (2014).

268. Ascione, F., Bianco, N., de' Rossi, F., Turni, G. & Vanoli, G. P. Green roofs in European climates. Are effective solutions for the energy savings in air-conditioning? *Appl. Energy* **104,** 845–859 (2013).

269. Block, A. H., Livesley, S. J. & Williams, N. S. G. Responding to the Urban Heat Island : A Review of the Potential of Green Infrastructure. *Vic. Cent.* 1–62 (2012).

270. Oke, T. R. Canyon geometry and the nocturnal urban heat island: Comparison of scale model and field observations. *J. Climatol.* **1,** 237–254 (1981).

271. Chen, Z. *et al.* Field measurements on microclimate in residential community in Guangzhou, China. *Front. Archit. Civ. Eng. China* **3,** 462 (2009).

272. Theeuwes, N. E., Solcerová, A. & Steeneveld, G. J. Modeling the influence of open water surfaces on the summertime temperature and thermal comfort in the city. *J. Geophys. Res. Atmos.* **118,** 8881–8896 (2013).

273. Nishimura, N., Nomura, T., Iyota, H. & Kimoto, S. Novel water facilities for creation of comfortable urban micrometeorology. *Sol. Energy* **64,** 197–207 (1998).

274. Steeneveld, G. J., Koopmans, S., Heusinkveld, B. G. & Theeuwes, N. E. Refreshing the role of open water surfaces on mitigating the maximum urban heat island effect. *Landsc. Urban Plan.* **121,** 92–96 (2014).

275. Saaroni, H. & Ziv, B. The impact of a small lake on heat stress in a Mediterranean urban park: the case of Tel Aviv, Israel. *Int. J. Biometeorol.* **47,** 156–165 (2003).

276. Lowe, D., Ebi, K. L. & Forsberg, B. Heatwave early warning systems and adaptation advice to reduce human health consequences of heatwaves. *Int. J. Environ. Res. Public Health* **8,** 4623–4648 (2011).

277. Ebi, K. L. & Schmier, J. K. A stitch in time: Improving public health early warning systems for extreme weather events. *Epidemiol. Rev.* **27,** 115–121 (2005).

278. Kovats, R. S. & Kristie, L. E. Heatwaves and public health in Europe. *Eur. J. Public Health* **16,** 592–599 (2006).

279. Hess, J. J. & Ebi, K. L. Iterative management of heat early warning systems in a changing climate. *Ann. N. Y. Acad. Sci.* 21–30 (2016). doi:10.1111/nyas.13258

280. Åström, C., Ebi, L. K., Langner, J. & Forsberg, B. Developing a Heatwave Early Warning System for Sweden: Evaluating Sensitivity of Different Epidemiological Modelling Approaches to Forecast Temperatures. *International Journal of Environmental Research and Public Health* **12,** (2015).

281. Bernard, T. E. & Kenney, W. L. Rationale for a Personal Monitor for Heat Strain. *Am. Ind. Hyg. Assoc. J.* **55,** 505–514 (1994).

282. Reid, C. E. *et al.* Evaluation of a Heat Vulnerability Index on Abnormally Hot Days: An Environmental Public Health Tacking Study. *Environ. Health Perspect.* **120,** 715–720 (2012).

283. Bernhard, M. C. *et al.* Measuring personal heat exposure in an urban and rural environment. *Environ. Res.* **137,** 410–418 (2015).

284. Nitschke, M. *et al.* Risk Factors, Health Effects and Behaviour in Older People during Extreme Heat: A Survey in South Australia. *International Journal of Environmental Research and Public Health* **10,** (2013).

285. Raja, I. A., Nicol, J. F., McCartney, K. J. & Humphreys, M. A. Thermal comfort: use of controls in naturally ventilated buildings. *Energy Build.* **33,** 235–244 (2001).

286. Gupta, S. *et al.* Electric fans for reducing adverse health impacts in heatwaves. *Cochrane Libr.* (2012).

287. Hajat, S., O'Connor, M. & Kosatsky, T. Health effects of hot weather: from awareness of risk factors to effective health protection. *Lancet* **375,** 856–863 (2010).

288. Zhao, L. *et al.* Interactions between urban heat islands and heat waves. *Environ. Res. Lett.* (2017). doi:10.1088/1748-9326/aa9f73